TENSION PILE STUDY

VOLUME VI

THEORY DEVELOPMENT AND CORRELATION

Report Number 82-200-5

* * *

Report to

CONOCO NORWAY, INC.

* * *

Through

DET NORSKE VERITAS
Oslo, Norway

By

THE EARTH TECHNOLOGY CORPORATION
Houston, Texas

February 1986

PREFACE

This is a final report for Task 10 - Theory Development and Correlation of Field Data. The work reported herein is part of a larger project sponsored by Conoco through Conoco Norway Research and Development to develop a better understanding of pile-soil interaction associated with foundation piles for tension leg platforms. The project is identified as CNRD 13-3. Also participating in support of the project were Chevron Oil Company, the American Bureau of Shipping, and the Minerals Management Service of the United States Department of the Interior. The development of concepts and background theory was originally accomplished under an in-house project supported by The Earth Technology Corporation before the initiation of the project with Conoco. Some modifications of the CASH (Cavity expansion with Axial SHearing) program and the analyses reported in this progress report were supported by Conoco.

The work was performed by The Earth Technology Corporation, acting as designated subcontractor to A. S. Veritec. The project team members and their roles in the project are summarized below. The majority of the work in this report was performed by Mr. Ignatius (Po) Lam. Mr. Hudson Matlock provided overall direction in the course of the study and reviewed the report. Mr. Dewaine Bogard furnished the field test data, served as the project manager and reviewed the report. Mr. Lino Cheang assisted in some of the CASH analyses. Dr. Jean Audibert, Manager of the Houston office, provided assistance in administrative matters.

TABLE OF CONTENTS

TABLE OF CONTENTS (Continued)

LIST OF FIGURES

TABLE OF CONTENTS

LIST OF FIGURES

TABLE OF CONTENTS

LIST OF FIGURES

TABLE OF CONTENTS

LIST OF TABLES

1. INTRODUCTION

Parallel to the experimental program, a task on theory development was undertaken to advance our understanding of pile behavior and to assist in extrapolation of pile load test data to prototype conditions. The choice of the analytical method summarized below has largely been guided by the perceived need for flexible, general-purpose tools that can be adjusted or modified to fit the experimental observations.

Some of the factors affecting side-friction capacity and deformational behavior of a pile are listed below and illustrated in Plate 1.1:

(1) In-situ soil stress conditions before pile installation.

(2) Changes in the soil conditions due to pile installation.

(3) Changes in the soil conditions from consolidation of the soil mass after installation.

(4) Changes in the soil conditions caused by subsequent static and cyclic axial loading.

A parallel experimental and analytical program was undertaken to improve our understanding on the above aspects. The experimental program included laboratory model tests performed by A. S. Veritec using one-inch diameter pile models and in situ load test programs performed by the Earth Technology personnel. Three types of in situ tests were conducted using the following equipment: (a) 3-inch diameter pile segments, (b) x-probes (1.72-inch diameter close-ended probes), and (c) a 359 ft long, 30-inch diameter pile. All the above equipment was instrumented to provide measurements of total lateral stress, pore water pressure, and side-shear resistance of the soil at various stages, including pile insertion, consolidation and static and cyclic pile loading.

Results of experiments from the 3-inch pile segment test have been reported in the Volume III report (Ref. 9). The 30-inch pile load test data has been reported in a recent report (Ref. 8).

A computer program, CASH (Cavity expansion with Axial SHearing), had been formulated to simulate the above factors and to provide improved t-z characterization as input to an overall soil-pile interaction analysis (e.g. using Program DRIVE (Ref. 14)). The following sections summarize (1) the concept behind CASH, (2) features of the soil stress-strain model, (3) preliminary backfitting analyses conducted in 1983 to simulate the 3-inch pile segment tests, (4) a series of sensitivity studies, and (5) backfitting analyses conducted for the 3-inch segment, the X-Probe and the 30-inch pile for two strata of soil layers (Strata II and III). Recommendations for future studies are also provided.

2. SINGLE-SLICE DISCRETE ELEMENT MODEL

2.1 General

This section summarizes the background theory behind the CASH program which can be used as a tool to better understand the changes in the surrounding soil during various stages in time, including: pile installation, consolidation and pile loading. Some of the key features of CASH are listed below:

(1) Analysis of an axisymmetric single slice of soil mass around a pile at a specific depth.

(2) Usage of a two-phase (solid and pore fluid) concept.

(3) Nonlinear constitutive soil model to characterize the soil skeleton stress-strain behavior.

(4) Large displacement effects.

The remaining sections (2.2 through 2.7) discuss the following topics:

- Section 2.2 - Configuration of the single slice of soil mass.
- Section 2.3 - The displacement degree of freedom at each soil node.
- Section 2.4 - Loading conditions (for pile driving, consolidation and axial shear).
- Section 2.5 - The governing equations.
- Section 2.6 - The two-phase (or effective stress) concept.
- Section 2.7 - Constitutive relation for the fluid phase.

- o Section 2.8 - Constitutive relation for the solid (soil skeleton) phase.
- o Section 2.9 - The computation scheme for nonlinearity.
- o Section 2.10 - Comparison of the CASH approach with other models by past researchers.

2.2 Configuration

The model used in program CASH is shown in Plate 2.1. An axisymmetric single horizontal slice of soil mass surrounding a cylindrical pile is used for the analysis. Either a plane-strain or a plane-stress condition can be assumed in the analysis.

The slice of soil mass is discretized in the radial direction in terms of a radial dimension r. To allow for the internal generation of a very thin shear zone during axial loading, the increments are very finely spaced near the pile wall. To accommodate large displacement effects, the geometry (discretization) representing the slice of soil mass is updated with time.

2.3 Degrees of Freedom

Displacement of the single-slice model is described by three degrees of freedom at each nodal point in the soil mass: (1) radial displacement u_r of the soil skeleton, (2) axial displacement u_z of the soil skeleton, and (3) radial displacement U_r of the pore fluid. During computation, the pore fluid movement at any point is characterized by its relative displacement with respect to the soil skeleton as shown in Plate 2.2.

2.4 Loading Conditions

Two components of a load-time history are used to simulate the effects of pile installation, consolidation and axial loading. These time-dependent input functions are prescribed independently as radial (expansion or contraction) and axial (shearing) displacements at the cylindrical cavity wall (representing the pile-soil interface). A variety of outer boundary conditions, such as zero displacement or constant stress conditions, can be specified in CASH.

2.5 Governing Equations

The three governing equations for the single slice model in CASH are based on (1) force equilibrium in the radial direction, (2) force equilibrium in the axial direction, and (3) Darcy's Law for the flow of pore fluid in the radial direction.

As shown in Plate 2.2, the slice of soil mass is first discretized into nodal points and elements. Different properties and increment length can be specified for each element. The stresses and pore pressures are sampled at the mid-point of each element and displacements of soil and pore fluid are computed at the nodal points.

Plate 2.3 illustrates the force components contributing to radial equilibrium. The equilibrium of forces at nodal point i leads to

$$\begin{aligned} & r_{i-1}\,\bar{\sigma}_{r,i-1} + 0.5\,\Delta h_{i-1}\,\bar{\sigma}_{\theta,i-1} + (r_{i-1} + 0.5\,\Delta h_{i-1})\,p_{i-1} \\ & -r_i\,\bar{\sigma}_{r,i} + 0.5\,\Delta h_i\,\bar{\sigma}_{\theta,i} + (r_i + 0.5\,\Delta h_i)\,p_i = 0 \end{aligned} \qquad (1)$$

where,

r_{i-1} , r_i = distances to center of elements,

Δh_{i-1} , Δh_i = increment lengths of elements,

$\bar{\sigma}_{r,i-1}$, $\bar{\sigma}_{r,i}$ = radial effective stress at elements,

$\bar{\sigma}_{\theta,i-1}$, $\bar{\sigma}_{\theta,i}$ = circumferential effective stress at elements,

p_{i-1} , p_i = pore fluid pressure at elements,

and the subscripts i-1 and i denote the element numbers.

The single force component acting in the axial direction is the shear force, thus resulting in the following equilibrium equation:

$$r_{i-1}\ \tau_{rz,i-1} - r_i\ \tau_{rz,i} = 0 \qquad (2)$$

where

$\tau_{rz,i-1}$; $\tau_{rz,i}$ = shear stress at elements i-1 and i respectively.

To model the pore fluid migration, Darcy's Law is applied which leads to the following equation

$$p_{i-1} - p_i = 0.5 \left(\frac{\gamma_{i-1}\ \Delta h_{i-1}}{k_{i-1}} + \frac{\gamma_i\ \Delta h_i}{k_i} \right) \dot{U}_{r,i} \qquad (3)$$

where

γ_{i-i} , γ_i = unit weight of fluid at elements i-1 and i respectively,

k_{i-1} , k_i = permeability at elements i-1 and i respectively,

$\dot{U}_{r,i}$ = flow velocity across the soil skeleton at node i.

The three governing equations (Eqs. 1 to 3) are written in terms of the effective stresses, pore pressure and fluid velocities. By applying stress-strain relationships for both soil skeleton and pore fluid, the stresses and pore pressure at an element can be related to displacements (u_r , u_z and U_r) at the two adjacent nodal points. Equations 1 to 3 can thus be written in terms of the three degrees of freedom in nodal displacements.

A space-wise implicit numerical operator is used in program CASH to solve the above governing equations. The operator ensures that static equilibrium (Eqs. 1 and 2) is satisfied at each time steps. An iterative scheme is used in adjustment and checking the stepwise linear (tangent) soil moduli and to ensure that the resultant error is tolerable even for a large increment of loading.

2.6 Two-Phase Saturated Soil Model

A two-phase effective stress model is used for the single-slice analysis. The stress condition at each point in the soil mass is characterized by an effective stress tensor $\bar{\sigma}_r$, $\bar{\sigma}_z$, $\bar{\sigma}_\theta$, and τ_{rz} plus a component of hydrostatic pore fluid pressure p .

The effective stress is the average stress transmitted through the soil skeleton and the pore fluid occupies the pore space between soil grains. When the soil mass is subjected to an external load, the load distribution between the pore fluid and soil grains is governed by the classical Terzaghi effective stress concept (Refs 18 and 2):

$$\sigma = \bar{\sigma} + p \qquad (4)$$

where

σ and $\bar{\sigma}$ are respectively components of total and effective normal stresses, and

p is the fluid pressure.

In accordance with the effective stress and the two-phase soil model concepts, the effective stress in the soil skeleton is assumed to be dependent only on the strain components of the soil skeleton. Similarly, the pore pressure is assumed to be dependent on the total specific volume of the pore fluid. An elastic bulk modulus of the fluid is assumed and can be adjusted to simulate the presence of entrapped gas.

2.7 Constitutive Relation for Pore Fluid

Concepts of the relation of pore pressure with displacements are shown in Plate 2.4. A bulk modulus K_f is used to relate pore fluid pressure to volume. The conventional equation of state of the fluid is used:

$$\Delta p = K_f \left(\frac{\Delta \gamma_f}{\gamma_f} \right) \tag{5}$$

where

Δp is change in pore fluid pressure, and

γ_f , $\Delta\gamma_f$ are the present density of the fluid and the change of density, respectively.

As shown in Plate 2.4, change in density of the pore fluid during loading is related to the movement of fluid with respect to the soil skeleton as well as the change in porosity:

$$\frac{\Delta\gamma_f}{\gamma_f} = \frac{\Delta\varepsilon_f + \Delta\varepsilon_s}{n} \tag{6}$$

where

$\Delta\varepsilon_f$ is the specific volume change of the pore fluid resulting from flow of fluid relative to soil skeleton,

$\Delta\varepsilon_s$ is the specific volume change of the soil skeleton, and

n is the porosity.

The specific volume change of the fluid mesh $\Delta\varepsilon_f + \Delta\varepsilon_s$ can be computed from the initial and deformed fluid mesh for element i (see Plate 2.4) as follows:

$$\text{Deformed Volume} = \pi (R_{i+1} + \Delta u_{r,i+1} + \Delta U_{r,i+1})^2 - \pi (R_i + \Delta u_i + \Delta U_{r,i})^2 \quad (7)$$

$$\text{Initial Volume} = \pi (R_{i+1})^2 - \pi (R_i)^2 \quad (8)$$

where R_i and R_{i+1} are the radial distances to node i and $i+1$, respectively.

$$\Delta\varepsilon_f + \Delta\varepsilon_s = \left(\frac{\text{Deformed Volume} - \text{Initial Volume}}{\text{Initial Volume}} \right)$$

$$\approx (0.5\frac{1}{r_i} - \frac{1}{\Delta h_i}) (\Delta u_{r,i} + \Delta U_{r,i}) + (0.5\frac{1}{r_i} + \frac{1}{\Delta h_i}) (\Delta u_{r,i+1} + \Delta U_{r,i+1}) \quad (9)$$

Finally, the pore pressure versus displacement relationship at element i is obtained from Eqs 5, 6, and 9 and given below:

$$\Delta p_i = \frac{K_{f,i}}{n_i} \left\{ (0.5\frac{1}{r_i} - \frac{1}{\Delta h_i}) (\Delta U_{r,i} + \Delta U_{r,i}) \right.$$

$$\left. + (0.5\frac{1}{r_i} + \frac{1}{\Delta h_i})(\Delta u_{r,i} + \Delta U_{r,i}) \right\} \quad (10)$$

2.8 Constitutive Relation for Soil Skeleton

The side-friction capacity and shear transfer characteristics of a pile depend to a large extent on the general stress-strain behavior of the soil mass. The major requirement placed on the formulation of the constitutive relation is flexibility for backfitting and correlation with any observed pile load test data. The adopted model should provide for reasonable simulations of (1) geologic loading leading to the in situ stress condition, (2) large shearing strains during pile installation, (3) consolidation, and (4) static and cyclic axial shearing during pile loading. Furthermore, the model must allow for considerable flexibility in input description of soil characteristics for backfitting purposes.

Most existing soil models do not meet the above requirements and have built-in physical and mathematical restrictions that do not arise from realistic considerations and are too limiting for the present backfitting purposes. To carry on this study, a new soil model was formulated. This soil model is formulated based on the perceived need of pile loading applications and is not necessarily intended to be used for other problems.

A Contrived Model. As the name (a contrived model) implies, the adopted constitutive model was artificially created to meet the perceived need of pile loading applications. At any time step, the incremental stress is related to the incremental strain by the following expressions:

$$\Delta\bar{\sigma}_{11} = \Delta\bar{\sigma}_{rr} = (K + \frac{4G}{3})\ \Delta\varepsilon_{11} + (K - \frac{2G}{3})\ \Delta\varepsilon_{22} + (K - \frac{2G}{3})\ \Delta\varepsilon_{33} - K\Delta\theta + f_1 \qquad 11(a)$$

$$\Delta\bar{\sigma}_{22} = \Delta\bar{\sigma}_{zz} = (K - \frac{2G}{3})\ \Delta\varepsilon_{11} + (K + \frac{4G}{3})\ \Delta\varepsilon_{22} + (K - \frac{2G}{3})\ \Delta\varepsilon_{33} - K\Delta\theta + f_2 \qquad 11(b)$$

$$\bar{\Delta\sigma}_{33} = \bar{\Delta\sigma}_{\theta\theta} = (K - \frac{2G}{3})\ \Delta\varepsilon_{11} + (K - \frac{2G}{3})\ \Delta\varepsilon_{22} + (K + \frac{4G}{3})\ \Delta\varepsilon_{33} - K\Delta\theta + f_3 \qquad 11(c)$$

$$\Delta\tau_{12} = \Delta\tau_{rz} = 2G^* \Delta\varepsilon_{12} + f_4 \qquad 11(d)$$

Eight coefficients (K , G , G^* , $\Delta\theta$, f_1 , f_2 , f_3 , and f_4) are necessary at each time step. With G^* set equal to G , $\Delta\theta$ and the f's vanish, the above expression is reduced to the conventional Hooke's Law written in terms of bulk modulus K and shear modulus G . The above eight constants are deduced for a given trial increment of strain at each time step.

The eight coefficients can be varied in accordance with the stress or strain history to achieve the necessary salient features of stress-strain behavior for volumetric and shear considerations (more description to follow). If the appropriate rules are followed, this model will be fundamentally correct in the following sense:

(1) The stress-strain behavior will be independent of the choice of the coordinate systems.

(2) Erroneous energy generation will not occur in monotonic or cyclic loading conditions.

Although the above model bears little resemblance to the classical plasticity theory (which is the framework for most current soil models), with the proper procedure to develop the model coefficients, it can satisfy the key concepts from plasticity theory:

(1) A yield function can implicitly exist to ensure that the model satisfies some failure criterion.

(2) The plastic strain increment would satisfy the plastic flow rule.

Additional discussion on the above will be given in this section.

Volumetric Considerations. K and $\Delta\theta$ are deduced based on volumetric considerations. As shown in Plate 2.5a, the soil model allows for nonlinear and inelastic stress-strain curves. Furthermore it allows for differences between initial loading and unloading. At the present, initial reloading is assumed to follow the same path as unloading. Volume change due to shearing is reflected by the translation of the volumetric stress-strain curve, controlled by the parameter θ. At each time step, an incremental change $\Delta\theta$ is determined to reflect monotonic behavior such as shear dilation and compaction as well as volume change from cyclic shear loading. The shear-volume change can be related to any variables such as the shear strain amplitudes, overconsolidation ratio (OCR) and the number of cycles of repeated loading.

Deviatoric Considerations. Upon determination of the constants K and $\Delta\theta$, the mean effective stress is known. The constants (G , G^* , f_1 , f_2 , f_3 , and f_4) are then deduced based on the anticipated deviatoric behavior of soil. In consideration of the constant G in Equations 11a through 11c, the octahedral shear stress and octahedral shear strain are computed as follows:

$$\tau_{oct} = \left[\frac{(\bar{\sigma}_{11} - \bar{\sigma}_{22})^2 + (\bar{\sigma}_{22} - \bar{\sigma}_{33})^2 + (\bar{\sigma}_{33} - \bar{\sigma}_{11})^2}{9} \right]^{0.5} \qquad (12)$$

$$\gamma_{oct} = \left\{ \frac{4}{9} \left[(\varepsilon_{11} - \varepsilon_{22})^2 + (\varepsilon_{22} - \varepsilon_{33})^2 + (\varepsilon_{33} - \varepsilon_{11})^2 \right] \right\}^{0.5} \qquad (13)$$

The stress and strain, τ_{oct} and γ_{oct}, are interpreted as the magnitude of induced shear stress and shear strain for the consideration of the shear modulus G and shear volume change $\Delta\theta$ due to straining in the normal directions. The small-strain modulus G_{max} is first computed from the estimated mean effective stress $\bar{\sigma}_m$ and some input numerical arrays relating G_{max} and τ_{max} to the mean effective stress $\bar{\sigma}_m$. The constant G is then computed from τ_{max},

G_{max} and a normalized backbone curve that relates the normalized stress (τ_{oct} / τ_{max}) to the normalized strain (γ_{oct} * G_{max} / τ_{max}) . The backbone curve of any desired form is input by a numerical array. Similar to the volumetric stress-strain curve, a linearly elastic unloading and reloading modulus is assumed. The linearly elastic unloading and reloading assumption is inappropriate for fully cyclic applications. However, fully cyclic loading is not expected (the normal stresses is expected to remain positive or compressive) for the normal stress directions and the above limitation is not expected to be too restrictive.

The constant G^* in Equation 11d that controls directly the deformational characteristics of the load-transfer (t-z) curve is basically governed by the same procedure as that for the constant G . The magnitudes of shear stress and shear strain are now directly τ_{rz} and γ_{rz} respectively and the normalized backbone curve is now the (τ_{rz} / τ_{max}) vs. (γ_{rz} * G_{max} / τ_{max}) curve. Furthermore, to allow for complete hysteretic treatments, the input backbone curve is used to generate an assembly of elastoplastic subelements similar to the soil support model used in the DRIVE program (Ref. 14). Thus, the resultant τ_{rz} vs. γ_{rz} curve is fully hysteretic and the stiffness and failure stress level can be related to the mean effective stress or the radial normal stress.

So far, consideration of the deviatoric model for the normal stresses (controlled by the constant G) is uncoupled from the shear stress (controlled by the constant G^*) . However, from past research on stress-strain modelling, the failure condition of soil is found to be dependent on all stress components. Components of the stress vector f_1 , f_2 , f_3 , and f_4 are introduced to arrive at the proper coupled failure characteristics. This stress

vector is determined by adopting classical plasticity treatments. A deviatoric failure criterion is assumed and is given below:

$$\zeta = \frac{1}{6}\left[(\bar{\sigma}_{11} - \bar{\sigma}_{22})^2 + (\bar{\sigma}_{22} - \bar{\sigma}_{33})^2 + (\bar{\sigma}_{33} - \bar{\sigma}_{11})^2 \right] + \tau_{12}^2 - (c_1 + c_2 \bar{\sigma}_m + c_3 \varepsilon_v)^2 \quad (14)$$

The stress increment in Equation 11 is first computed along the steps outlined previously assuming that f's are zero. The resulting stress is then tested for failure by the above equation. If ζ is found to be less than zero, ultimate failure condition does not occur and the above stress increment is appropriate. If ζ is found to be larger than zero, plastic flow occurs and f_1 through f_4 need to be determined. The physical aspects of the stress vector f_1, f_2, f_3, and f_4 are briefly summarized.

For a given increment of strain, the vector $\{f\}$ is primarily a tool to arrive at a final stress state which is compatible with the three dimensional failure criterion (as shown in Equation 14). The stress vector $\{f\}$ is characterized by the direction and the magnitude. The direction of this vector is chosen such that no change in mean effective stress will be introduced. Furthermore the vector $\{f\}$ depends only on the current state of stress and does not depend on the direction of loading. The above consideration leads to the following expressions.

$$\begin{aligned} f_1 &= \lambda s_{11} = \lambda (\sigma_{11} - \bar{\sigma}_m) \\ f_2 &= \lambda s_{22} = \lambda (\sigma_{22} - \bar{\sigma}_m) \\ f_3 &= \lambda s_{33} = \lambda (\sigma_{33} - \bar{\sigma}_m) \\ f_4 &= \lambda s_{12} = \lambda \tau_{12} \end{aligned} \quad (15)$$

where

s_{11}, s_{22}, s_{33}, and s_{12} are the components of the deviatoric stress tensor.

The quantity λ is a scalar with a magnitude so determined that the final state of stress in Equation 11 will produce the proper final failure condition (or ζ in Equation 14 equal to zero).

Comparison to Classical Plasticity Models. If the elastic parameters (G, G* and K) in equation 11 were maintained to be constant (through specification of the $\tau_{oct} - \gamma_{oct}$ and the $\tau_{rz} - \gamma_{rz}$ relationships), the contrieved model would be reduced to a elasto-plastic plasticity model with a failure criterion defined by Equation 14. The plastic strain increment would be non associative in the volumetric sense, but associative in the deviatoric subspace. Some of the CASH solutions applying the above classical plasticity concept has been reported by Matlock et al. (Ref. 15). It was concluded, in the course of this project that none of the currently available general soil model (that can be used for general boundary problems) has all the necessary features to account for the observed pile behavior. The model reported in this report is the product of a series of effort of trial and back fitting of experimental data. Some of the soil modeling features motivated by the observation of field experiment data are:

(1) Accounting for the effect of cyclic remolding on the shear strength characteristics similar to Hvorslev's concept. (Ref. 12). Further discussion of this is provided in Section 3.3.

(2) A flexible framework to incorporate shear volume change effect in cyclic loading conditions (See Section 3.2).

Inputs to the above soil model are primarily a number of numerical arrays describing the physically intuitive stress-strain curves (see Plate 2.5). Any curve fitting prior to analysis is unnecessary for the above described soil model. This aspect is expected to facilitate backfitting and iterative adjustment for observed pile load test data.

2.9 Computational Scheme for Nonlinear Soil Behavior

The structure of the CASH program is designed to allow for flexibility in treatment of all the above mentioned aspects of soil behavior including (1) shear-volume change, (2) nonlinear hysteretic response and (3) shear failure behavior of soil. Some of the features for flexibility include the following:

(1) An iterative approach is used to adjust for the proper representation of soil behavior. At every element, and at every time step, the strain increment from successive trial solutions are compared and tested for convergence (to some specified level of tolerance). If convergence is not achieved, the last trial increment of strain is then used to obtain revised soil stiffness representation for the next trial solution. The iterative process continues until convergence is achieved.

(2) The numerical scheme in CASH allows for a very flexible treatment of soil stiffnesses. It permits the use of any combination of (a) tangent modulus concepts and (b) load adjustment concepts to represent the stress-strain behavior of soil in the overall single slice solution.

(3) The constitutive subroutines are arranged in modular form such that any soil model can be assigned to any element. Besides the soil model described above, the CASH program currently has two other simpler soil models: (a) a linear elasticity model, and (b) an elasto-perfectly plastic soil model (Ref 15).

Due to the above treatments, the basic calculation module can be made to follow any desired soil model or constitutive relation. In effect, any postulate on soil behavior can be easily implemented in the CASH analyses.

To accommodate the large displacement effects, the configuration of the single slice of soil mass is continually updated in time by updating the coordinates of each nodal point. The governing equations (described in Section 2.4) are reformulated with respect to the updated geometry at each time step.

In addition to the above, the discrete element model does not assume any form of smooth displacement functions across the boundary between two elements. The only continuity assumption across the boundary of two elements arises from the need to satisfy equilibrium and the continuity of the flow of pore fluid at the nodal points between adjacent elements.

To avoid unnecessary complexity in the mathematical treatments, incremental deformations of an element (strain) are related to displacements at the nodal points by an infinitesimal strain assumption and higher order terms are neglected. However, the coordinate of every node is updated and the governing equations are reformulated in accordance to the new configuration to account for large displacement effects.

2.10 Comparison of the CASH Analysis with Past Researches

Several researchers have attempted to solve for the state of stress and skin friction capacity of piles by cavity expansion solutions (Refs 5, 10, 11, 13, 15-18). The most well-known approach is the effort arising from the ESACC (Effective Stress Axial Pile Capacity Cooperative) project (Refs 10, 11, 13). Several methods for predicting axial pile capacity were developed from the results of that project. All of them incorporate implementations of cavity expansion solutions to various degrees to account for the variation of soil properties and pile installation effects. The cavity expansion solutions from the above mentioned researchers arbitrarily separate pile driving, consolidation and axial shear loading into distinctly different processes. Separate analyses, each employing incompatible assumptions (e.g., soil model and drainage conditions) were conducted to account for pile installation effects. Pile installation is simulated by a radial cavity expansion solution. The stress state and the pore pressure at the end of expansion are then input to a separate program for consolidation analysis. The state of effective stress at the end of consolidation is then used to predict the frictional capacity.

The major improvement that the CASH program has over past solutions lies in its flexibility and coherence in accounting for the pile driving, consolidation and axial shear loading effects. The improvements on the two-phase concept

(pore-fluid and soil-skeleton) as well as the addition of the degree of freedom for axial soil displacement has enabled CASH to mingle the cavity expansion, consolidation and axial shear in any manner. Arbitrary assumptions in various processes, drainage conditions, and other incompatibilities (e.g., in the soil model at various stages) are avoided. In addition, CASH also allows for a more flexible treatment in modelling soil behavior. Various restrictions imposed by most conventional generalized models are avoided by the use of a contrived soil model which at the present development is not general enough to be applied to boundary value problems beyond the one dimensional axi-symmetric pile solutions. However, the contrived soil model provides for flexibility in simulating any physically based stress-strain behavior (e.g., remolding and shear-volume change effects). More specific comments to compare the CASH approach to the previous cavity expansion approach (the above cited references) are given below:

(1) Previous methods account for the pile driving effect by performing cavity expansion solutions using a single-phase soil model. An undrained assumption is used in conjunction with a nonlinear soil model to assess the state of stress and pore pressure caused by pile installation. The two-phase soil model in CASH eliminates the need of the undrained assumption. Dissipation (or redistribution) of pore pressure is accounted for at all times. In addition, axial displacement can be prescribed on the cavity wall simultaneously with the radial expansion to assess the effects of axial shear associated with pile driving (Ref. 15).

(2) In the earlier approach, the state of stress and the pore pressure distribution at the end of the cavity expansion is input to an alternate program to perform the consolidation analysis. In the course of the earlier research efforts, several consolidation solutions were developed, with progressive improvements on the two-phase concept and the constitutive model. The final version is fairly compatible with the one used by CASH in terms of the two phase concept. Dissipation of pore pressure is handled approxi-mately the same by the two approaches. The change of effective stresses during consolidation depends to a large extent on the adopted soil model. The modified Cam Clay model, although more mathematically elegant, is not as flexible as the one in CASH which can accommodate any postulate of soil behavior.

(3) In the earlier approach, the state of effective stress at the end of consolidation is used directly with the effective stress soil model parameters to predict the skin friction capacity. Instead of rigorously simulating the axial shear versus the axial displacement characteristics (t-z curves), as in CASH, the earlier approach postulated various approximate equations to solve for the skin friction capacity which is appropriate only for the specific assumed conditions (e.g., drainage condition and distribution of stresses). Various forms of equations have been postulated making use of the radial effective stress, or the mean normal effective stress, as the stress parameter in the prediction. In addition to the state of stress, various forms of shear strength equations have been postulated. In contrast, the introduction of the degree of freedom for axial displacement in CASH enables us to actually solve for the complete t-z curves (including monotonic or cyclic loading conditions) at any stage of cavity expansion or consolidation.

The above has provided a contrast of the CASH approach versus the approach by previous researchers. Actual solutions from CASH will be presented in later sections. Further comments on the similarities and differences between the CASH solutions and the solutions obtained by previous researchers will be given.

Three series of CASH analyses have been conducted for the Conoco project. The first series of analyses were conducted around December 1983 to backfit the 3-inch pile segment tests. Only a very limited number of analyses were conducted in that series but they provided qualitative explanations to some interesting observations. This series of analyses are summarized in Section 3. The second and the third series of analyses were conducted in March and April of 1985 after the large-scale 30-inch pile test which had undergone 111 days of consolidation. In the second series, some parametric analyses were conducted to evaluate the sensitivity of a few factors. This series of analyses is presented in Section 4. The third series of analyses was conducted to compare against a wider collection of field data (including the 3-inch pile segment tool, X-Probe and 30-inch pile data at both stratum II and stratum III). This series of analyses is presented in Section 5.

3. PRELIMINARY BACKFITTING OF SMALL SCALE SEGMENT TESTS (FIRST SERIES)

3.1 General

The first series of CASH analyses was conducted in December 1983 to backfit the initial series of 3-inch pile segment tests (Ref 9). Emphasis was placed on providing qualitative explanations to observed measurements to improve our knowledge of factors and mechanisms governing side friction behavior of piles. The backfitting analyses reported below are the first set of trial solutions. Further analyses have been performed to provide better matching of experimental data. Furthermore, analyses were performed for only one series of load tests. The following discussion pertains to only the series of tests conducted at hole 1 at a depth of 63.4 m (208 feet). The test data has been fully documented in the Volume III report (Ref 9).

3.2 In Situ Measurements

A detailed report on the field measurements has been presented in the "Final Report on Small Diameter Pile Segment Tests" (Ref 9). Some of the observations that are relevant to the subsequent CASH simulations are briefly summarized below.

Installation and Consolidation Effects. Plate 3.1 summarizes the time histories of pore pressure, total normal stress and effective normal stress measured on the pile wall during consolidation. The estimated initial ambient levels prior to pile driving are also identified in the plate. Pile driving caused an increase in both the total normal stress and pore pressure. However, the effective normal stress decreased during pile driving. During consolidation, both the total stress and the excess pore pressure decreased with time. The effective normal stress, however, increased during consolidation and ultimately rose above the initial ambient level.

Axial Shear Load Tests. Two series of axial pile segment load tests were conducted in Hole 1 at 63.4 m (208 feet) depth: (1) an immediate test shortly after driving, and (2) a series of cyclic two-way tests at the end of approximately 72 hours of consolidation (long term test). The two series of axial load tests caused some change in the pore pressure and the normal stresses (total and effective). However, the permanent change induced by shear loading was relatively small as compared to the general trend of consolidation (see Plate 3.1).

Measured t-z Curves. The measured shear transfer versus pile displacement curves for the two series of axial pile load tests (immediate and long term tests) are presented in Plates 3.2 and 3.3, respectively. For both series of tests, the t-z curves exhibit only very minor strain softening tendencies during initial loading. The cyclic test shown in Plate 3.3 reveals some amount of cyclic degradation effects at the first few cycles of loading. However, the cyclic degradation of shear strength was not very severe.

Stress-Paths. The shear transfer versus effective normal stress for the two series of tests (immediate and long term) are summarized in Plate 3.4. As discussed in the "Report on Small Diameter Pile Segment Tests" (Ref 9), there was a distinct radial effective stress drop associated with the degradation of friction from the first to the second cycle. Subsequent cycling results in a reduction in measured friction with no associated reduction in radial effective pressure. In fact, with continued slippage, there is an increase in radial effective stress concurrent with a slight drop in measured friction. The composite plot of stress paths for the immediate and the long term tests showed that some failure envelopes can be constructed. However, the experimental data

does not support the existence of a unique failure envelope (a unique set of cohesion intercept, c and friction angle, ϕ). Further discussions on this aspect will be given in the following section on CASH simulations.

Pressure Response During Cyclic Shearing. The total radial stress, pore pressure and radial effective stress measured during the immediate test are cross-plotted against the corresponding axial displacement and are shown in Plate 3.2. The corresponding plots for the long term tests are summarized in Plate 3.3. The variations in the total normal stress are relatively small. Larger amplitudes of variations are measured for the pore pressure and the effective stress. After the second cycle of loading, the pore pressure and the effective stress are repetitively cyclic in nature. When plotted against displacement, a figure-eight configuration is shown for both the pore pressure and the effective stress plots. An increase of pore pressure is recorded at the initial stage of loading for both tension and compression loading. The pore pressure decreases after plastic slippage occurs. The effective normal stress responds as a mirror image of the pore pressure. An increase in pore pressure coincides with a decrease in radial effective stress and vice versa as the pore pressure decreases.

Soil Cake Around the Pile. Besides the above field measurements, some observations were made during the field tests that may be of significance to our understanding of pile behavior. One such observation is that after the pile segments have been pulled from the soil, one or more thin layers of clay were found adhered to the pile wall. Similar observations have been reported for laboratory model tests in clay by Bogard and Matlock (Ref 3). It has been postulated that during axial pile loading in marine clays, plastic slippage may not occur on the pile wall, but at a slight distance away. The plane of

slippage has been termed the "shear-zone" by Bogard and Matlock (Ref 3). The physical evidence in the field reinforced the above hypothesis. CASH analyses were performed and are summarized in the next section to investigate the mechanisms resulting in the formation of the shear planes.

3.3 CASH Simulations

The above described phenomena observed during pile installation, consolidation and cyclic axial shear are simulated by a series of CASH solutions. Emphasis is placed not merely on the conventional aspects of shear transfer behavior (t-z curves and side-friction capacities), but also on the mechanisms affecting the side friction behavior of piles. A number of the observations from the field measurements could potentially be important in leading to an understanding of pile behavior and attempts are made in the CASH simulations to at least provide qualitative matches of these observations. They have been described in the previous section and are briefly listed below:

(1) In contrast to most cavity expansion solutions, effective stresses on the pile wall actually diminish during pile driving.

(2) The total normal stress does not remain constant, but diminishes during consolidation.

(3) Layers of clay are found adhering to the pile wall after extraction.

(4) The figure-eight pattern arises when the pore pressure and the effective stress are plotted against the axial displacement under large amplitude cyclic loading conditions.

Two series of CASH solutions were made and are presented in the following section. The first series simulates the pile driving and consolidation processes. The second series simulates the process of cyclic axial pile loading. The selection of the soil and the pore fluid material parameters are partially based on the results of the previously conducted laboratory testing

program (Ref 9). However, it was necessary to adjust some of the parameters in the backfitting process to account for remolding due to pile driving and pile loading effects which were not accounted for in the laboratory program.

Plate 3.5 summarizes the input to the first series of CASH solutions to simulate the pile driving and consolidation effects. Radial displacement is prescribed on the cavity wall between 0 and 10 seconds to simulate the effects of lateral soil displacement caused by driving the tip of the pile past the depth considered. The magnitude of the prescribed radial displacement was chosen such that the increase in total stress matches the field measurement prior to consolidation. Shear volume compaction is expected for the under-consolidated clay. Thus, some amount of shear volume compaction has been prescribed to the soil model during the cavity expansion process. The amount of compaction can be prescribed to match the solution of the other soil models (e.g., the Modified Cam Clay Model). Shear dilation can also be easily prescribed in CASH to simulate other soil conditions (say over consolidated clay). The Cam-Clay Model used by many other researchers may not be appropriate for heavily over consolidated clay conditions.

The computed radial distributions of pore pressure and radial effective stress at the end of the cavity expansion (time = 10 sec) are plotted in Plates 3.6 and 3.7 respectively. The resultant solution from the curve at time of 10 sec does not agree with the field observation at the pile wall. The computed effective stress is higher than the initial ambient level while the field measurement indicates a reduction in effective stress. It can be postulated that a simple cavity expansion may not fully account for the pile driving process. In reality, the soil will experience very large cyclic shearing during pile driving which can remold the soil close to the pile wall.

To provide a better simulation of the axial shearing during pile driving, axial displacement is imposed on the cavity wall between 10 and 30 seconds in the CASH solution as shown in Plate 3.5. To simulate the remolding effects, additional shear volume compaction is prescribed on the soil during the axial shearing process. The analysis performed was not intended to duplicate the actual driving in all details, but to merely provide a means to initiate some remolding effects. The magnitude of axial displacement at the pile wall was varied until the computed effective stress and the pore pressure approximated the field measurement at the beginning of the consolidation process. The radial distribution of pore pressure and effective stress at the end of the pile driving simulation (time = 30 sec) are plotted as the solid lines in Plates 3.6 and 3.7, respectively.

Consolidation Simulation. After the end of the pile driving simulation, the CASH solution was continued up to a time of 72 hours (see Plate 3.5) to allow the pore pressure (which was built up during pile driving) to dissipate. As the pore pressure dissipates back to the ambient level, the soil consolidates, resulting in an increase in shear strength. The CASH solution of pore pressure, effective radial stress and total normal pressure versus the time of consolidation is summarized in Plate 3.8. The radial distributions of pore pressure and radial effective stress at various times of consolidation are presented in Plates 3.9 and 3.10.

Axial Shear Simulation. After consolidation, CASH solutions were continued to provide simulations of the axial pile loading process. Emphasis is placed on providing explanations of the formation of slip planes (shear zone) close to the pile wall and on the response of the pore pressure and effective stress during cyclic loading.

The formation of slip planes away from the pile can be explained by the remolding characteristics of the soft marine clay. The soft clay found at the test site tends to reduce in volume during remolding. During undrained loading (approximating the pile driving condition), the shear induced volume compaction caused an increase in pore pressure and a corresponding decrease in effective stress. During consolidation, the pore pressure dissipates, and the soil skeleton consolidates along some remolded compressibility line (e-p curve) as the effective stress increases. The above process is schematically depicted in Plate 3.11 and has been implemented in the previously discussed pile driving and consolidation simulations. The magnitude of volume reduction differs for each soil element and was assumed to be dependent on the shear strain amplitude. Each soil element consolidates along a different remolded compressibility curve. In addition, the CASH analyses accounted for the difference in the compressibility of the soil between the virgin loading path and the unloading-reloading paths. As a result of the remolding effects (especially the axial shear remolding), the void ratio can vary very abruptly over a small radial distance (within half an inch) away from the pile wall at the end of the consolidation even though the stresses and pore pressure must be fairly uniform due to the need to satisfy equilibrium conditions. The CASH solution for the radial change of volumetric strain (compression is positive) and radial effective stress at the end of consolidation is shown in Plate 3.12. The above described remolding phenomenon has a profound implication on the shear transfer mechanism around the pile as described below.

Shear strength characteristics of soils have conveniently been expressed through the effective stress concepts in terms of the c and ϕ parameters. There has been much speculation by the effective stress theory, that the cohesion (c) indicates the magnitude of the true bonding between particles and ϕ is a true

measure of the frictional components of shear resistance. For the very plastic marine clay, it seems unlikely that the situation is so simple. The increase in shear resistance for an increase in effective stress may very well be due to the corresponding decrease in void ratio, thus increasing the amount of interlocking and bonding between clay platelets. Thus, the parameter ϕ may only be a convenient (but indirect) expression of the shear strength of soil, and the clay may not exhibit true frictional behavior. As a result, the c and ϕ parameters may not be unique for a given soil. The shear resistance offered by bonding between clay platelets may depend on other factors (besides effective stress) such as time and the structure of the clay platelets. The change of void ratio (see Plate 3.12) is an important measure of the structural characteristics of the soil very close to the pile wall. The change in the structure of clay (related to the void ratio change) can be very dramatic very close to the pile wall due to the above discussed remolding effects. Thus, it may be important to reexamine the conventional effective stress concept to accommodate the large remolding effects caused by pile installation. Hvorslev (Ref 12) has found from testing of clay remolded to different water contents (void ratios) that the c and ϕ parameters are indeed not unique for clay, but depend also on the water contents. He proposed that there are different sets of c and ϕ for different water contents. The above idea was implemented into the CASH program and was found to provide a reasonable explanation of the observed formation of the shear zone. In the CASH analyses for cyclic axial shear loading, the following failure criterion is used.

$$\text{Axial Shear Strength} = c_1 + c_2 \bar{\sigma}_m + c_3 \varepsilon_v \qquad (16)$$

where

c_1, c_2 and c_3 are material parameters, $\bar{\sigma}_m$ is the mean normal effective stress and ε_v is the volumetric strain (related to the change of void ratio).

Besides the shear strength and shear stiffness characteristics discussed above, the shear-volume change behavior needs to be prescribed for the cyclic axial shear analysis. Understanding of the shear-volume change of the soil under cyclic loading was found to be important in explaining the figure-eight behavior of the measured pore pressure and effective stress during cyclic loading (see Plate 3.3). An algorithm for cyclic shear-volume change was implemented in CASH and is shown schematically in Plate 3.13. The shear straining of the soil initially causes a reduction in the volume of the soil skeleton. As the shear strain approaches the plastic slippage, the soil skeleton dilates up to a certain value. No further volume change occurs as shear strain continues to increase far beyond plastic slippage. Upon reverse loading, the above shear volume change characteristic simply repeats itself by initially compacting in volume, then followed by some dilation behavior. The above is consistent with the concept that soil behavior should show no preference to the direction of shear. The shear-volume change during positive shear should be the same as that during negative shear.

The above described soil behavior, that is, (1) remolding effects on shear strength and (2) cyclic shear-volume change, were implemented in a series of CASH simulations of cyclic axial shear loading. The problem is described in Plate 3.14. At the end of the consolidation (after 72 hours), cyclic axial displacement is prescribed on the cavity wall. This series of solutions is sequential to the previously described pile driving and consolidation solutions. The radial geometry, the three components of normal stresses and the pore pressure at the end of the consolidation were retained for each element. However, the axial displacement and the axial shear stress were reinitialized to zero. This reinitialization merely reflects a datum shift and does not represent actual soil movements.

The resultant t-z curve from the CASH solution is presented in Plate 3.15. The radial distribution of the axial displacement at the time instant A is presented in Plate 3.16. Plastic slippage was found to occur at about 0.1 inch away from the wall of the 3-inch diameter pile. The soil elements immediately adjacent to the pile wall in effect have a higher shear strength due to remolding and consolidation, thus causing slippage to occur some distance away from the pile.

It can further be postulated that once the slip plane is initiated, the concentration of shear strain on this plane will likely focus continuing remolding effects to occur on the slip plane under cyclic loading conditions. After one series of load tests, when pore pressure is allowed to dissipate, the remolded soil will then consolidate in the immediate vicinity of the slip plane, resulting in additional increase in shear strength. When a subsequent series of pile load tests is conducted, the weak link where slippage initiates will then occur at some small distance away from the previous slip plane. When a number of series of tests are conducted with consolidation allowed in between tests, a few layers of soil can form around the pile as a result of the successive remolding and consolidation processes. The above was physically observed from the 3-inch segment tests. The number of soil cake layers correlated well with the number of series of load tests during consolidation. Implementation of Hvorslev's concept of a non-unique failure criterion to account for the remolded shear strength was needed to create the slip plane away from the pile wall. Otherwise, failure will always occur on the pile wall-soil interface which is the point of maximum shear stress. A unique failure criterion in the Cam Clay Model so far has predicted that failure always occurs on the pile-soil interface (Ref 17).

The response of pore pressure, effective stress and total pressure were also cross-plotted against the axial displacement and presented in Plates 3.17, 3.18 and 3.19, respectively. Through the interpretation of the above CASH solution, the figure-eight response of pore pressure and effective stress revealed the following points which may be valuable for understanding of shear transfer behavior of piles.

(1) A large component of the figure-eight phenomenon can be explained by the shear-volume behavior of soil. Under undrained condition, the shear-volume change tendency of soil will result in an opposite response between pore pressure and effective stress. If an increase (decrease) in pore pressure is compensated by a corresponding decrease (increase) in effective stress, the total stress in the element will be unchanged. If the above behavior occurs on all the elements, the global equilibrium is unaffected and the total normal stress on the pile wall will remain constant during cyclic shear loading. However if some of the shear volume compaction is not just merely cyclic but permanent in nature, then the induced pore pressure will dissipate in time resulting in some reduction in total stress on the pile wall. Such reduction in total stress will merely be a function of consolidation time and will not depend on the direction of shearing.

(2) There is a subtle message from the figure-eight phenomenon. The mirror image response between pore pressure and effective stress strongly suggests that the figure-eight phenomenon is related to the shear-volume behavior of soil. Since soil should show no preference in the direction of loading (positive versus negative shear), the t-z characteristics should in turn be similar between compressive and uplift pile loading. However, other factors (e.g. pile top or pile tip end effects) may result in differences between compressive and uplift shear behavior near the boundaries. Such end effects are expected to be insignificant in the design of a long offshore pile. Simulation of the figure-eight phenomenon requires extension of the soil model to account for shear-volume change effects for cyclic loading situations. Most current soil models (including the Modified Cam-Clay Model) cannot account for such cyclic phenomena. The ability to simulate the figure-eight behavior illustrates the flexibility of the contrived soil model model to accommodate any desired postulate of soil behavior in pile loading analyses.

4. SENSITIVITY STUDY OF VARIOUS PARAMETERS

4.1 General

The second phase of backfitting analyses were conducted in March and April 1985. At that time, the processing of the 30-inch field pile load test data (Ref. 8) was essentially complete (except the retest). An abundance of data has been collected for the 3-inch pile segment, the X-Probe and the 30-inch pile. Emphasis is being placed on providing a reasonable fit to a wide range of conditions (different depths and various types of data). The objective of this phase of analyses is to develop a better basis for design. CASH analyses were conducted for two soil strata: (Stratum II at the 45-meter or 148-foot depth and Stratum III at the 63-meter or 208-foot depth). Using one consistent set of soil parameters, analyses were conducted to simulate the 3-inch pile segment, the X-Probe and the 30-inch pile condition. Prior to the actual backfitting of the field data, a series of parametric studies was conducted to develop a feel for the sensitivity of various factors. The sensitivity analyses are summarized below.

4.2 Problem Description

The input parameters for a benchmark case was first established. Then, the input parameters were varied to evaluate the following factors:

(1) The effects of various cavity expansions

(2) The effects of different shear strength of soil

(3) The effects of different soil stiffness

(4) The effects of pile diameter

Soil Model. The soil model used for the second series (sensitivity) and the third series (backfitting) analyses is simpler than the one used in the first series of preliminary backfitting analyses. The parameters in this soil model

can readily be measured in conventional laboratory test programs. The basic features of the soil model are schematically presented in Figure 2.5. The volumetric behavior is nonlinear and inelastic for the virgin curve. The unloading and reloading behavior is assumed to be linearly elastic.

In addition to the above, the shear volume change is also considered. The prescribed shear-volume change behavior is assumed to be dependent only on the octahedral strain, γ_{oct} (see Plate 4.1) and thus can account for only monotonic loading behavior. The shear volume change under cyclic loading (e.g. resulting in the figure-eight phenomenon discussed in section 3) is not activated. This simplification was chosen for a more stable CASH solution. The observed figure-eight behavior although very definite (it can be seen in numerous sets of data), is not very pronounced in magnitude (the cyclic component of pore pressure is small as compared to the static component). Therefore, the above simplification should not result in unacceptable error for the current soil condition. The magnitude of shear volume change is obtained by backfitting analyses such that the pore pressure generated after cavity expansion approximates the pore pressure measured by the 3-inch pile segment after installation. The deviatoric model is schematically shown in Plate 4.2. The shear behavior is nonlinear and hysteretic. The undrained shear strength (τ_{max}) and the small strain modulus (G_{max}) are both assumed to be linearly proportional to the mean confining stress. The benchmark input parameters for the deviatoric model is summarized below:

	Stratum I (80 ft - 160 ft)	Stratum II (160 ft - 240 ft)
Shear strength parameter, C_2 in Eq. 16	0.38	0.38
Shear stiffness parameter, G_1, where $G_{max} = G_1 \bar{\sigma}_m$	60	600

The above shear strength parameter is based directly on the direct simple shear test results (Ref. 6). The small strain shear modulus parameter (G_1) is based on backfitting the 3-inch pile data. The resultant values of C_1 and G_1 are consistent with what is commonly assumed in conventional practice. Other relevant input parameters and the problem description in the sensitivity study is summarized in Plate 4.3. In the sensitivity study, the pile driving effect is simulated by a simple cavity expansion. The initial radius of the cavity in the CASH model and the amount of expansion is varied in different analyses such that the final interior cavity radius (after expansion) is equal to the pile radius. After the cavity expansion, radial consolidation continues to 2800 hours. The consolidation time of 2800 hours is long enough to approximate the ultimate consolidated condition. Then axial shear displacement is prescribed at the pile wall to solve for the t-z backbone curve.

4.3 Discussion of CASH Solution

A total of 6 cases were considered in the sensitivity study. The solutions are summarized in Table 4.1. The benchmark case correspond to the soil condition at the 45 m (148 ft) depth (Stratum II). The CASH solution for the state of stress at the end of cavity expansion and at the end of consolidaton is presented. The ultimate skin friction f during axial shear and the ratio β of skin friction to the radial effective stress at the beginning of axial shear is also tabulated. Some of the important findings are summarized below.

Consolidation Time. Curves are presented in Plate 4.4 for the normalized pore pressure at the pile wall (normalized with respect to the maximum value immediately after expansion) versus normalized consolidation time (time divided by the square of the pile radius). It can be seen that the consolidation time does not merely depend on the pile diameter.

A comparison among Runs 1, 2 and 3 reveals that the consolidation curve also depends on the amount of expansion which is probably related to the pile wall thickness. The amount of 3.2 cm (1.25 inch) cavity expansion in Run 2 represents essentially a closed-end pile situation. The pore pressure for a bigger cavity expansion extends to a larger radial distance. Therefore a longer consolidation time is needed to reach a certain degree of consolidation. The above phenomenon is supported by a comparison between the 3-inch and the 30-inch pile data and is also in general agreement with some of our other test data (Ref 7). Other factors such as shear strength and stiffness may affect the magnitude of pore pressure on the pile wall, but showed minor effects in consolidation time. The dependence of consolidation time on wall thickness was not observed by past researchers.

Amount of Cavity Expansion. The solution of the incremental (change over the in situ condition) total and radial effective stress at the end of cavity expansion and after consolidation is presented in Plate 4.5. It may be seen that the radial effective stress changes abruptly at a small amount of cavity expansion. After some amount of cavity expansion, a further increment of cavity expansion induces only small changes in the radial effective stress. This phenomenon suggests that the radial effective stress can be significantly different for small variation of wall thicknesses for a thin-wall open-ended pile. In addition to the above observation in the magnitude of radial effective stress, it may be seen (Table 4.1) that the ultimate unit skin friction (f) does not vary significantly even though the radial effective stress after consolidation is significantly higher for Run 3 (3.2 cm or 1.25 inch expansion). The β coefficient appears to decrease for a bigger cavity expansion. The above is supported by a comparison between the X-Probe data and the open-ended pile data

(for both the 3-inch Probe and the 30-inch pile). These CASH analyses assumed that the undrained shear strength depends on the mean effective stress rather than on the radial effective stress. In the vicinity of the pile wall, both the mean effective stress and the induced shear stress tend to increase (for a bigger cavity expansion) during consolidation. Proper consideration of axial shear resistance at the end of consolidation requires accounting for the increase in shear strength due to the increase of confinement as well as the increase in shear stress in the soil. The earlier cavity expansion approaches consider only the variation of the radial or the mean effective stress and are not expected to be adequate. Furthermore, such solutions assume that the amount of cavity expansion is large enough to achieve the ultimate plastic condition. Therefore the state of stress at the end of consolidation becomes totally dependent on the shear strength and will be unique for a given soil. The ultimate radial effective stress measured by the open-ended pile (3-inch segment and the large scale pile) was found to be very different from that measured by the X-Probe (see Table 5.1 and discussed further). This suggests that the appropriate amount of expansion for an open-ended offshore pile is insufficient to achieve the ultimate effective stress level. For most open-ended offshore piles, the effective stress level will be very sensitive to the amount of expansion which depends on the flow pattern of soil at the pile tip.

Soil Shear Strength. The solution from Runs 1 and 4 can be compared to evaluate the sensitivity of the shear strength characteristics of soil. The shear strength parameter (C_1 of 0.38 was based on a friction angle of 21 degrees from direct simple shear tests (see Ref 6). A C_1 of 0.64 (used in Run 4) was based on a friction angle of 25 degrees from triaxial tests (see Ref 6). The ratio of the ultimate unit skin friction between Run 1 and Run 4 was found to

be roughly proportional to the shear strength parameter C_1 which is a direct measure of the undrained shear strength of the soil. The pore pressure generated during cavity expansion and the effective stress at the end of consolidation were found to be dependent on the shear strength of the soil. This is consistent with the findings by other researchers.

Soil Modulus. The solution from Runs 1 and 5 can be compared to evaluate the implication of the modulus characteristics of soil. In general, a higher value in the radial effective stress results from a stiffer shear modulus. In addition to the above, the incremental total stress appears to remain at an approximately constant level during consolidation for most of the runs except for Run 5 which has a significantly higher shear modulus. The incremental total radial stress decreases from 0.7 MPa to 0.37 MPa (14.8 ksf to 7.8 ksf) during consolidation. A significant decrease in the total radial stress during consolidation was observed in the X-Probe tests at all depths and in the open-ended pile tests at stratum III, supporting the fact that the total radial stress can vary during consolidation of soil around a pile. A stiffer shear modulus appears to cause a bigger reduction in total radial stress during consolidation. Such a phenomenon is very different from conventional consolidation of soil under a footing where the static loading does not change.

Diameter Effects. A comparison between Run 1 and 6 indicates that so long as all the dimensions (e.g. wall thickness) are strictly directly proportional to pile diameter, the CASH solution in all aspects (pore pressure, effective stresses, and t-z curves normalized by diameter) would be strictly identical at any stage of consolidation. The consolidation time would be strictly proportional to the inverse of the square of the pile diameter.

When the above sensitivity study is tested against the field data, the CASH solutions were found to provide for a reasonable match to the field data qualitatively in two aspects: (1) dependence of consolidation on wall thickness and (2) a lower β coefficient for the X-Probe. The biggest uncertainty arises from the complexity introduced during pile driving and the uncertainty on the effective amount of expansion which in turn must be related to the flow pattern at the pile tip. Another key observation can be made from the above sensitivity study. The long term skin friction capacity for static loading has been the most important parameter in the design of a long offshore pile. The variation of the long term skin friction capacity is surprisingly small except in Run 4 which has a significantly higher shear strength value. Even though there is a wide scatter in the solution of pore pressure and effective stresses caused by the cavity expansion effect, the frictional capacity for static loading tends to converge to some stable value for a given set of shear strength parameters. The above observation supports the conventional belief that rational design of an offshore pile could be independent of the choice of the procedure (total stress or effective stres approach) so long as the "proper shear strength" has been used.

Table 4.1. Summary of Sensitivity Study

Run	Description	Solution After Expansion			Solution at End of Consolidation			
		σ_r' (ksf)	Δp (ksf)	$\Delta\sigma_r$ (Total) (ksf)	σ_r' (ksf)	$\Delta\sigma_r$ (Total) (ksf)	f (ksf)	$\beta = \frac{f}{\sigma_r'}$
1	Bench Mark	0.64	1.17	0.61	1.74	0.57	0.50	0.29
2	Radial expansion increased to 1.25"	0.55	1.92	1.27	1.90	1.21	0.50	0.26
3	Radial expansion decreased to 0.02"	0.89	0.71	0.40	1.58	0.39	0.49	0.31
4	Shear strength increased to C_1 = 0.64	0.73	1.77	1.30	2.31	1.16	0.87	0.38
5	Shear modulus increased to G_1 = 600	0.74	2.17	1.71	2.06	0.92	0.45	0.22
6	Pile radius increased to 15"	0.62	1.19	0.61	1.74	0.57	0.50	0.29

Bench Mark Parameters:

(1) Pile radius = 1.5 in
(2) Radial expansion = 0.0625 in
(3) Shear strength parameter C_1 = 0.38 where $\tau = C_1 * \sigma_m'$ (see Eq. 13)
(4) Shear modulus parameter G_1 = 60 where $G_{max} = G_1 * \sigma_m'$
(5) 1 inch = 2.54 cm
(6) 1 ksf = 0.0479 MPa

5. BACKFITTING SMALL AND LARGE SCALE TESTS

5.1 General

A third series of CASH analyses were conducted to backfit a wider collection of field tests including (a) solutions for the 3-inch pile segment, the X-Probe and the 30-inch pile tests at the 148 feet depth (Stratum II soil) and (b) solutions for the 3-inch pile segment and the 30-inch pile tests at the 63.4 m (208 feet) depth (Stratum III soil).

The CONOCO project yielded an abundance of data from the 3-inch segment tool, the x-probe, and the 30-inch large scale pile. It is of interest to compare the CASH solution to all the above data to evaluate the validity of the analytical procedure. However, numerous CASH solutions are required to provide direct comparison with all the test data to match the proper depth, consolidation time, and loading sequences. Therefore, selected sets of field data were used to provide direct comparison with the CASH solution at different consolidation times. The following sets of data were thought to be representative of the appropriate design condition and are compared to the CASH solutions.

(1) The probe 4 test data collected during the test series conducted during December 1982 was used to compare against the 3-inch pile simulation at both the 45 m (148 feet) and the 63.4 m (208 feet) depth.

(2) The X-Probe test data collected during the test series conducted during December 1983 was used to compare against the X-Probe pile simulation at 45 m (148 feet) depth.

(3) The 30-inch large scale pile test data collected during December 1983 was used. Interpolation between the measured data points was made to obtain the comparison against the CASH solutions.

5.2 Problem Description

Amount of Expansion. The following table summarizes the dimensions (diameter and wall thicknesses) for the 3-inch segment, the X-Probe and the 30-inch pile.

Type	Radius	Wall Thickness	w.t./Radius
30-inch pile	15 in (38 cm)	0.75 in (1.9 cm)	0.05
3-inch segment	1.5 in (3.8 cm)	0.125 in (0.32 cm)	0.083
X-Probe	0.86 in (2.2 cm)	Fully Plugged	1.0

In the absence of a more definitive study the amount of expansion for the 30-inch pile, the 3-inch segment and the X-Probe was assumed to be 0.375, 0.0625 and 0.7 inches respectively at both 148 feet and 208 feet depth. The amount of expansion is half of the wall thickness for the 3-inch segment and the 30-inch pile(both open-ended). A fully plugged condition cannot be analyzed because the zero initial radius would cause numerical difficulties. The amount of expansion assumed for the X-probe was thought to be sufficiently large.

The sensitivity study in Section 4 indicates that the increase in total stress from expansion of half of the wall thickness approximately matches the 3-inch segment data. The above rule of thumb could not account for some of the details (e.g. the configuration of the cutting shoe). The half wall thickness was adopted here for simplicity although a case-by-case fitting analysis would lead to a better match of the CASH solution to the field data.

In all the analyses, the cavity expansion occurs between 0 to 10 seconds. The condition is essentially undrained during cavity expansion.

Axial Shear and Consolidation. Following the cavity expansion, consolidation and axial shear were solved by CASH. Only a quarter cycle of axial shear to full plastic slippage was prescribed at each sequence of axial shearing. The resultant t-z curve represents the initial loading path. Cyclic loading was not attempted.

The extent of cyclic degradation was not very severe for the soil condition encountered in this project except at greater depth (the Stratum III soil).

It would be more fruitful to account for cyclic degradation by the discrete sub-element model in the DRIVE program. Further development in constitutive modeling is needed to reliably account for cyclic degradation effect in the CASH type of approach. The physical evidence in the field strongly supports the presence of a slip plane. Under cyclic loading conditions, concentration of shear strain will likely focus continuing degradation on the slip plane. Therefore understanding the slip plane phenomenon will be essential to expand current analytical efforts to cyclic loading situations. The present concepts of constitutive models rely heavily on concepts of continuous solids. If the appropriate developments were made to accommodate the remolding concept, continuum solutions can solve for the position and how the slip plane is initiated. However, the continuum concept may be too restrictive to track the discontinuous slippage on the shear plane under cyclic loading conditions. Incorporation of some discontinuous element may be needed to fully account for the cyclic degradation plenomenon. Present understanding of clay structure probably would support only an empirical description of the cyclic degradation behavior.

The sequence of consolidation and axial shear analyzed by CASH in the back-fitting analysis is summarized below.

30-inch Pile at Both Depths

(1) Immediate test after cavity expansion (pile driving).

(2) Long term test after 2700 hours consolidation which is very close to the actual consolidation time in the field.

3-inch Segment at 148 ft.

(1) First stage test after 8-hour consolidation.

(2) Second stage test after 20-hour consolidation.

(3) Third stage test after 44-hour consolidation.

3-inch Segment at 208 ft.

(1) First stage test after 8-hour consolidation.

(2) Second stage test after 16 hour consolidation.

X-Probe at 148 ft.

(1) First stage test after 1-hour consolidation.

(2) Second stage test after 25-hour consolidation.

5.3 Discussion of CASH Solutions

A total of five CASH analyses were conducted consisting of four solutions for the 30-inch pile and the 3-inch segment at both depths of 45 m (148 ft) and 63.4 m (208 ft). An additional analysis was conducted for the X-Probe at the 45 m (148 feet) depth. Plates 5.1 through 5.5 summarize the histories of total radial stress, pore fluid pressure, and effect radial stress on the pile wall for the five CASH analyses. The shear transfer versus axial displacement curves at various stages of axial loading is presented in Plates 5.6 through 5.10.

A comparison between the CASH solutions and the field data are also presented in Table 5.1 and Table 5.2, respectively. The following general comments can be made regarding the comparison.

(1) Although the CASH solution accounted for a slight but definite reduction of the β coefficient (ratio of maximum skin friction to radial effective stress) for the X-Probe, the solution under-predicts the normal total and effective stress significantly. Further development of the constitutive model is needed to account for the major direction change from severe normal loading to axial shearing. Current knowledge on the effect of change in direction of loading on soil behavior is very limited.

(2) The solution of time histories of total stress, pore fluid, pressure and effective stress reasonably accounted for the field measurements in many aspects including (1) the dependence of consolidation on both pile radius and wall thickness; (2) the CASH solution accounting for the change in both total and effective radial stress.

Table 5.1. Comparison of CASH Solution to Field Data at 148 Feet

Test Type	Load Stage	σ_r' (ksf)		f (ksf)		β	
		CASH	Experiment	CASH	Experiment	CASH	Experiment
3-Inch Segment	8-hr. test	1.29	1.16	0.4	0.34	0.31	0.29
	20-hr. test	1.47	1.10	0.47	0.39	0.32	0.35
	44-hr. test	1.58	1.30	0.52	0.3	0.33	0.23
30-Inch Pile	Immediate	1.76	1.10	0.20	0.22	0.26	0.22
	2700-hr. test	1.50	1.66	0.50	0.50	0.33	0.29
X-Probe	1-hr. test	0.71	2.75	0.16	0.51	0.23	0.19
	25-hr. test	1.27	4.36	0.39	0.77	0.31	0.18

Notes:

(1) σ_r' is the radial effective stress on the pile wall prior to axial shear
(2) f is the peak value in the initial cycle of axial shear
(3) β is the ratio of f to σ_r'
(4) The 3-inch segment data is obtained using Probe 4 in 1982.
(5) The 30-inch pile data is interpolated from the field data in 1983.
(6) The X-Probe data was recorded in 1983.
(7) 1 ksf = 0.0479 MPa

6. FURTHER EVALUATION OF CASH AND OTHER DESIGN PROCEDURES

6.1 General

In the previous sections (Section 3 and 5), detailed CASH solutions of pore pressure, radial effective stress as well as initial t-z curves at various stages of consolidation have been compared to specific sets of field data. The Conoco project has yielded an abundance of high quality test data especially for the 3-inch pile segment tests. This section summarizes the most important measurements (the long term radial effective stress and maximum skin friction at the initial cycle of loading) from all the tests. Then, the CASH solutions are compared to all of the relevant test data. In addition to the above, solutions were obtained from other design procedures (e.g., the A.P.I. recommendation (Ref.1) and the effective stress method (Refs. 4, 5, 17 and 19). Their predictions, along with our CASH solutions, are compared to the Conoco test data.

6.2 Three-Inch Segment Test Data

All the available 3-inch segment tests at 45 m (148 feet) and 63.4 m (208 feet) depth are listed in Table 6.1 and Table 6.2, respectively. The key information from each test has been summarized in the table. The peak skin friction values measured during the initial cycle of loading are plotted and compared to the CASH solution in Plate 6.1. The data point from Test No. 6 was not plotted because the consolidation time is too short to approximate the ultimate long term condition. The CASH solution of the maximum skin friction value is also indicated in the plate. It could be noted that the CASH solution falls within the range of scatter of the field data at both depths.

6.3 30-Inch Large Scale Test Data

This section provides further comparison of the CASH solutions to the 30-inch large scale pile data. Furthermore, the long-term skin friction capacity is computed using the effective stress procedure (Ref 17) and the A.P.I. recommendation (Ref 1) at 45 m (148 feet) and 63.4 (208 feet) depth. They are also compared to the large scale pile data along with the CASH solution.

The measured pore water pressures and total radial pressures immediate after pile driving are presented in Plate 6.2. The CASH solutions (same solutions as those in Section 5) of the pore pressure and total radial pressure at the 45 and 63.4 m (148 and 208-foot) depths are shown in the plate. The CASH solution under-predicts the pore pressure and the total radial pressure at the 45 m (148 feet) depth. The prediction is quite good at 63.4 m (208 feet) depth.

The profiles of pore pressure, total radial stress, and radial effective stress measured after 111 days of consolidation are presented in Plate 6.3. The CASH solutions (same solutions as those in Section 5) are also presented in the figure. The CASH solutions were in general agreement with the field data.

The maximum skin friction at the initial cycle of loading obtained from the field test of the 30-inch pile are presented in Plate 6.4. Two curves are presented: (1) the one obtained immediately after pile driving, and (2) the one obtained after about 111 days of consolidation. The measured maximum skin friction profile is plotted as step functions with respect to depth since the field data provided information on only the average shear transfer value in between two strain modules. In reality the shear transfer versus depth would

be a continuous curve instead of a step function. The interpreted shear strength profile (Ref 6) is also plotted on the figure for cross reference.

The CASH solutions of the peak skin friction capacities at 148 feet and 208 feet depth (presented in Section 5) are further summarized in the figure. In addition to the CASH solutions, skin friction capacities are further computed using the A.P.I. procedure (Ref 1) and the effective stress method (Ref 17). In the A.P.I. approach, multiplication factors (α) of 0.09 and 0.61 were applied on the undrained shear strength of 0.033 and 0.062 MPa (0.7 and 1.29 ksf), at 45 m (148 feet) and 63.4 m (209 feet) depth, respectively. In the effective stress method (Ref. 17), Randolph et al., traced through the history of radial effective stress throughout the cavity expansion and consolidation processes. The state of effective stress at the end of consolidation is used to assess the equivalent undrained shear strength value for pile design. The value of the ultimate undrained shear strength for a normally consolidated clay was found to be about 1.51 times the initial undrained shear strength before pile driving. The shear transfer calculated by this method are 0.051 and 0.093 MPa (1.06 and 1.95 ksf) at 45 and 63.4 m (148 and 208-foot) depth, respectively. Later researchers of the effective stress method lowered the skin friction prediction by a factor of about 0.23 by various arguments (Ref 13). The skin friction capacity predicted by the effective stress method after the above adjustments are 0.039 and 0.072 MPa (0.82 and 1.5 ksf), respectively.

Plate 6.4 can be examined to evaluate the validity of various approaches. The effective stress method (Ref 17 and 13) grossly overpredicted the skin friction capacity of the Conoco pile. The A.P.I. approach yielded reasonable predictions at the shallower depth (e.g. at 45 m or 148 feet), but tends to

underpredict the pile capacity at deeper depth. The CASH solution yielded reasonable solutions especially at the deeper depth. It also accounted for the increase in pile capacity versus consolidation time. It is noteworthy to mention that the interpreted shear strength profile which does not consider any pile driving (cavity expansion) and consolidation effects approximated the long term skin friction profile reasonably well. The skin friction capacity may approach even closer to the undrained shear strength profile for a longer consolidation time. The above discussion relates to design for static loading conditions only. The field data indicates that the skin friction capacity degrades under cyclic loading condition and our design procedure should accommodate this aspect.

7. SUMMARY, CONCLUSIONS AND RECOMMENDATIONS

7.1 Summary

A computer program CASH has been utilized to interpret sample results from the Conoco tests. This program has been designed to provide improved t-z characterization (such as side-friction capacity and soil stiffness) as input to an overall soil-pile interaction analysis that might be done with the DRIVE program (Ref 14). CASH takes the following factors into account in the development of the t-z curves:

(1) In-situ soil condition.

(2) The effects of pile driving.

(3) The effects of consolidation of soil mass after pile driving.

(4) The effects of subsequent static and cyclic axial shear loading.

Program CASH models a single horizontal slice of soil layer surrounding an imaginary cylindrical cavity at a specific depth. The effects of displacement of soil during pile driving is accounted for by the radial expansion of the cylindrical cavity. The vertical movement of the surrounding soil during pile driving can also be simulated by prescribing vertical soil displacement on the cavity wall. This feature (vertical soil displacement) can further be used to solve for the t-z characteristics at any stages of consolidation. The major features of the program CASH are listed below:

(1) A general two-phase soil model to account for the state of effective stress and pore water pressure throughout the pile driving, consolidation and pile loading processes.

(2) Large displacement capability.

(3) A flexible framework to incorporate any postulate (e.g., nonlinear failure and shear volume change effects) of stress-strain behavior of soil in the assessments of t-z characteristics.

One major advantage of the CASH program over some of the earlier developments (Refs 4, 5, 10, 11, 13, 16-19) lies in the flexibility of the program in the treatment of stress-strain behavior of soil. CASH is not restricted by current knowledge on constitutive modeling techniques. Any postulate on the physical behavior of soil can easily be implemented into the CASH analysis. Another major advantage in CASH is its flexibility to co-mingle any of the three loading processes: (1) cavity expansion, (2) consolidation, and (3) axial shear loading. By so doing, many of the incompatibilities between stages of solution and the associated arbitrary assumptions that were inherent in the earlier development efforts have been circumvented.

Description of the theory behind CASH has been given in Section 2 of the report. Three series of analyses have been conducted in the course of the Conoco project. The first series of CASH analyses was performed to backfit only one series of 3-inch pile segment test (Probe 1 test conducted in December 1982). Emphasis was placed on providing qualitative explanations to the field observation and measurements at that time. In this first series of analysis, CASH has been found to have the potential to account for the t-z behavior and the variation of normal stresses (total and effective) on the pile wall at various stages (immediately after driving, consolidation and cyclic pile loading). The CASH solutions have provided interesting explanations on the formation of slip planes around the pile and the pore pressure and normal stress responses during cyclic pile loading conditions. This series of analysis have been discussed in Section 3.

After the initial confirmation of the CASH approach, a second series of sensitivity analyses were conducted in March, 1985 to investigate the effects of varying various parameters, including the following:

(1) Amount of cavity expansion.

(2) Shear strength of soil.

(3) Shear stiffness of soil.

(4) Pile diameter.

This series of parametric studies are documented in Section 4.

A third series of CASH solutions was also performed to compare the CASH solutions to a wider sampling of field tests in Section 5. In this series of analyses, CASH solutions were obtained and compared to the 3-inch segment, the X-Probe and the 30-inch large scale pile tests at both 45 and 63.4 m (148 and 208-foot) depths. One-to-one comparison at various consolidation times were attempted for all the above sets of tests. After making the comparisons further evaluation of the various commonly used skin-friction predicted methods (the A.P.I. recommendation, the effective stress method (Refs 17, 11) and the CASH solutions) were made in Section 6. In Section 6, the CASH solutions for the most important design parameter, long-term skin friction capacity, were compared to samples of the available Conoco data, along with the solutions by the various predictive methods. A brief summary, along with conclusions and recommendations are presented in this section.

7.2 Conclusions

The CASH analyses conducted so far, although can not account for all the field measurements in all quantitative details, did provide a reasonable explanation account of many of the phenomena observed in the field. The CASH analyses have provided a reasonable approximation for the t-z curves (capacity and stiffness) as well as the pore water pressure and effective stress responses

observed immediately after pile driving consolidation and cyclic axial shear loading. On the basis of the CASH solutions, the following interpretation can be made:

(1) The state of effective stress after consolidation is very sensitive to the initial amounts of cavity expansion. After some threshold, further amounts of expansion will lead to insignificant changes in the ultimate effective stress. On the basis of the available Conoco data, the amount of cavity expansion for an open-ended thin wall pile is small in comparison with this threshold level and is expected to be related to the wall thickness of the pile. Therefore the state of stress will be very sensitive to the wall thickness.

(2) In addition to controlling the state of stress, the time of consolidation was also found to be dependent on the wall thickness, a thicker wall pile could create a larger zone of disturbance and thus lead to a longer time of consolidation.

(3) One major conclusion from the parametric study is that the skin friction capacity at the end of consolidation depends on not just one component of stress (such as the radial effective stress or the mean effective stress) as suggested by previous researchers (Refs 5, 10, 11, 13, 17 and 19). The long term skin friction capacity from the cavity expansion method, depends on the complete state of stress in the soil adjacent to the pile. Furthermore, even though there is a wide scatter in the solution of pore pressure and effective stresses caused by the cavity expansion effect, the ultimate frictional capacity tends to converge to some value. The ultimate frictional capacity depends largely on the shear strength characteristics. This supports the conventional belief that rational design of an offshore pile for static loading could be independent of the choice of the analytical procedures (total or effective stress approach), so long as the "proper shear strength" has been incorporated.

(4) The formation of a slip plane at a small distance away from the pile wall was supported by the physical evidence in the field. This has been related to the remolding characteristics of soil from the CASH analyses. The implication of the existence of the slip plane suggests that further cyclic loading will focus further degradation on the slip plane. Therefore, understanding the behavior of the slip plane will hold the key to future understanding of cyclic degradation phenomena.

(5) The response of the normal stresses under cyclic loading support the fact that the skin friction of a long pile is independent of the loading direction (tension versus compression).

(6) The total radial stress does not remain constant during consolidation, especially for a stiffer soil.

7.3 Recommendations

The following areas of research are proposed to further advance our understanding of skin-frction behavior of long offshore piles:

(1) Further testing programs and backfitting analyses to evaluate the flow pattern of soil at the pile tip to establish the effective amount of the laterally compressed and sheared zone around the pile.

(2) Basic research on constitutive behavior of soil is needed to investigate (1) the effects of major change in the direction of plastic shear on soil, and (2) cyclic degradation phenomena, especially the aspect related to discontinuous modeling of the slip plane. Furthermore, implementation of concepts of remolding, cyclic shear volume change characteristics are also needed.

(3) The CASH solution has been found to yield reasonable solutions for open-ended piles in soft clay. Further analyses and testing programs are needed for different conditions including (a) applications to closed-end piles, and (b) other soil conditions.

(4) The pile load test data along with the CASH interpretation confirmed that conventional design practice such as the API procedure provided good solutions for the static long term skin friction pile capacity for the highly plastic marine soft clay soil condition. However, it is necessary to properly account for the degradation effects under cyclic loading conditions. At the present time, it could be more practical to account for cyclic degradation effects empirically using the available test data.

(5) The cavity expansion type analytical approach, when properly formulated, can provide reasonable solutions of the static long term skin friction capacity of a pile. However, any arbitrary assumptions would likely introduce significant error in the solution. It is necessary to account for the complete state of stress in the soil element adjacent to the pile wall to yield reasonable pile solutions.

REFERENCES

(1) American Petroleum Institute, "API Recommended Practice for Planning, Designing and Constructing Fixed Offshore Platforms," API-RP2A, Fifteenth Edition, October 22, 1984.

(2) Bjerrum, L., "Theoretical and Experimental Investigations on the Shear Strength of Soils," Norwegian Geotechnical Institute Publication No. 5, Oslo, 1954, 113 pp.

(3) Bogard, D., and Matlock, H., "A Model Study of Axially Loaded Pile Segments, Including Pore Pressure Measurements," Report to the American Petroleum Institute, University of Texas, May, 1979.

(4) Carter, J. P., J. R. Booker and J. C. Small, "The Analysis of Finite Elasto-Plastic Consolidation," International Journal for Numerical and Analytical Methods in Geomechanics, Volume 3, No. 2, April-June 1979.

(5) Carter, J. P., M. F. Randolph, and C. P. Wroth, "Stress and Pore Pressure Changes in Clay during and after the Expansion of a Cylindrical Cavity," International Journal for Numerical and Analytical Methods in Geomechanics, Volume 3, No. 4, October-December 1979.

(6) Earth Technology Corporation, "Tension Pile Study, Volume I, Site Investigation and Soil Characterization Study at Block 58 West Delta Area, Gulf of Mexico," Report to Conoco Norway, Inc., through Det Norske Veritas, Report No. 82-200-1, April, 1982.

(7) Earth Technology Corporation, "Small-Diameter Pile Segment Test at Empire, Louisiana, Volume I," Final Report to a Joint Industry Project, August 30, 1984.

(8) Earth Technology Corporation, "Tension Pile Study, CNRD 13-3, Volume IV, Instrumented Pile in Soft Clay," Report to Conoco Norway, Inc., through Veritec, A. S., Report No. 82-200-4, June 1985.

(9) Earth Technology Corporation, "Tension Pile Study, CNRD 13-2, Volume III, Final Report on Small Diameter Pile Segment Tests," Report to Conoco Norway, Inc., through Det Norske Veritas, Report No. 82-200-03, June, 1983.

(10) Esrig, M. I., Kirby, R. C., Bea, R. G., and Murphy, B. S., "Initial Development of a General Effective Stress Method for the Prediction of Axial Capacity for Driven Piles in Clay," Proceedings, Ninth Offshore Technology Conference, Houston, Texas, Vol. 3, 1977, pp. 495-506, OTC 2943.

(11) Esrig, M. I., and Kirby, R. C., "Advances in General Effective Stress Method for the Prediction of Axial Capacity of Piles Driven in Clay," Proceedings, Eleventh Offshore Technology Conference, Houston, Texas, Vol. 1, pp. 437-448, OTC 3406.

(12) Hvorslev, M. J., "Uber die Festigkeitseigenschafften gestorter bindiger Boden," Kbn. (Gad) 1937, 159 p.

(13) Kirby, R. C., M. I. Esrig, and B. S. Murphy, "General Effective Stress Method for Piles in Clay, Part I - Theory", Proceedings, Geotechnical Practice in Offshore Engineering, at University of Texas at Austin, Austin, Texas, April 27-19, 1983.

(14) Matlock, Hudson and Stephen H. C. Foo, "Axial Analysis of Piles Using a Hysteretic and Degrading Soil Model," Proceedings, International Conference on Numerical Methods in Offshore Pilings, London, May 1979.

(15) Matlock, Hudson, Ignatius Lam, and Lino Cheang, "Analytical Interpretation of Pile Installation and Axial Performance," Proceedings, 2nd International Conference on Numerical Methods in Offshore Piling at the University of Texas at Austin, April, 1982.

(16) Palmer, A. C., "Undrained Plane-Strain Expansion of a Cylindrical Cavity in Clay: A Simple Interpretation of the Pressuremeter Test," Geotechnique Vol. 22, No. 3, September 1972, pp. 451-457.

(17) Randolph, M. F., Carter, J. P., and Wroth, C. P., "Driven Piles in Clay --The Effects of Installation and Subsequent Consolidation," Geotechnique Vol. 29, No. 4, December, 1979, pp. 361-393.

(18) Randolph, M. F., and C. P. Wroth, "An Analytical Solution for the Consolidation Around a Driven Pile," International Journal for Numerical and Analytical Methods in Geomechanics, Volume 3, No. 3, July-September 1979.

(19) Randolph, M. F., and B. S. Murphy, "Shaft Capacity of Driven Piles in Clay," Proceedings, Seventeenth Offshore Technology Conference, Houston, Texas, 1985, pp. 371-378, OTC 4883.

(20) Terzaghi, K., From Theory to Practice in Soil Mechanics, New York: Wiley, 1960.

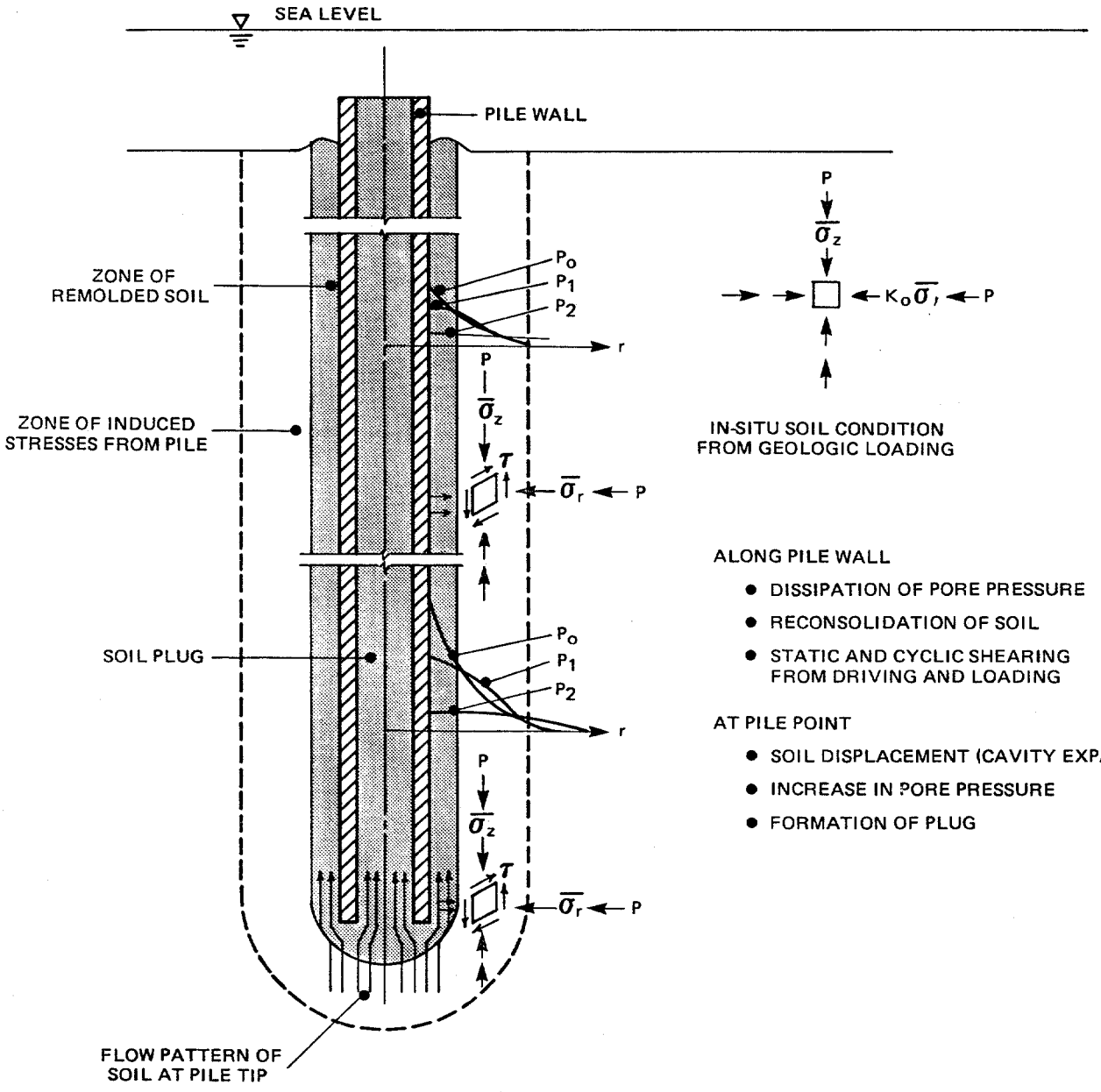

DESCRIPTION OF PILE LOADING PROCESSES

PLATE 1.1

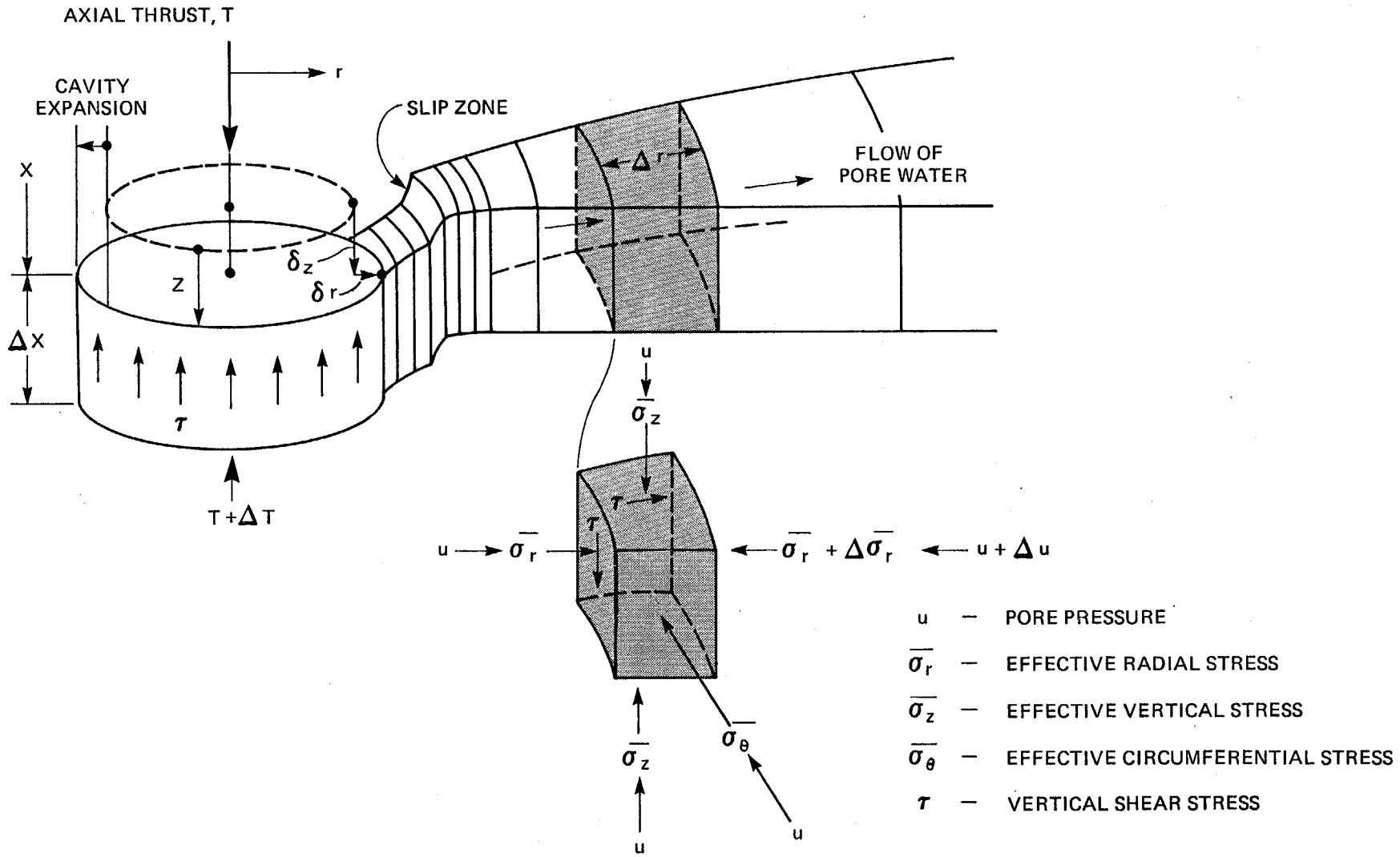

SINGLE–SLICE MODEL USED FOR SIMULATION OF PILE INSTALLATION, CONSOLIDATION AND LOADING

PLATE 2.1

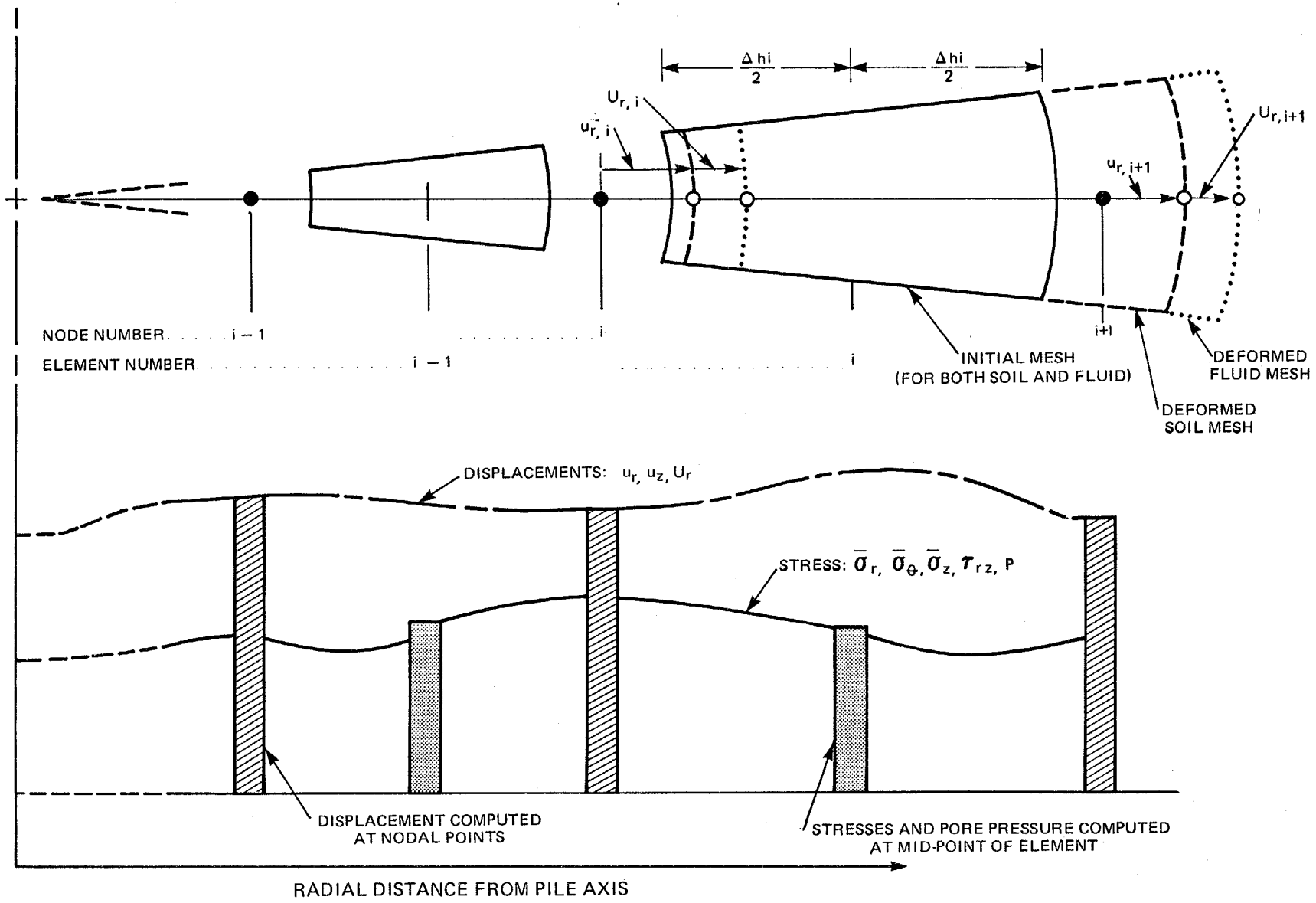

LOCATIONS WHERE SAMPLES OF DISPLACEMENT, STRESSES AND PRESSURE ARE TAKEN

PLATE 2.2

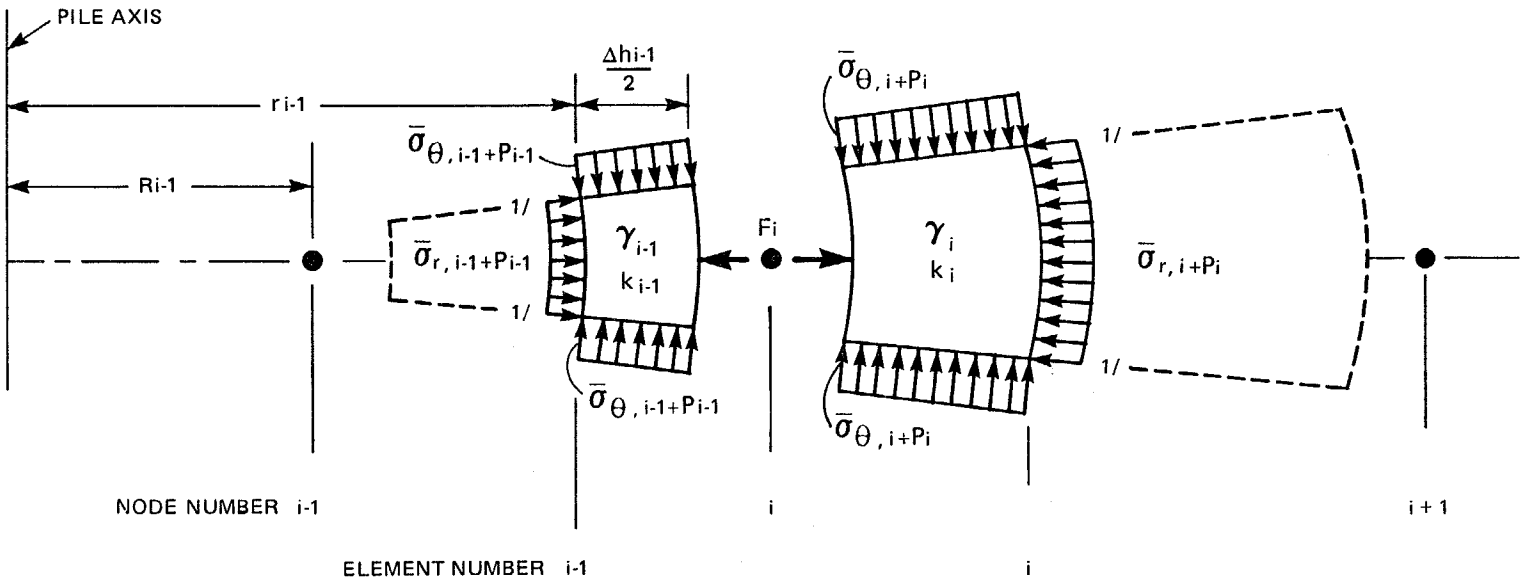

R = RADIAL DISTANCE TO NODAL POINT

r = RADIAL DISTANCE TO MID-POINT OF ELEMENT

Δh = INCREMENT LENGTH

$\bar{\sigma}_\theta$ = CIRCUMFERENTIAL STRESS

$\bar{\sigma}_r$ = RADIAL STRESS

P = PORE FLUID PRESSURE

Fi = BALANCE FORCE FOR EQUILIBRIUM

γ = UNIT WEIGHT OF PORE FLUID

k = PERMEABILITY

FORCE COMPONENTS FOR RADIAL EQUILIBRIUM IN DISCRETE ELEMENT MODEL

PLATE 2.3

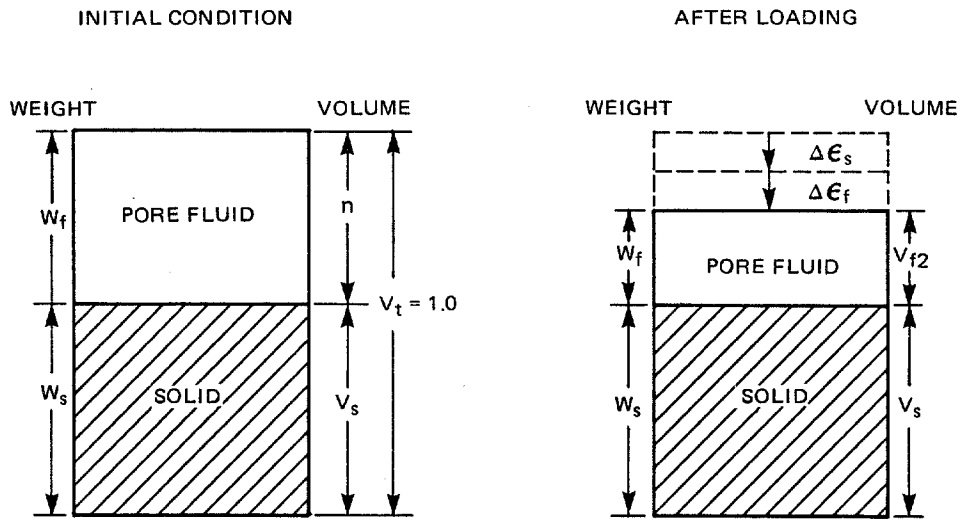

n = INITIAL POROSITY

$\Delta\epsilon_s$ = VOLUMETRIC STRAIN IN SOIL SKELETON (POSITIVE FOR COMPRESSION)

$\Delta\epsilon_f$ = VOLUMETRIC STRAIN DUE TO RELATIVE MOVEMENT OF PORE FLUID WITH RESPECT TO SOIL SKELETON (POSITIVE FOR COMPRESSION)

γ_{f_1} = INITIAL DENSITY OF PORE FLUID = $\frac{W_f}{n}$

γ_{f_2} = DENSITY OF PORE FLUID AFTER LOADING = $\frac{W_f}{V_{f2}} = \frac{W_f}{n - \Delta\epsilon_f - \Delta\epsilon_s}$

$$\therefore \quad \Delta\gamma_f = \gamma_{f2} - \gamma_{f1} = w_f \left(\frac{1}{n - \Delta\epsilon_f - \Delta\epsilon_s} - \frac{1}{n} \right)$$

$$\text{AND} \quad \frac{\Delta\gamma_f}{\gamma_{f1}} = n \left(\frac{1}{n - \Delta\epsilon_f - \Delta\epsilon_s} - \frac{1}{n} \right)$$

$$\approx \frac{\Delta\epsilon_f + \Delta\epsilon_s}{n}$$

$$\text{THEREFORE,} \quad \Delta_p = K_f \left(\frac{\Delta\gamma_f}{\gamma_f} \right) = \frac{K_f}{n} \left(\Delta\epsilon_f + \Delta\epsilon_s \right)$$

CONSTITUTIVE RELATION OF PORE FLUID AT EACH ELEMENT

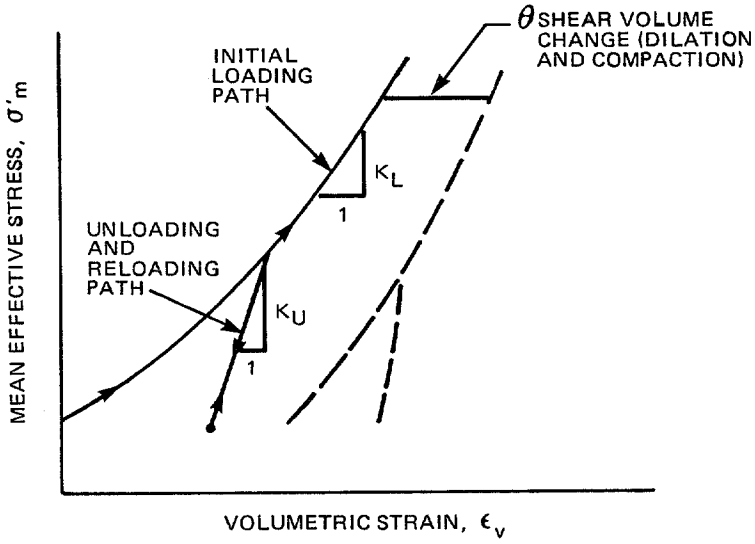

(a) VOLUMETRIC BEHAVIOR

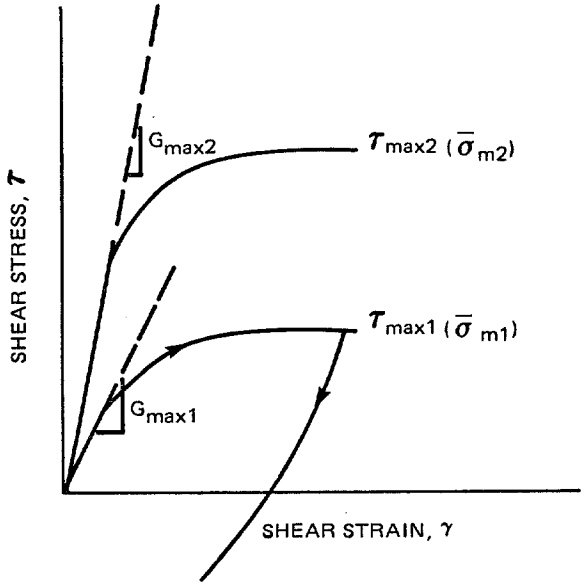

(b) SHEAR BEHAVIOR

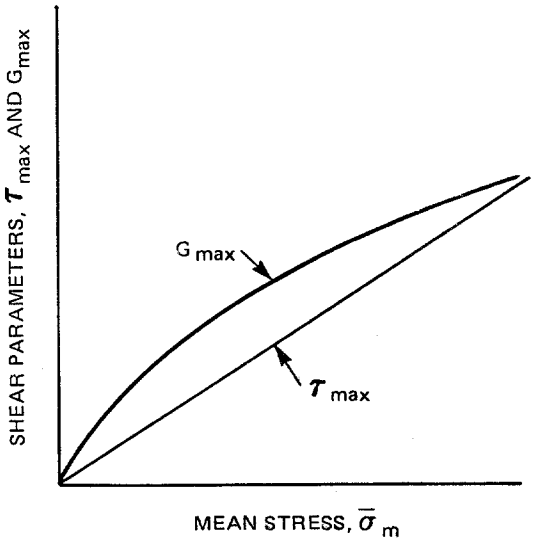

(c) RELATIONSHIP OF SHEAR PARAMETERS ON CONFINEMENT

INPUT DESCRIPTION OF SOIL MODEL

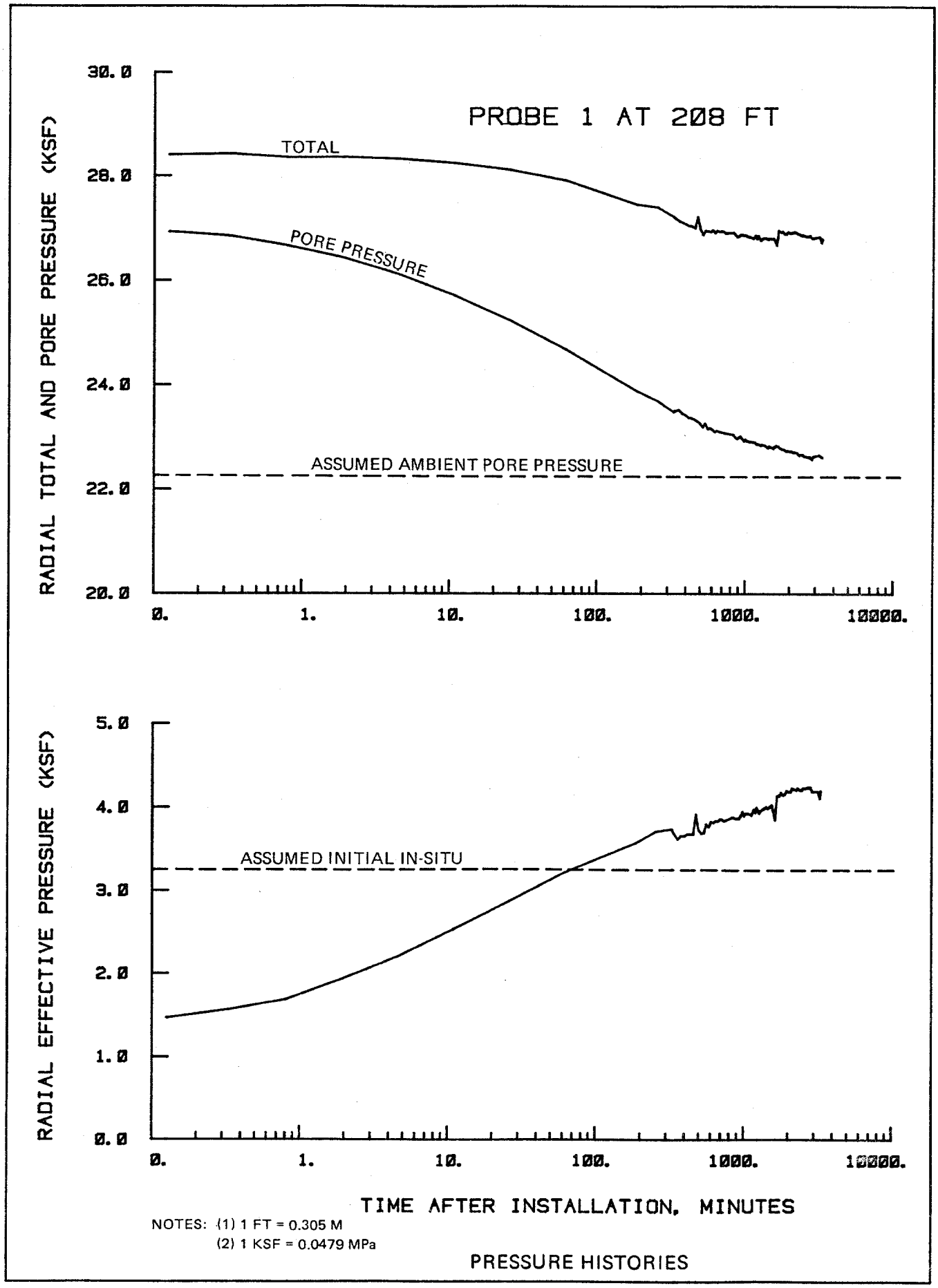

NOTES: (1) 1 FT = 0.305 M
(2) 1 KSF = 0.0479 MPa

PRESSURE HISTORIES

PLATE 3.1

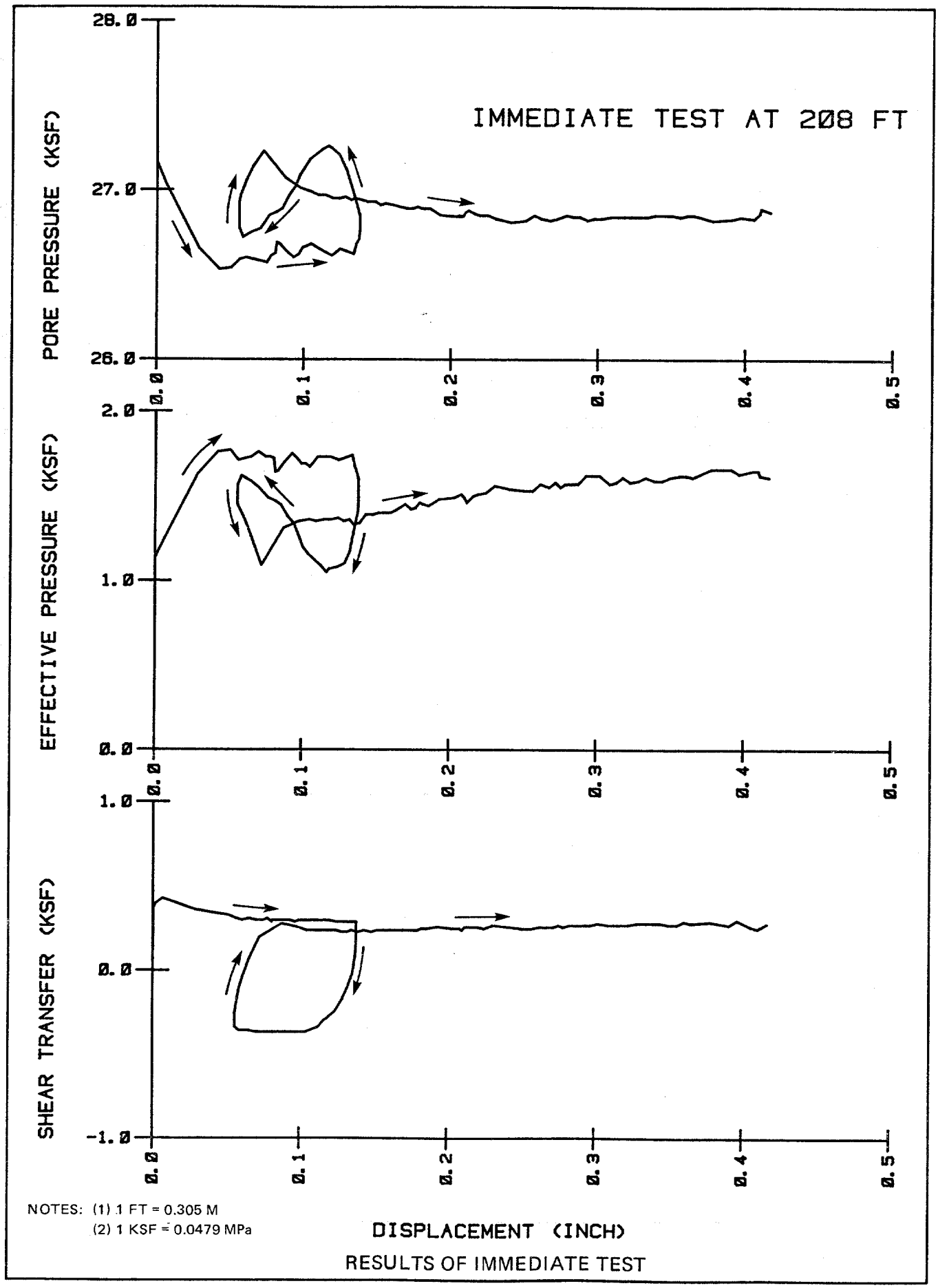

NOTES: (1) 1 FT = 0.305 M
(2) 1 KSF = 0.0479 MPa

RESULTS OF IMMEDIATE TEST

PLATE 3.2

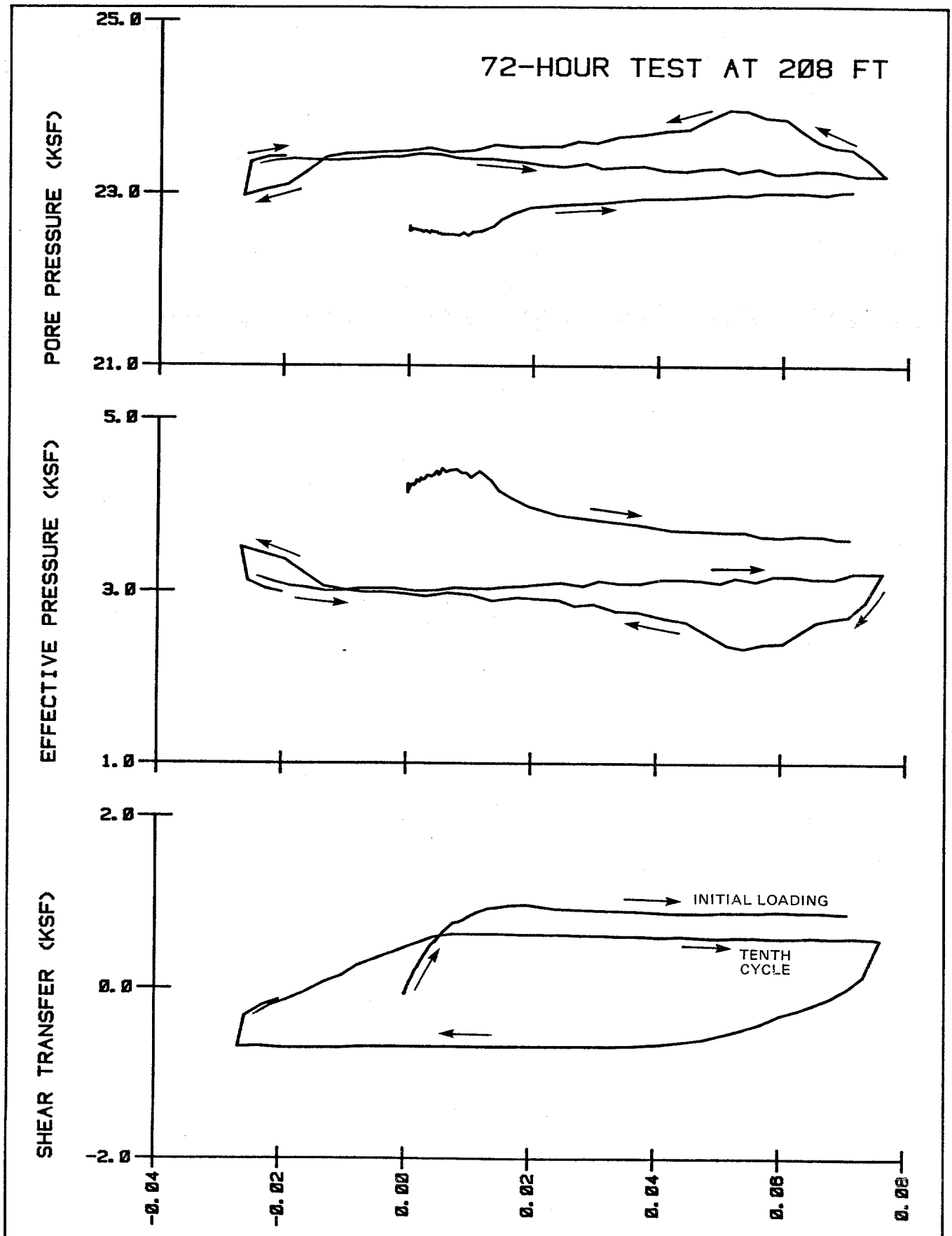

NOTES: (1) 1 FT = 0.305 M
(2) 1 KSF = 0.0479 MPa

RESULTS OF LONG-TERM TEST

PLATE 3.3

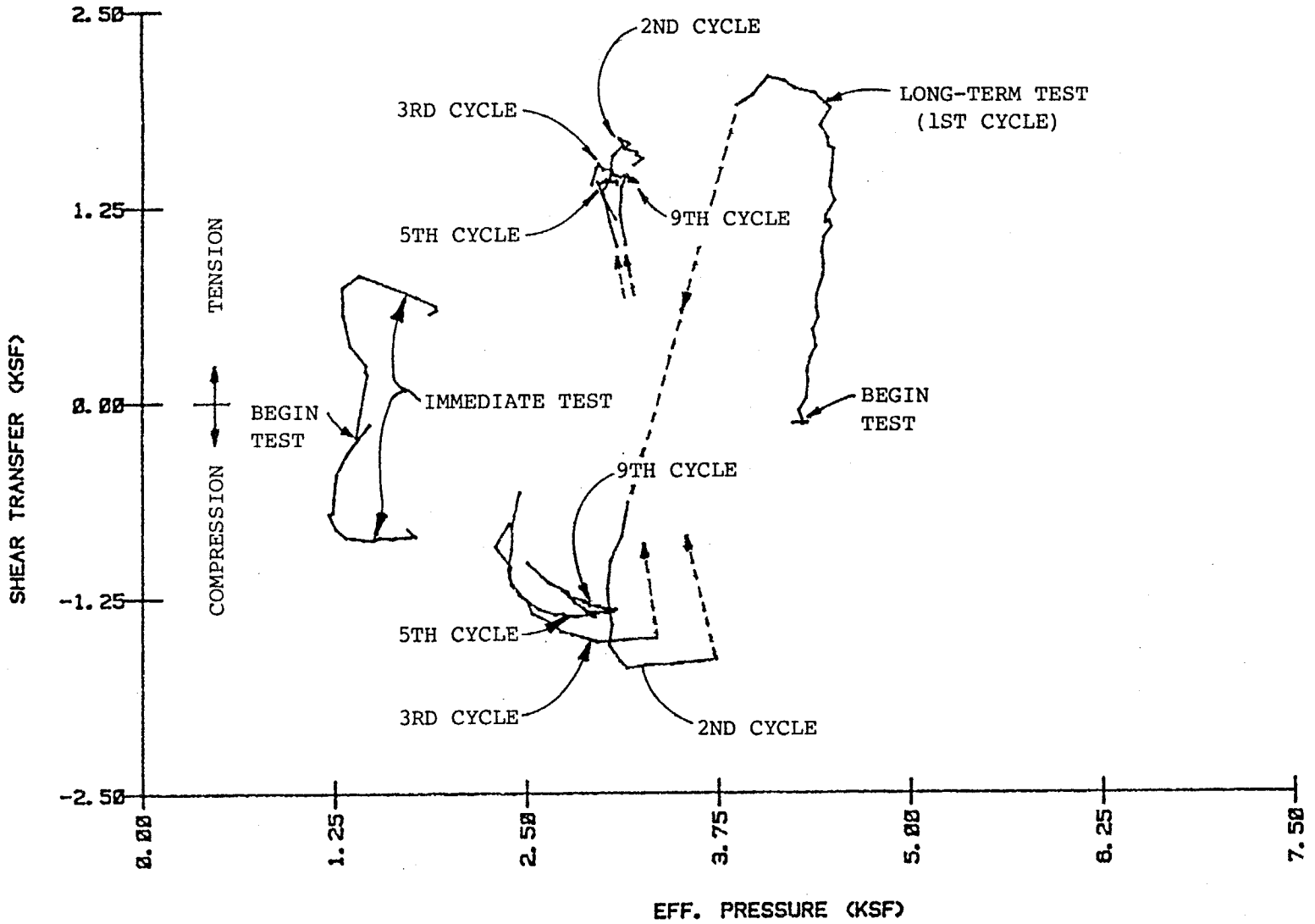

NOTE: 1 KSF = 0.0479 MPa

STRESS PATHS 208 FT. DEPTH WEST DELTA BLK 58A

PLATE 3.4

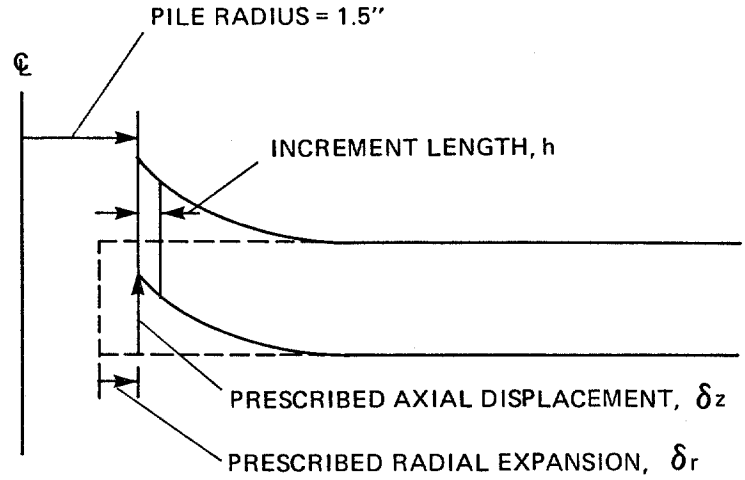

LOAD – TIME HISTORIES

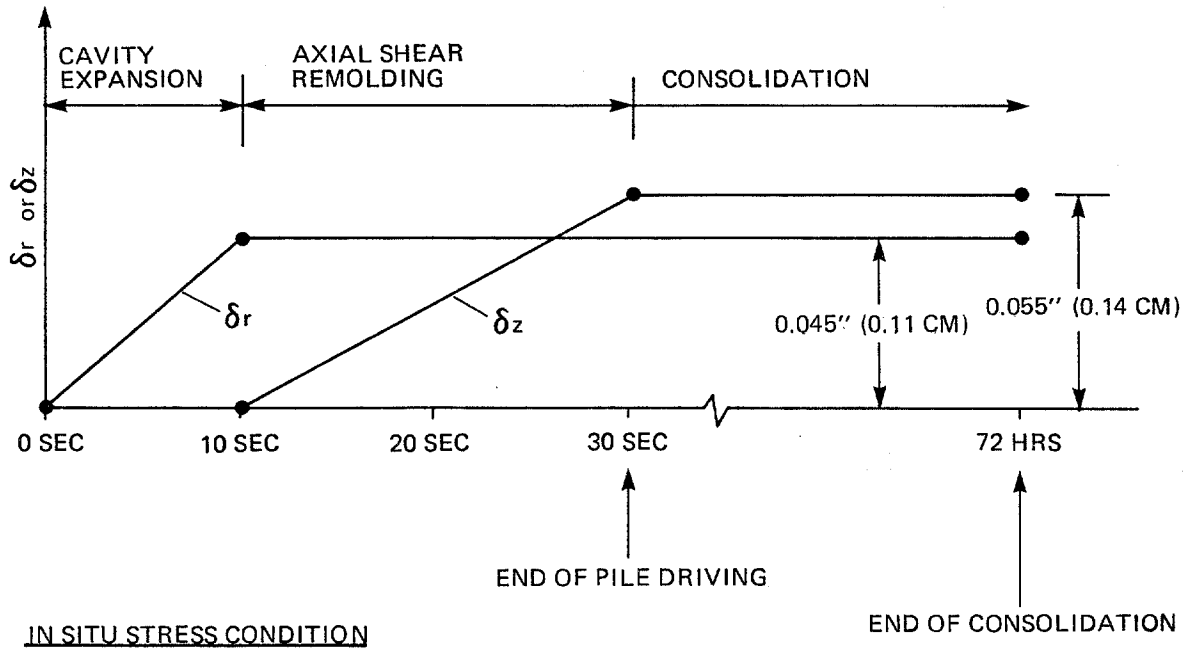

IN SITU STRESS CONDITION

VERTICAL STRESS = 4.3 KSF (0.206 MPa)

HORIZONTAL STRESS = 3.23 KSF (0.155 MPa)

PORE FLUID PRESSURE = 22.2 KSF (1.06 MPa)

PROBLEM DESCRIPTION OF FIRST SERIES OF CASH SOLUTION TO SIMULATE PILE DRIVING AND CONSOLIDATION

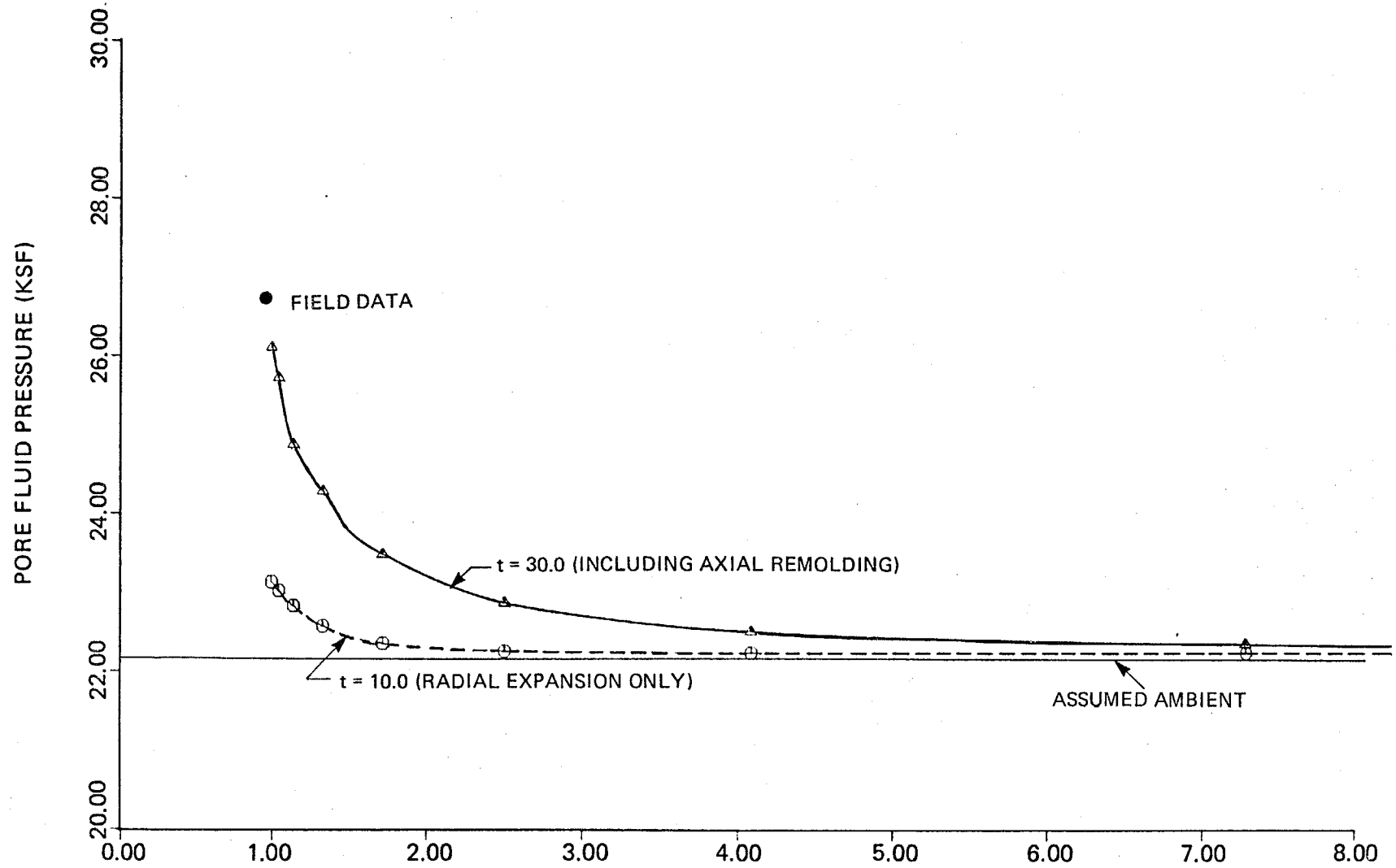

NOTE: 1 KSF = - 0.0479 MPa

RADIAL DISTRIBUTION OF PORE PRESSURE FROM CASH SOLUTION SIMULATING PILE DRIVING

PLATE 3.6

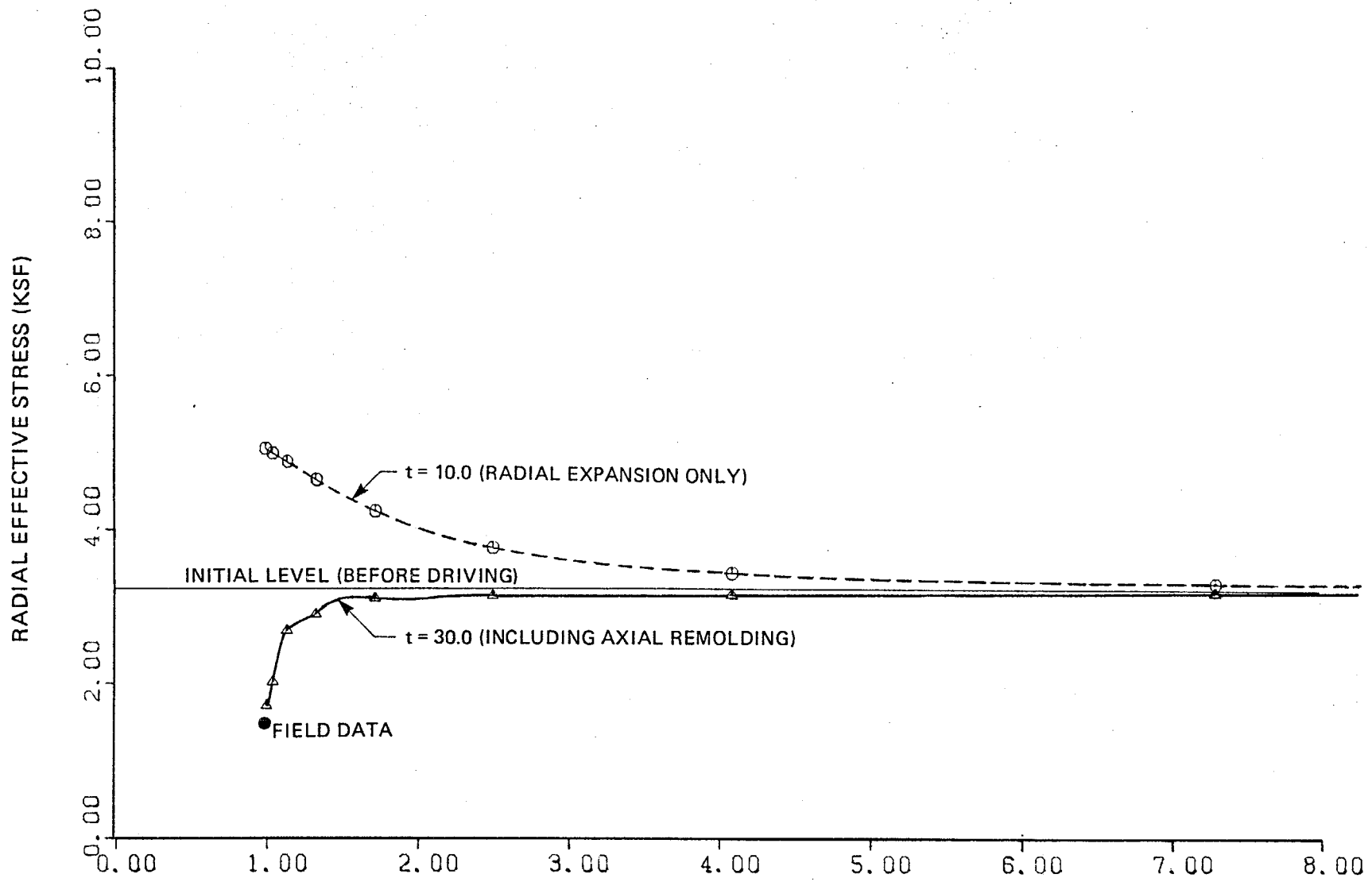

NOTE: 1 KSF = 0.0479 MPa

RADIAL DISTRIBUTION OF EFFECTIVE STRESS FROM CASH SOLUTION SIMULATING PILE DRIVING

PLATE 3.7

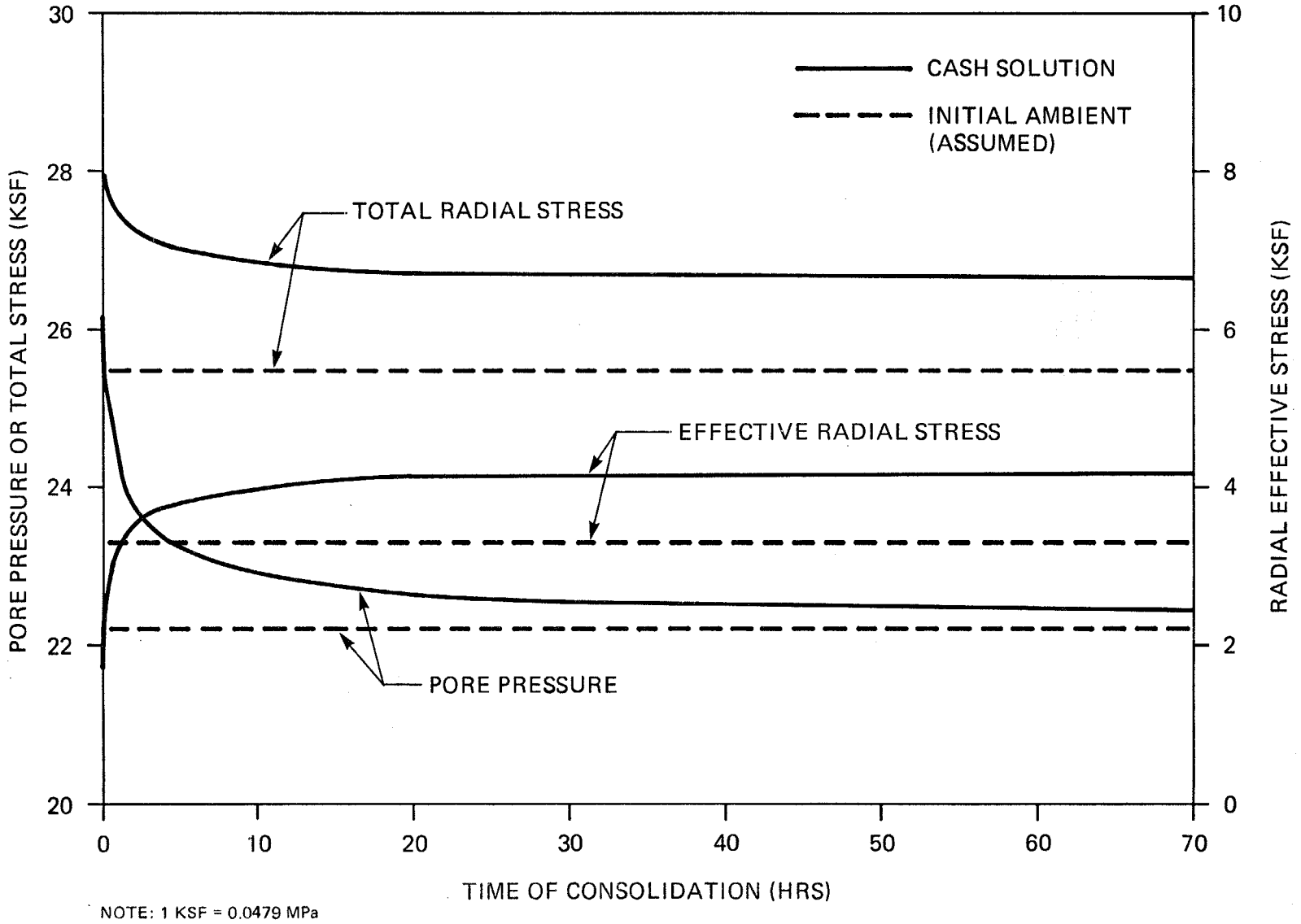

NOTE: 1 KSF = 0.0479 MPa

TIME HISTORIES OF PORE PRESSURE, TOTAL AND EFFECTIVE STRESSES FROM CASH SOLUTION OF THE CONSOLIDATION PROCESS

PLATE 3.8

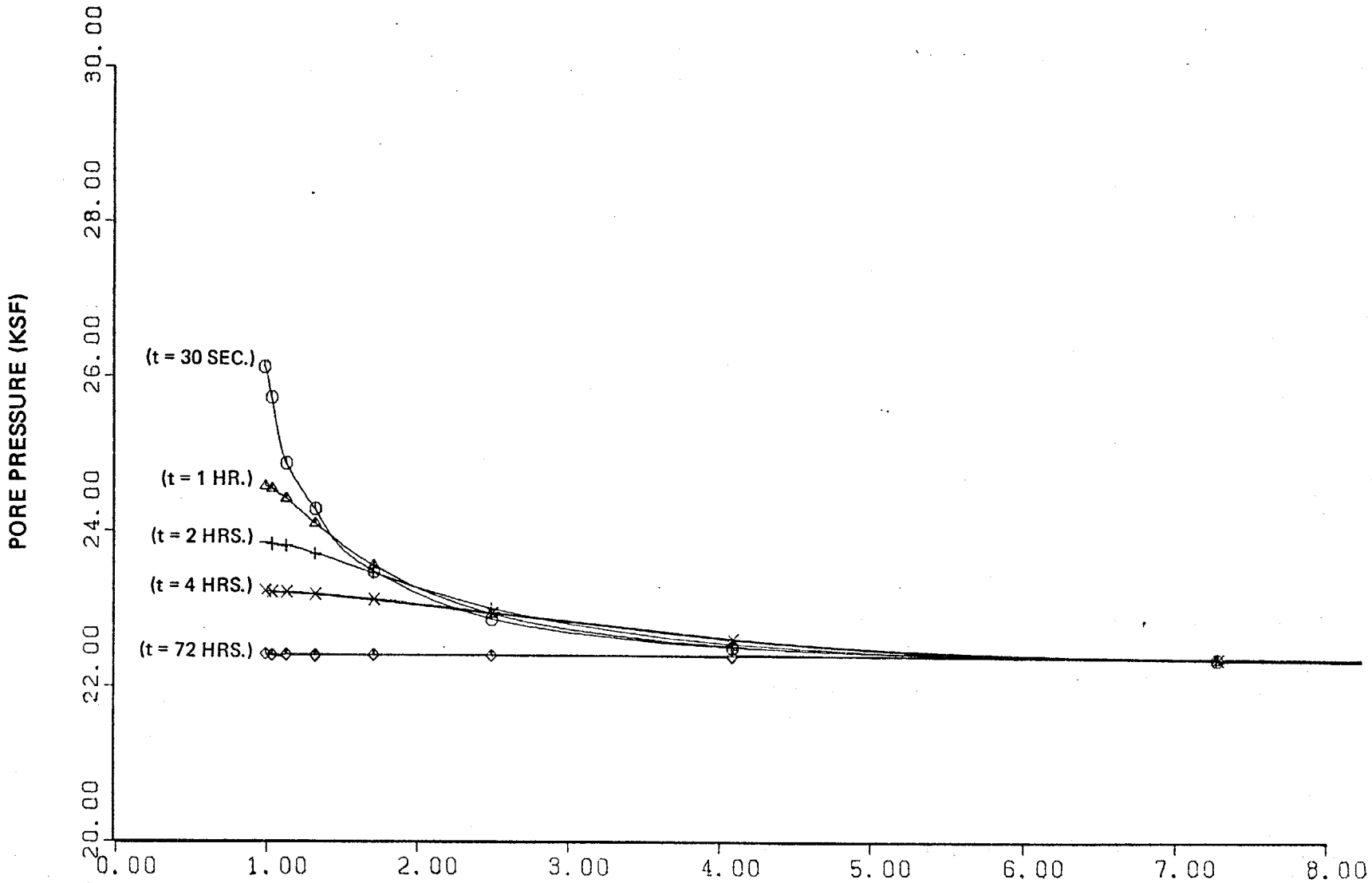

NOTE: 1 KSF = 0.0479 MPa

RADIAL DISTRIBUTION OF PORE PRESSURE FROM CASH SOLUTION SIMULATING THE CONSOLIDATION PROCESS

PLATE 3.9

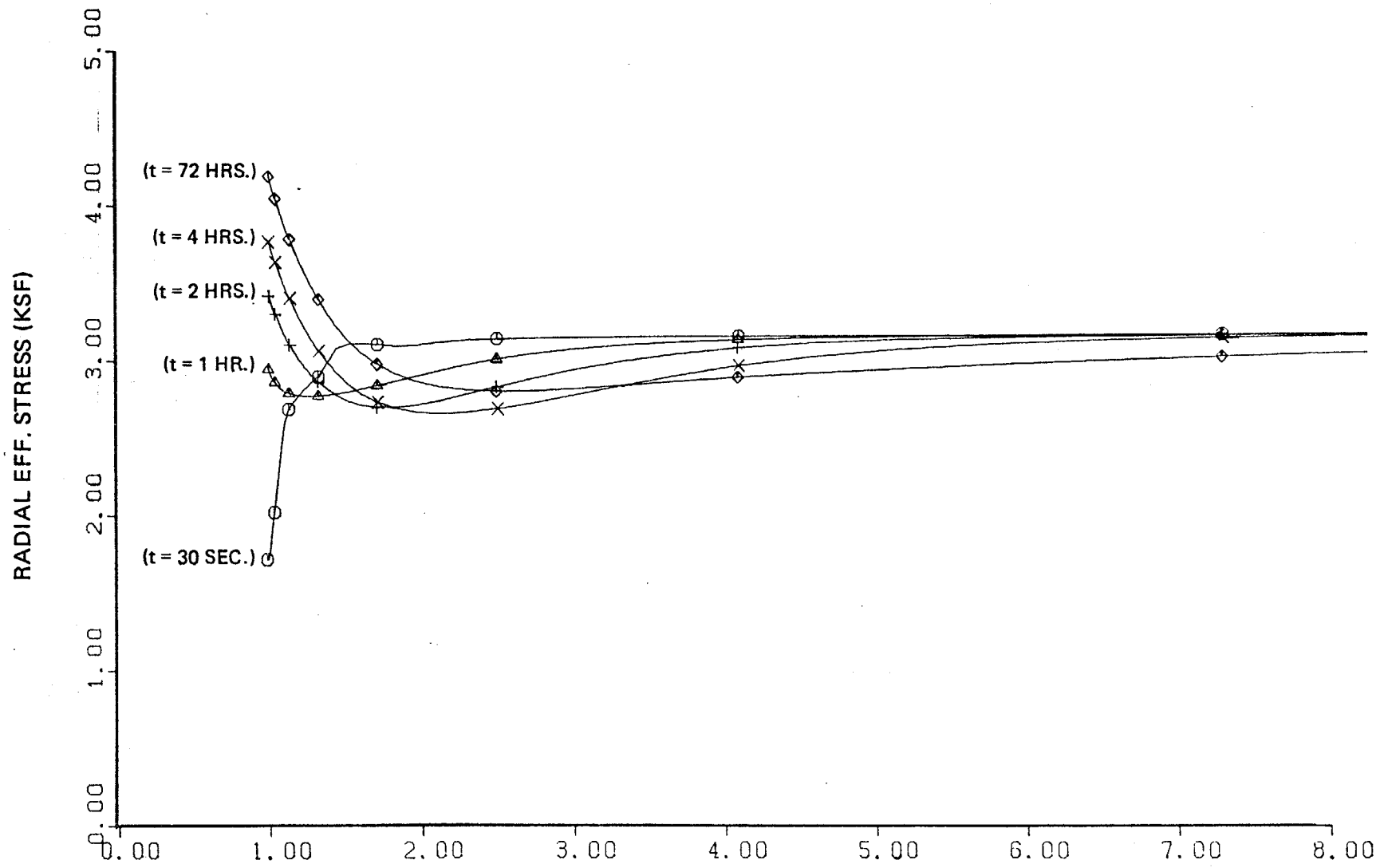

NOTE: 1 KSF = 0.0479 MPa

RADIAL DISTRIBUTION OF EFFECTIVE STRESS FROM CASH SOLUTION SIMULATING THE CONSOLIDATION PROCESS

PLATE 3.10

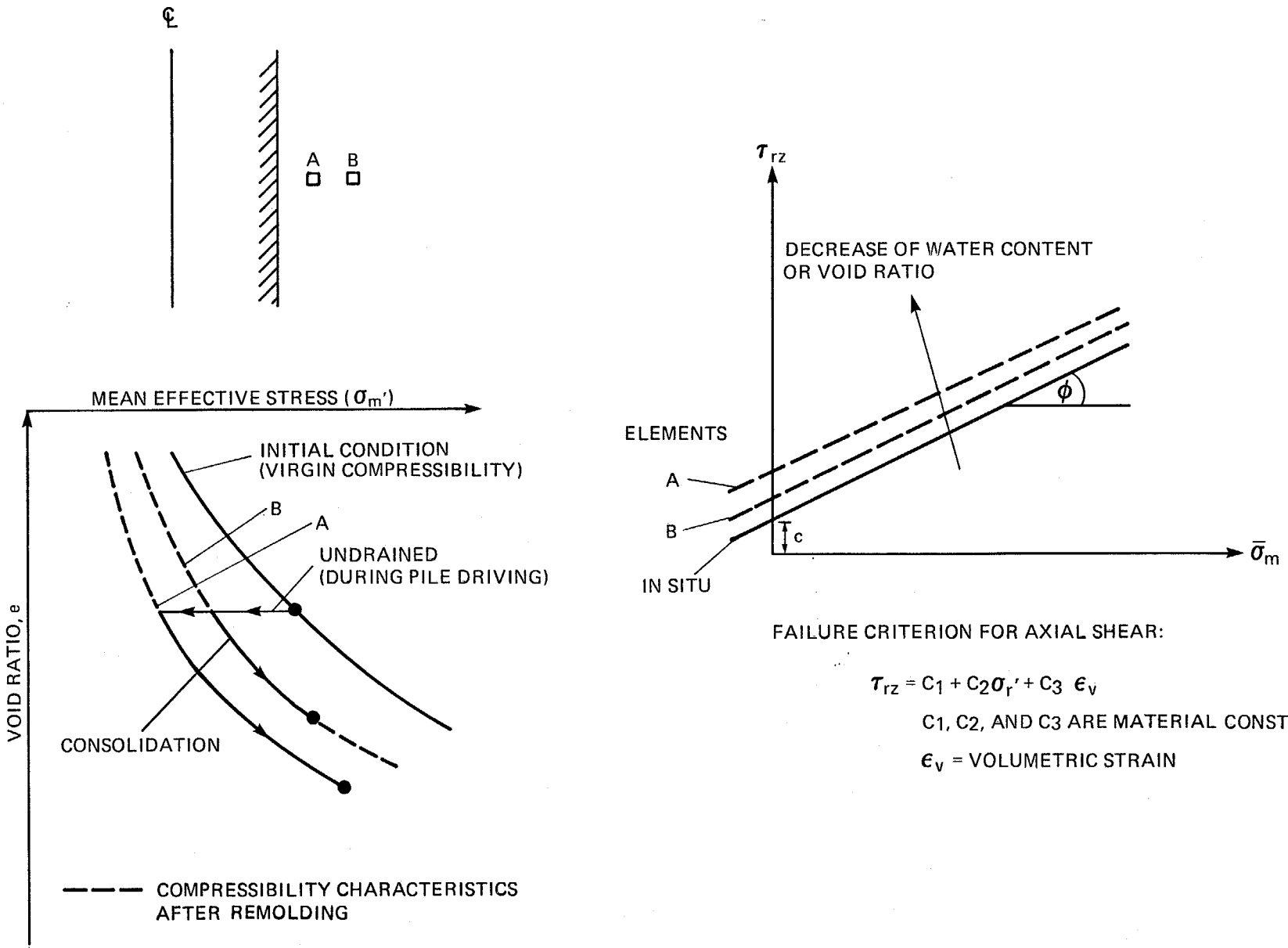

(a) REMOLDING EFFECTS ON VOLUME

(b) REMOLDING EFFECTS ON SHEAR STRENGTH

REMOLDING AND CONSOLIDATION PROCESSES DURING AND AFTER PILE DRIVING

PLATE 3.11

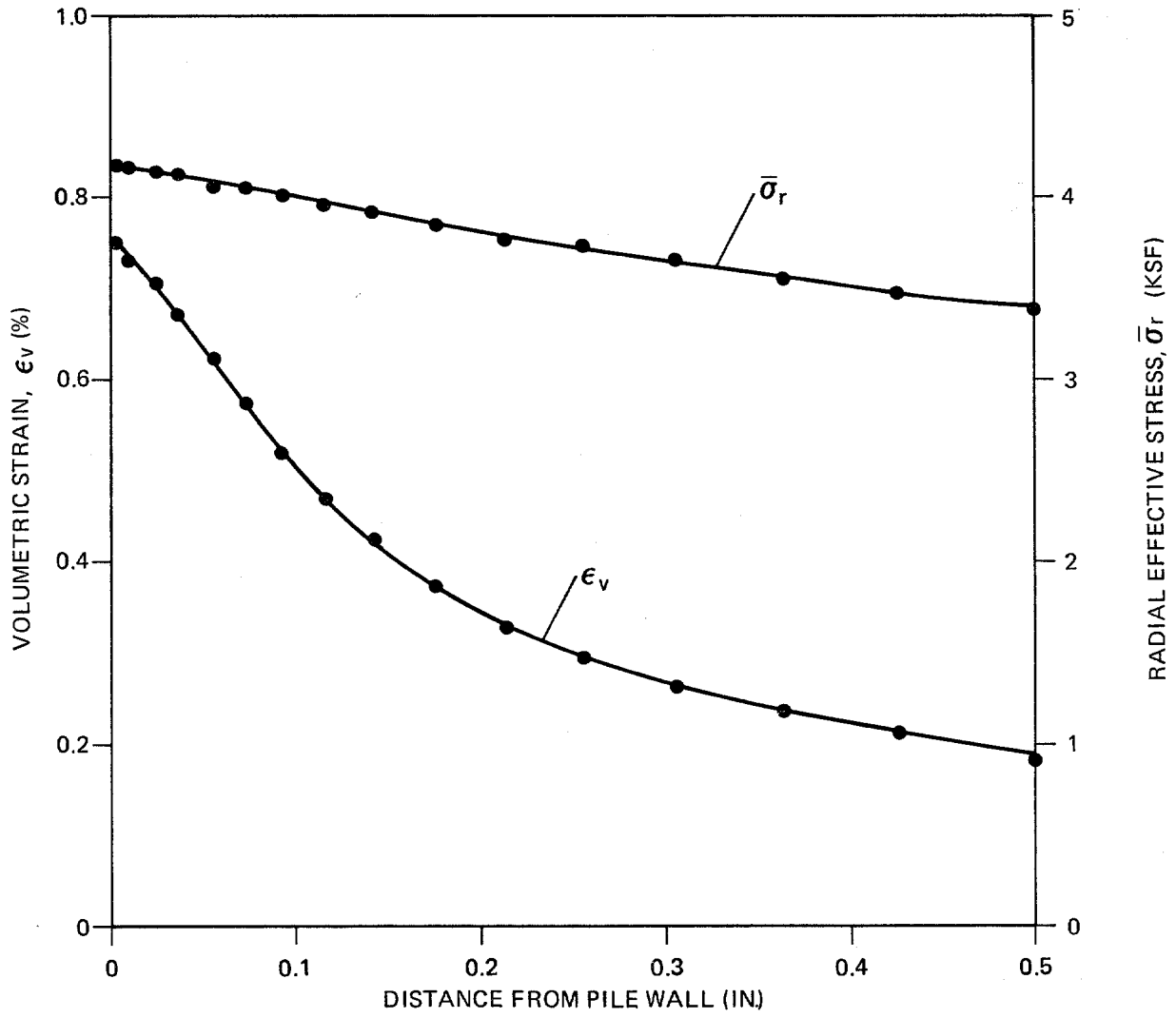

NOTES: (1) THE VOLUMETRIC STRAIN IS POSITIVE FOR COMPRESSION

(2) $\epsilon_v = \frac{-\Delta e}{1 + e_o}$ WHERE Δe AND e_o ARE INCREMENTAL AND ORIGINAL VOID RATIO, RESPECTIVELY.

CASH SOLUTION OF VARIATION OF VOID RATIO
AND EFFECTIVE STRESS CLOSE TO THE PILE WALL

PLATE 3.12

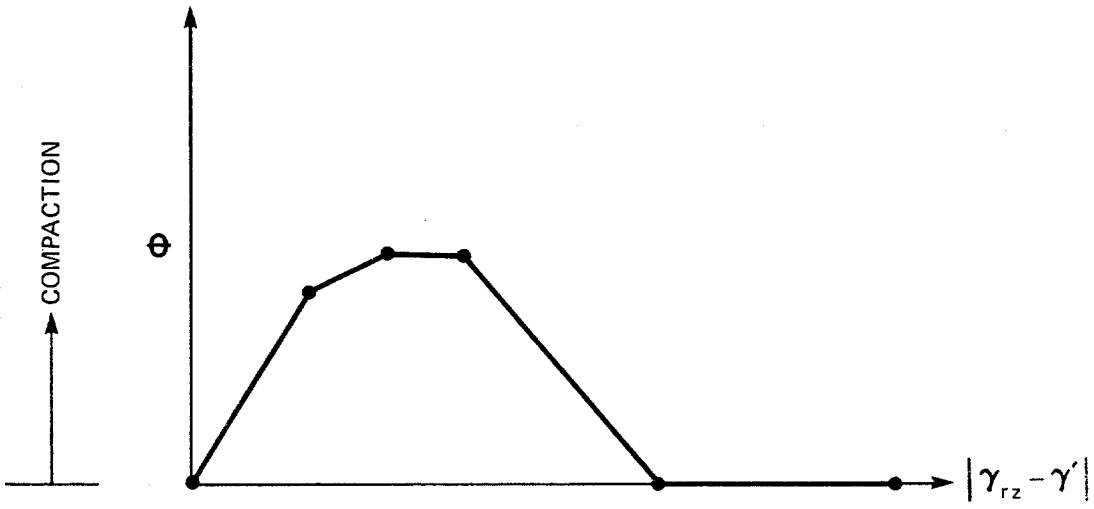

$|\gamma_{rz} - \gamma'|$ — ABSOLUTE VALUE

γ_{rz} —— CURRENT SHEAR STRAIN

γ' —— SHEAR STRAIN WHERE LAST REVERSAL OCCURS

SCHEMATIC DESCRIPTION OF SHEAR–VOLUME CHANGE ALGORITHM FOR CYCLIC AXIAL SHEAR LOADING

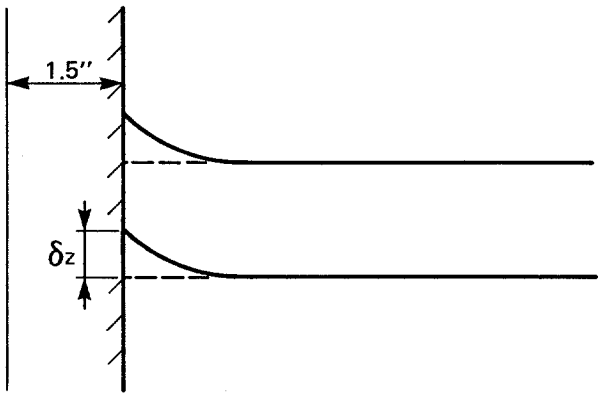

LOAD – TIME HISTORIES

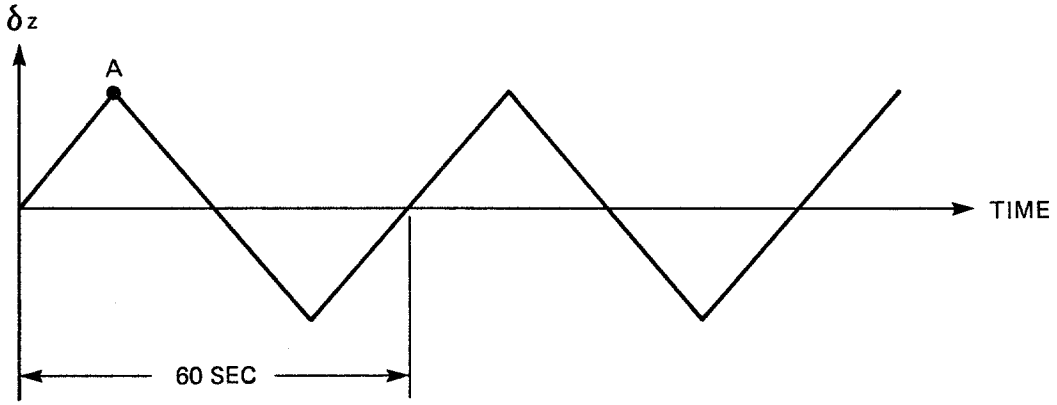

NOTES: 1 INCH = 2.54 CM

PROBLEM DESCRIPTION OF SECOND SERIES OF CASH SOLUTION TO SIMULATE CYCLIC AXIAL SHEAR LOADING

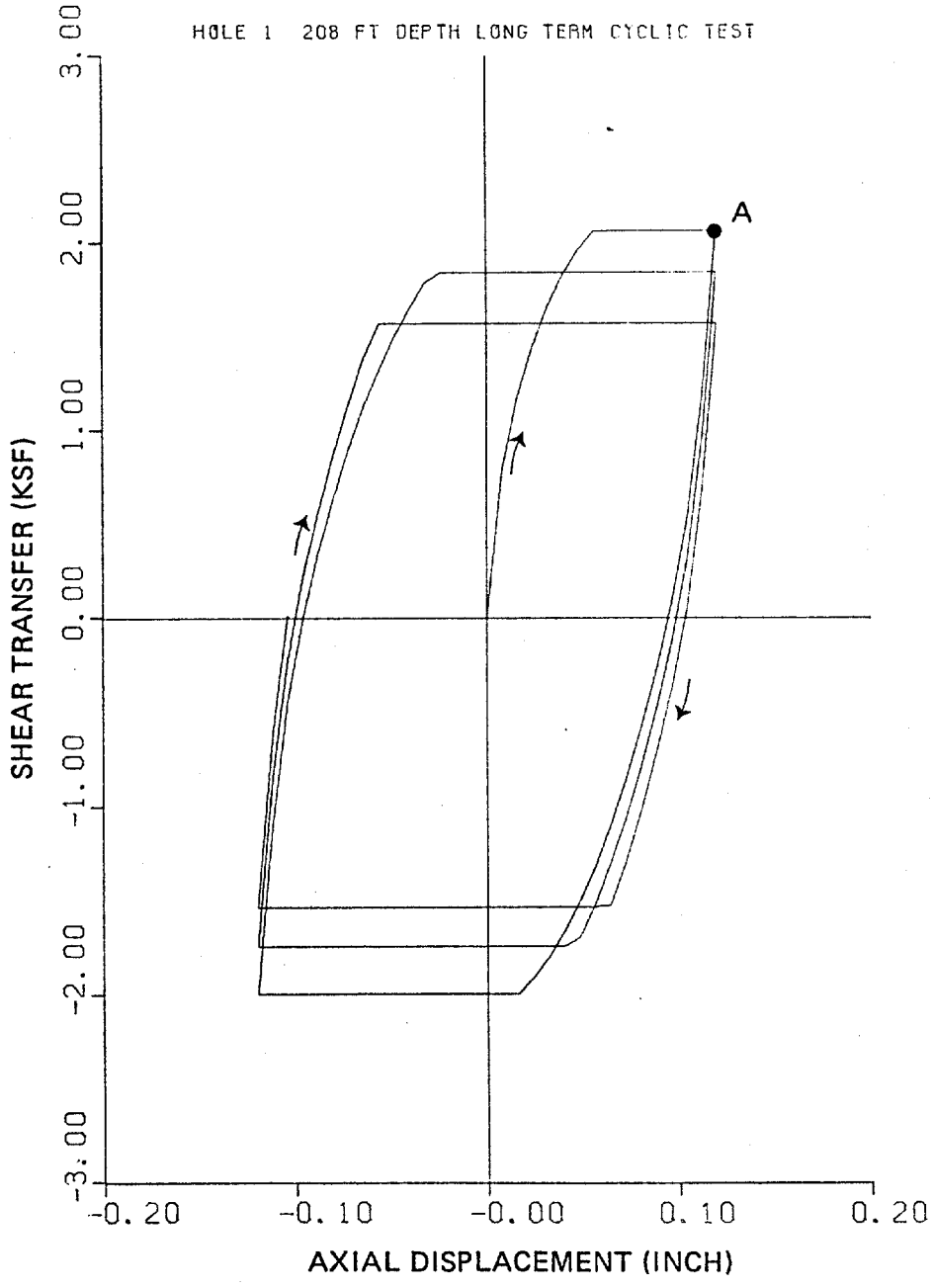

NOTES: (1) 1 INCH = 2.54 CM
(2) 1 FT. = 0.305 M
(3) 1 KSF = 0.0479 MPa

CASH SOLUTION OF SHEAR TRANSFER VS.
AXIAL DISPLACEMENT FOR CYCLIC SHEAR LOADING

PLATE 3.15

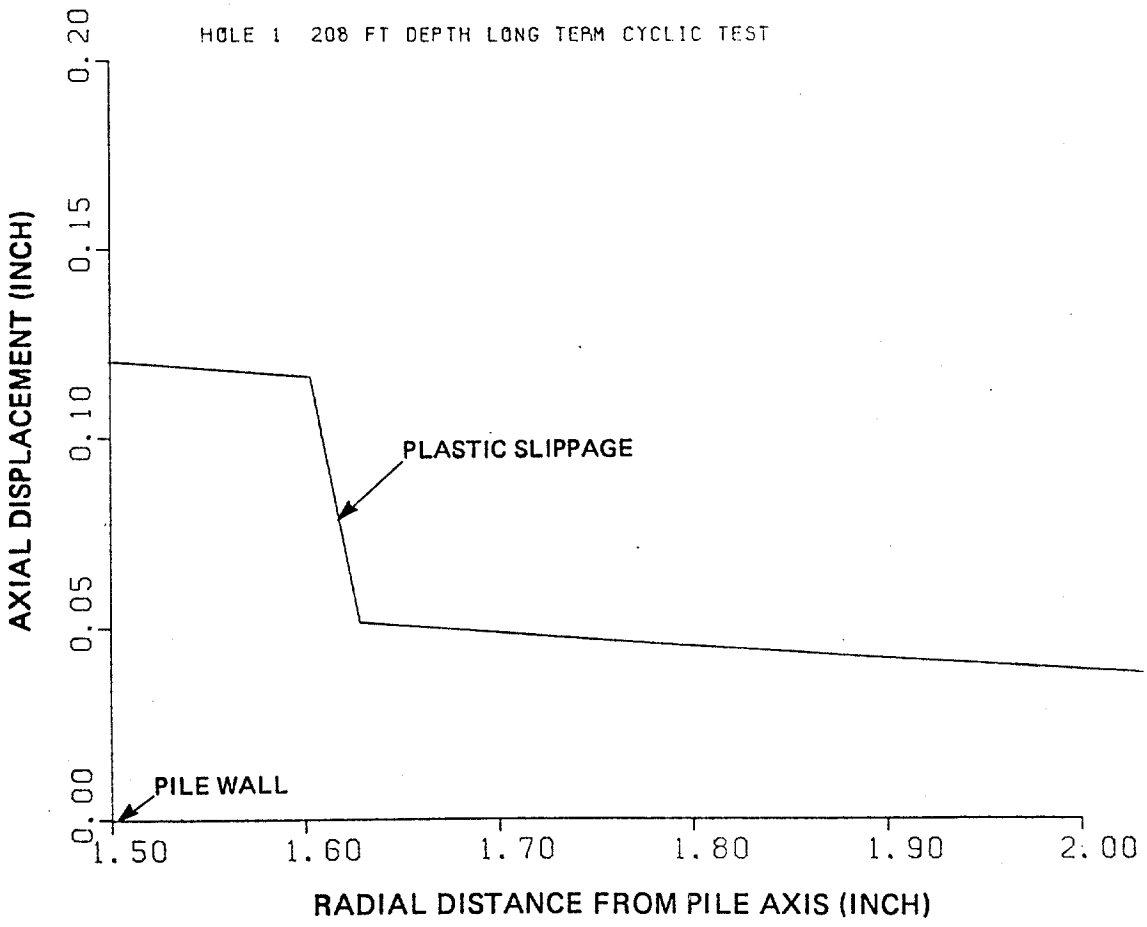

NOTES: (1) 1 INCH = 2.54 CM
(2) 1 FEET = 0.305 M

CASH SOLUTION OF THE SOIL AXIAL DISPLACEMENT WITH RESPECT TO RADIAL DISTANCE FROM PILE WALL AT TIME INSTANT A

(SEE PLATE 3.15)

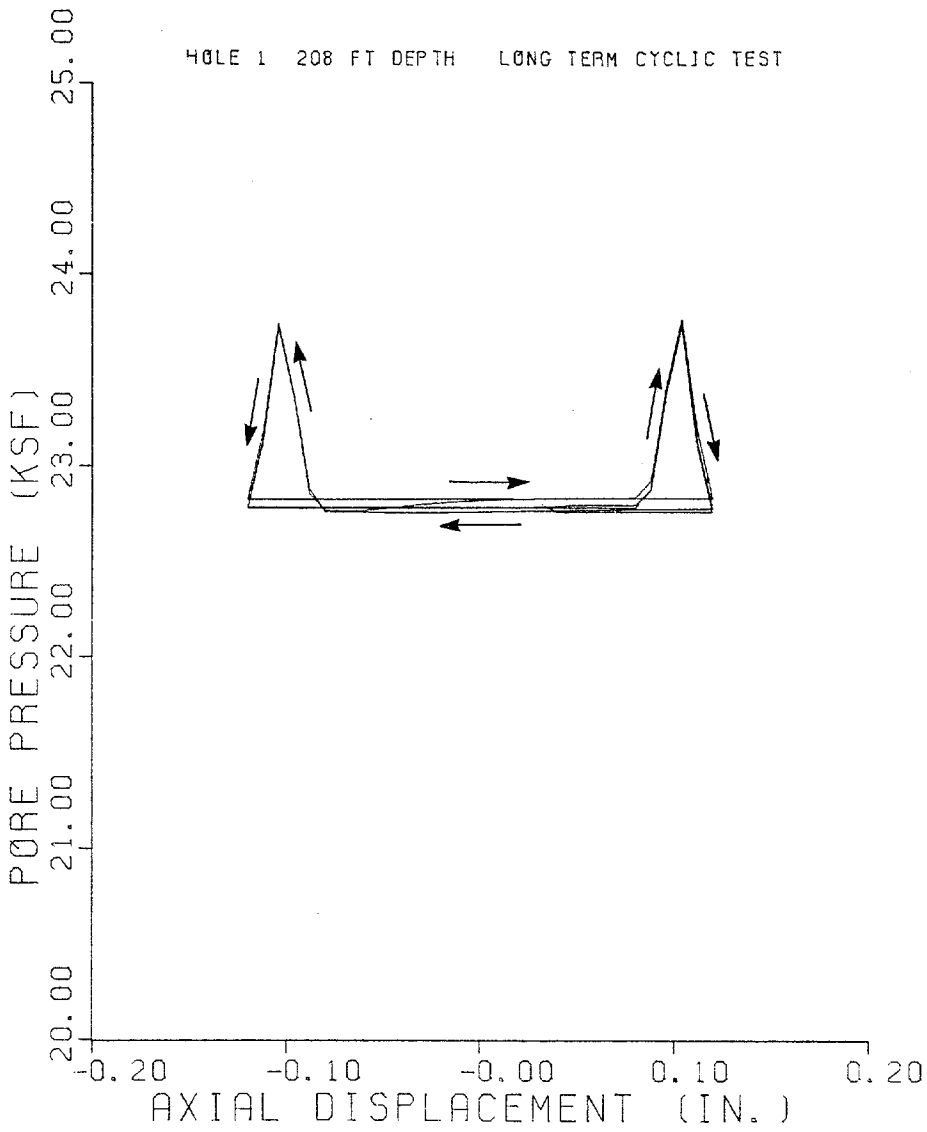

NOTES: (1) 1 INCH = 2.54 CM

(2) 1FT. = 0.305 M

(3) 1 KSF = 0.0479 MPa

CASH SOLUTION OF PORE PRESSURE CROSS–PLOTTED AGAINST AXIAL DISPLACEMENT DURING CYCLIC LOADING

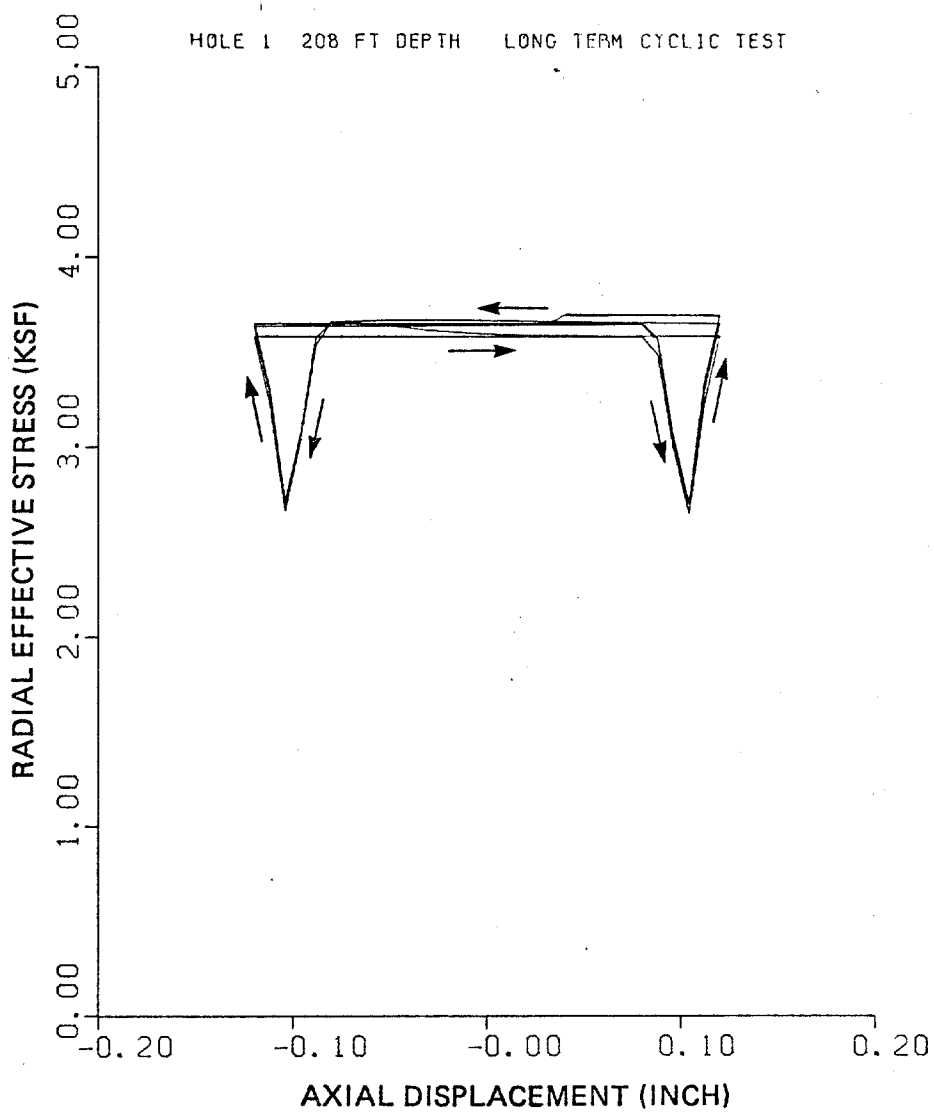

NOTES: (1) 1 INCH = 2.54 CM
(2) 1 FT. = 0.305 M
(3) 1 KSF = 0.0479 MPa

CASH SOLUTION OF EFFECTIVE STRESS CROSS–PLOTTED AGAINST AXIAL DISPLACEMENT DURING CYCLIC LOADING

PLATE 3.18

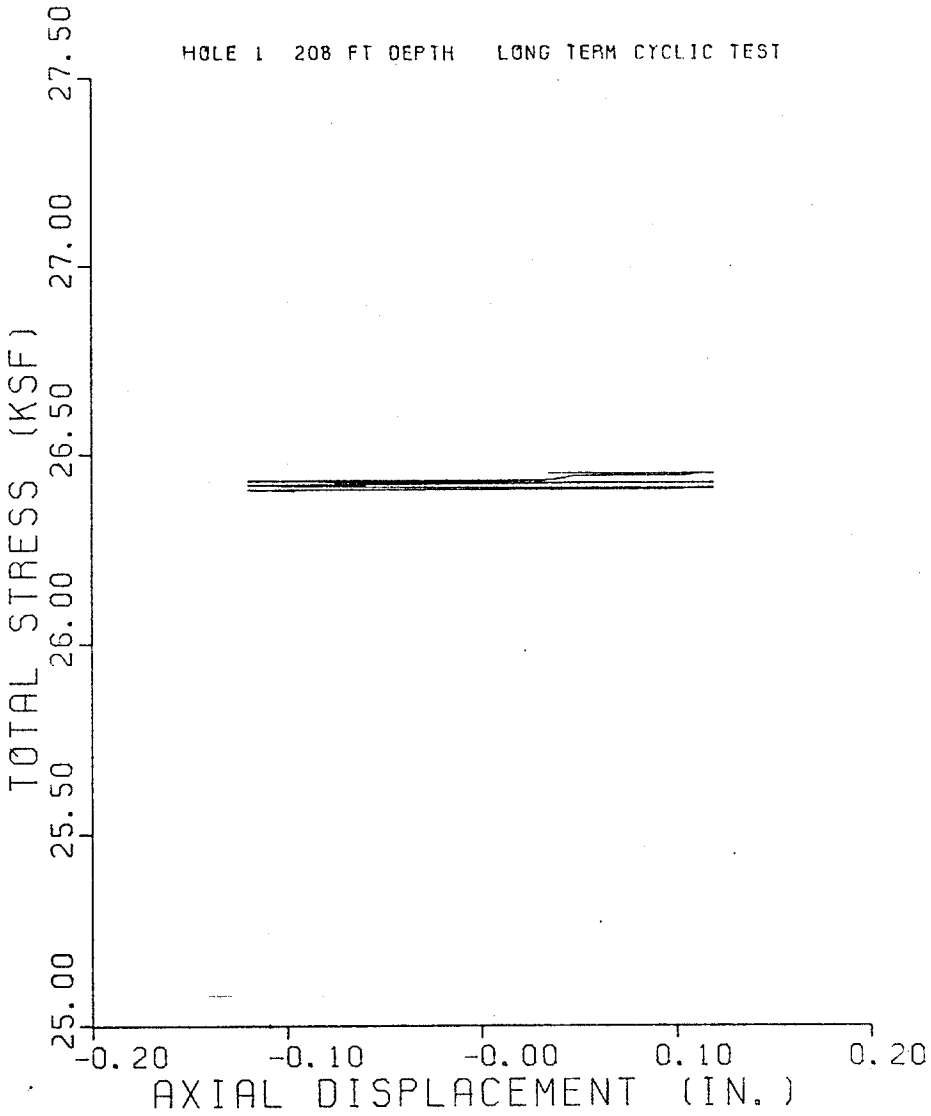

NOTES: (1) 1 INCH = 2.54 CM

(2) 1 FT. = 0.305 M

(3) 1 KSF = 0.0479 MPa

CASH SOLUTION OF TOTAL STRESS CROSS–PLOTTED AGAINST AXIAL DISPLACEMENT DURING CYCLIC LOADING

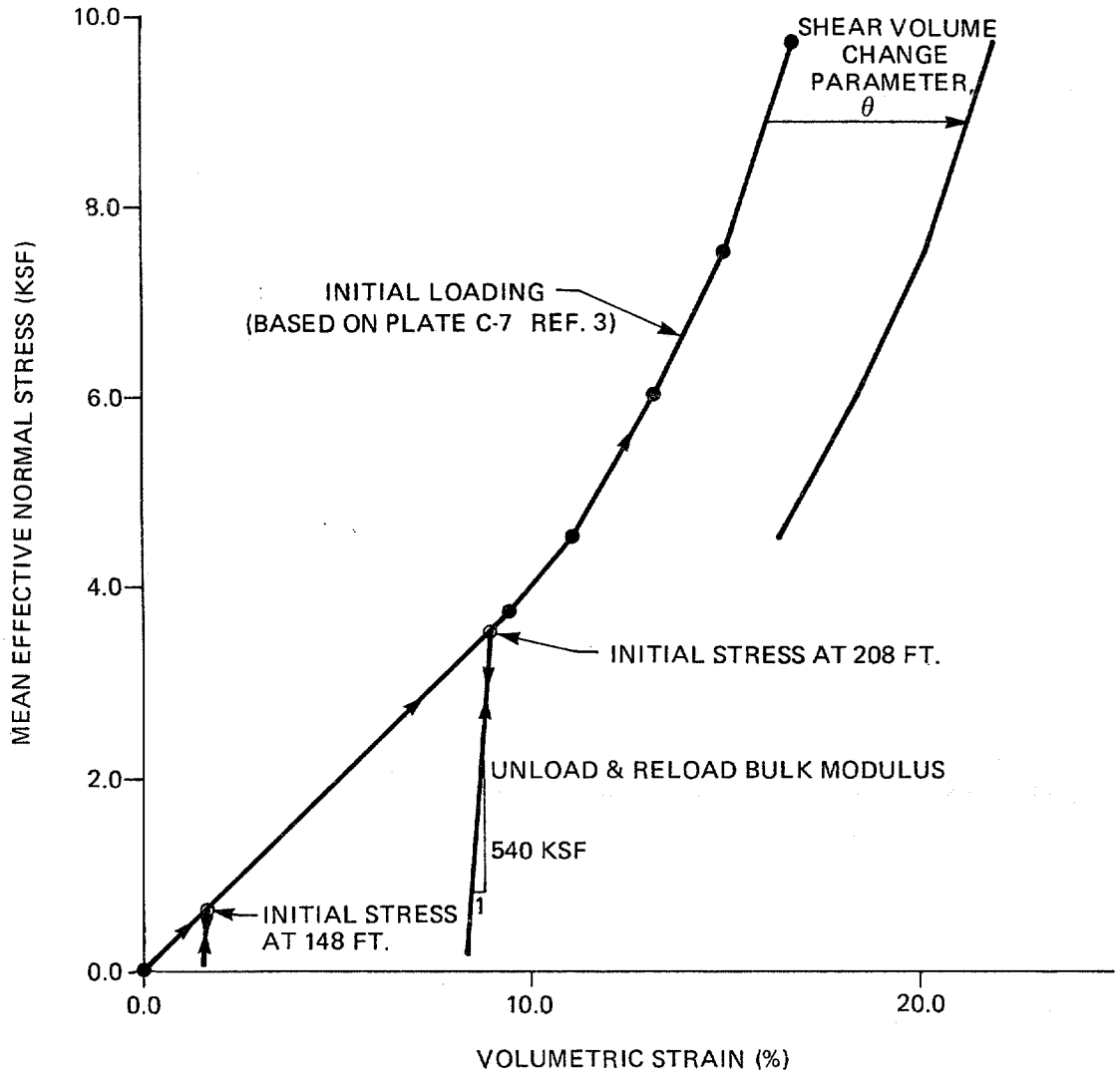

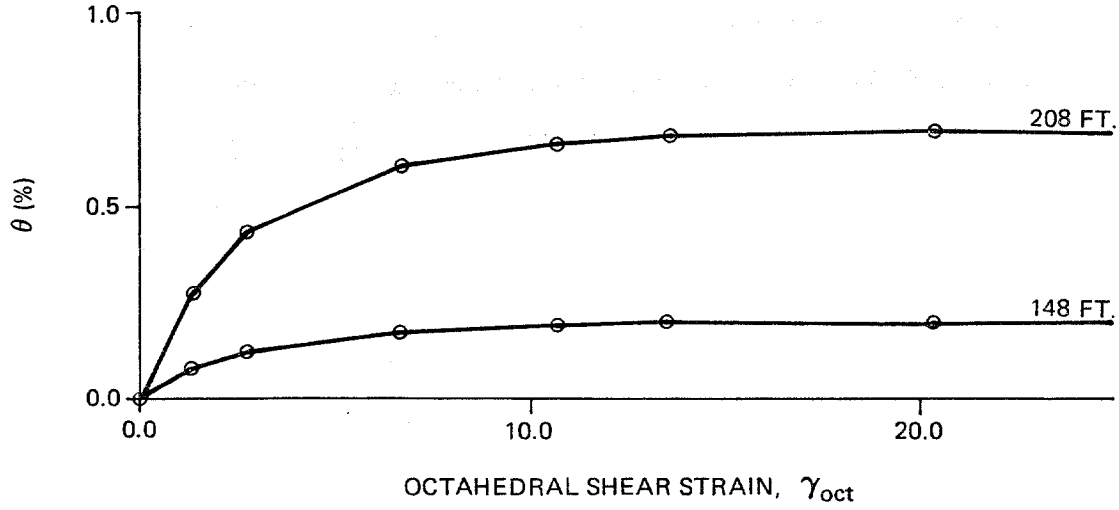

NOTES: (1) 1 FT. = 0.305 M

(2) 1 KSF = 0.0479 MPa

VOLUMETRIC BEHAVIOR FOR SENSITIVITY AND FINAL BACKFIT ANALYSES

PLATE 4.1

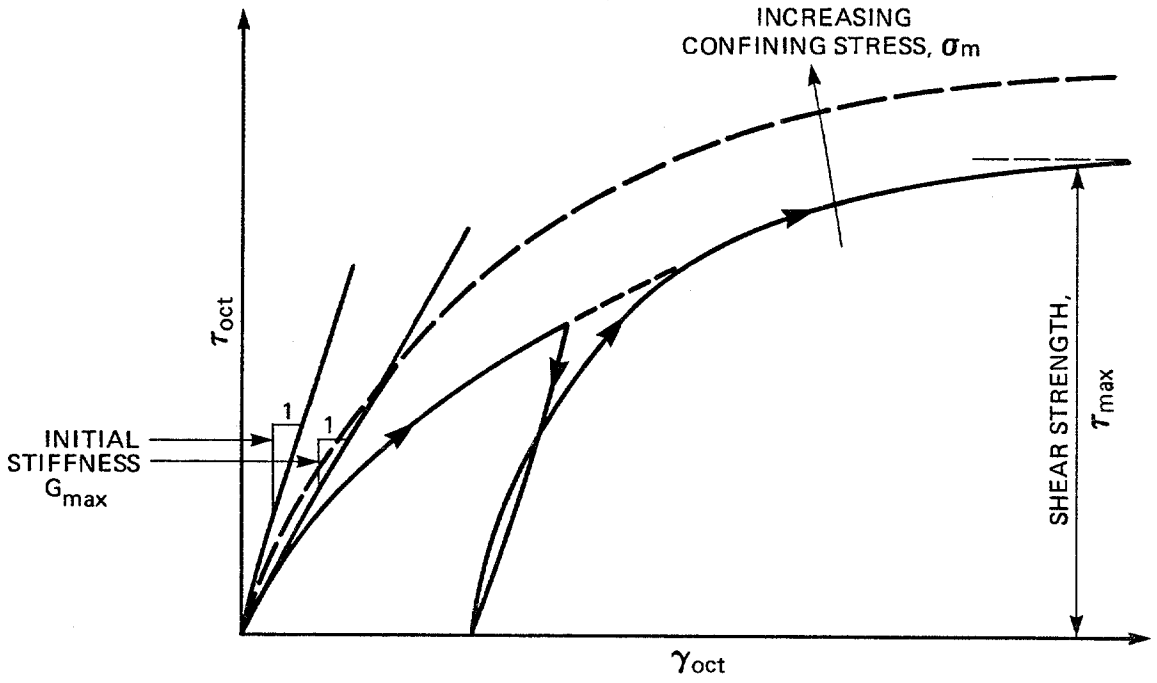

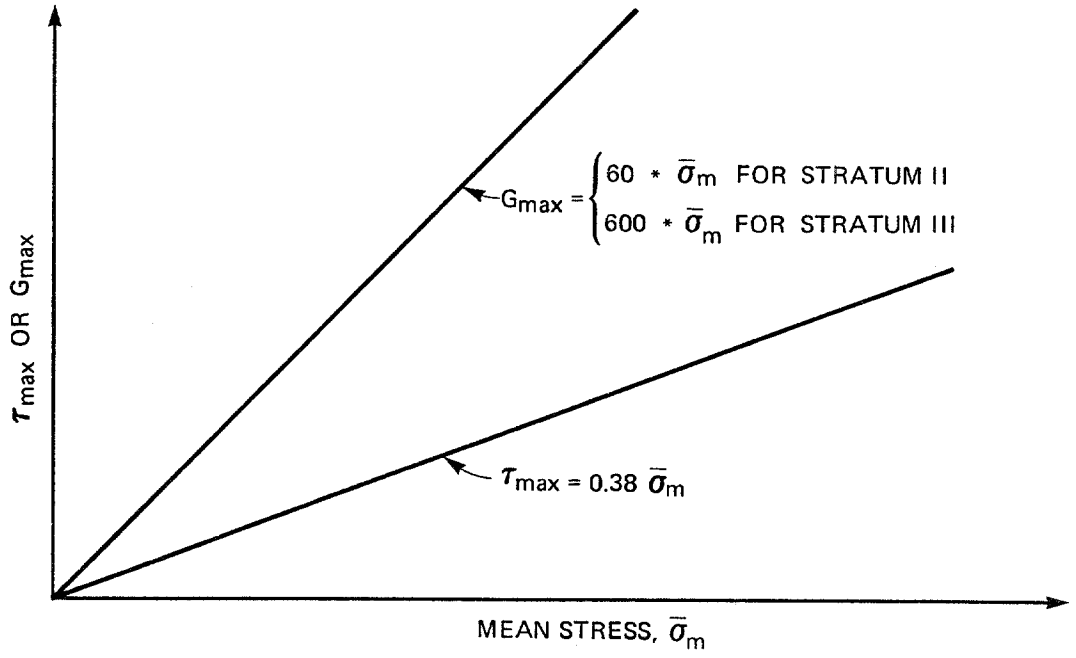

DEVIATORIC MODEL FOR SENSITIVITY AND FINAL BACKFIT ANALYSES

PLATE 4.2

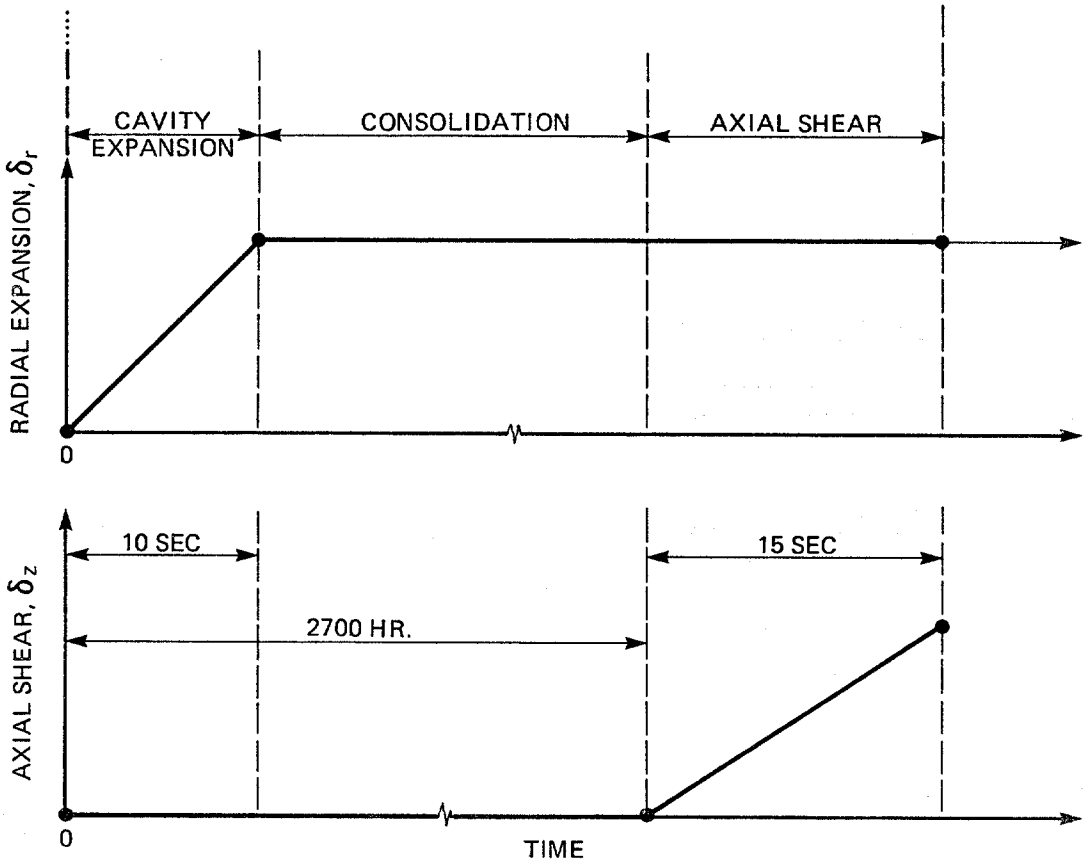

(a) LOADING CONDITION IN SENSITIVITY STUDY

UNIT WT. OF PORE FLUID = 64 PCF (10.00 KN/M3)

PERMEABILITY FOR BOTH STRATUM II & III = 2.5×10^{-9} cm/sec.

BULK MODULUS OF PORE FLUID = 4.6×10^{4} KSF (2,200 MPa)

IN SITU STRESS:	148 FT.	208 FT.
VERTICAL STRESS (KSF)	1.90	4.30
HORIZONTAL STRESS (KSF)	1.20	3.23
PORE FLUID PRESSURE (KSF)	16.60	21.00

1 KSF = 0.0479 MPa

(b) OTHER INPUT PARAMETERS IN SENSITIVITY AND FINAL BACKFIT ANALYSES ARE DESCRIBED IN PLATES 4.1 AND 4.2.

LOADING CONDITIONS AND IN SITU CONDITION FOR CASH

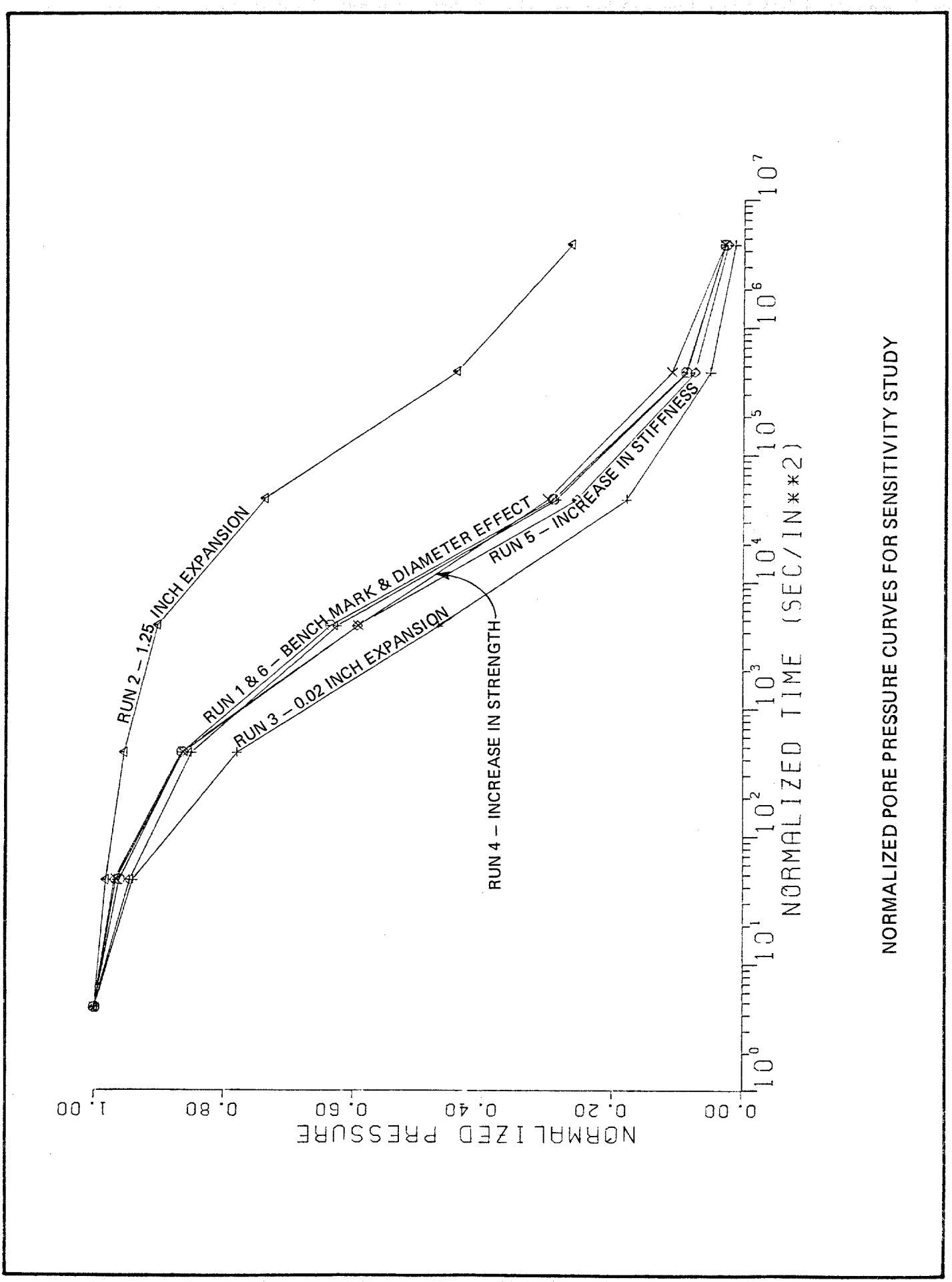

NORMALIZED PORE PRESSURE CURVES FOR SENSITIVITY STUDY

PLATE 4.4

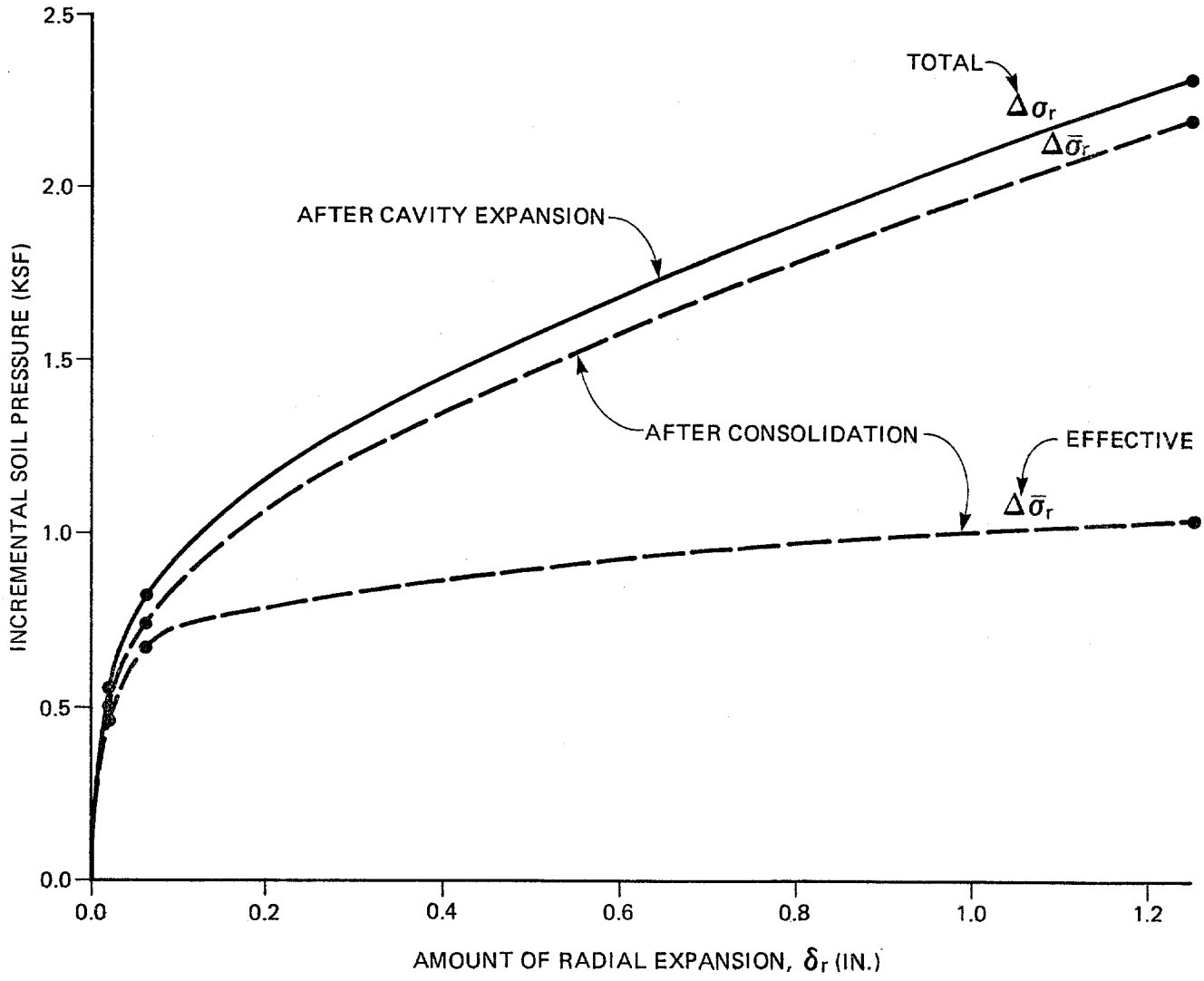

NOTES: (1) 1 INCH = 2.54 CM
(2) 1 KSF = 0.0479 MPa

CHANGE IN RADIAL NORMAL STRESSES AFTER CAVITY EXPANSION AND AFTER CONSOLIDATION

PLATE 4.5

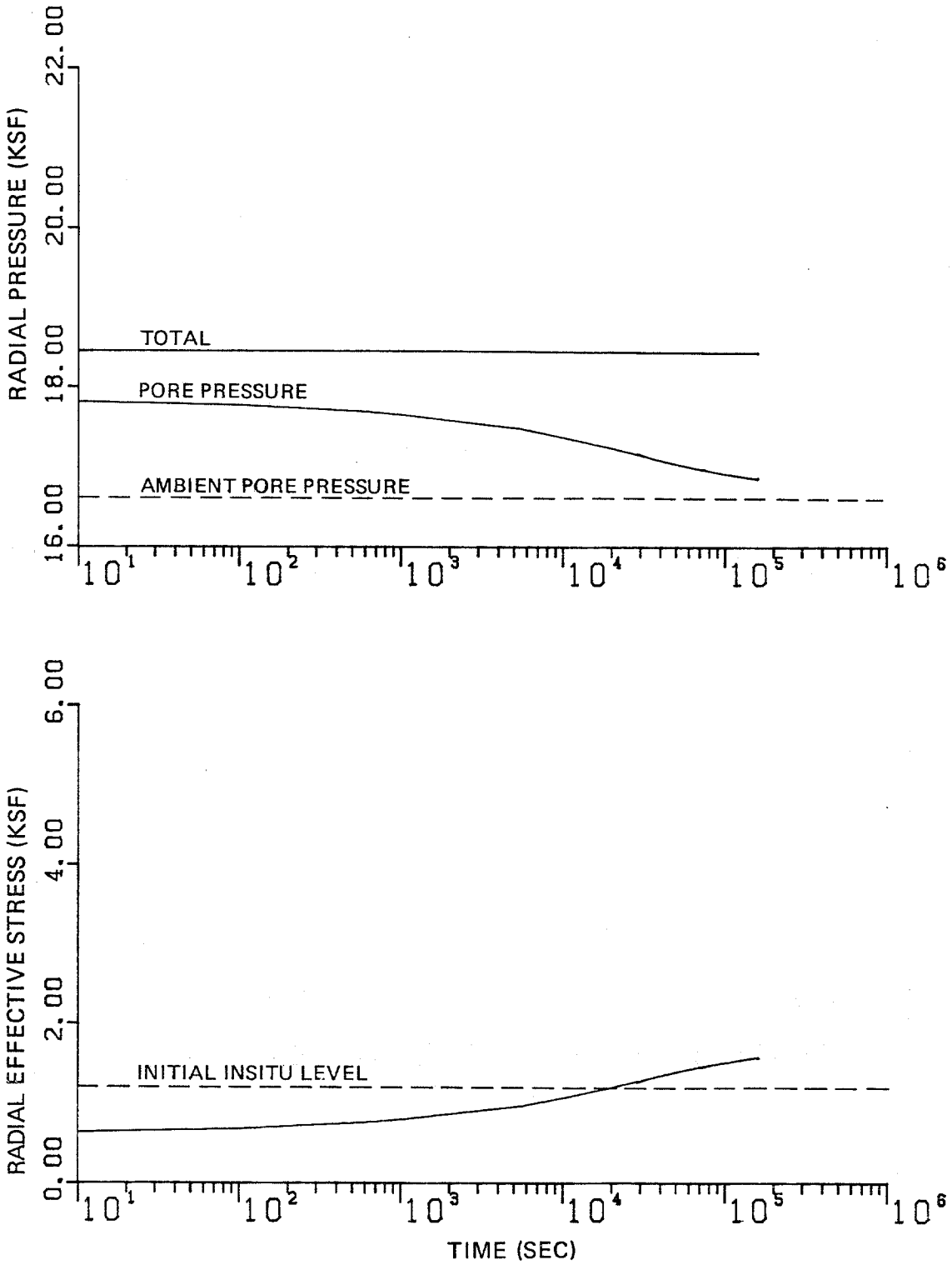

NOTE: 1 KSF = 0.0479 MPa

SOLUTION OF CONSOLIDATION HISTORY AT 148 FT. FOR 3–INCH SEGMENT

PLATE 5.1

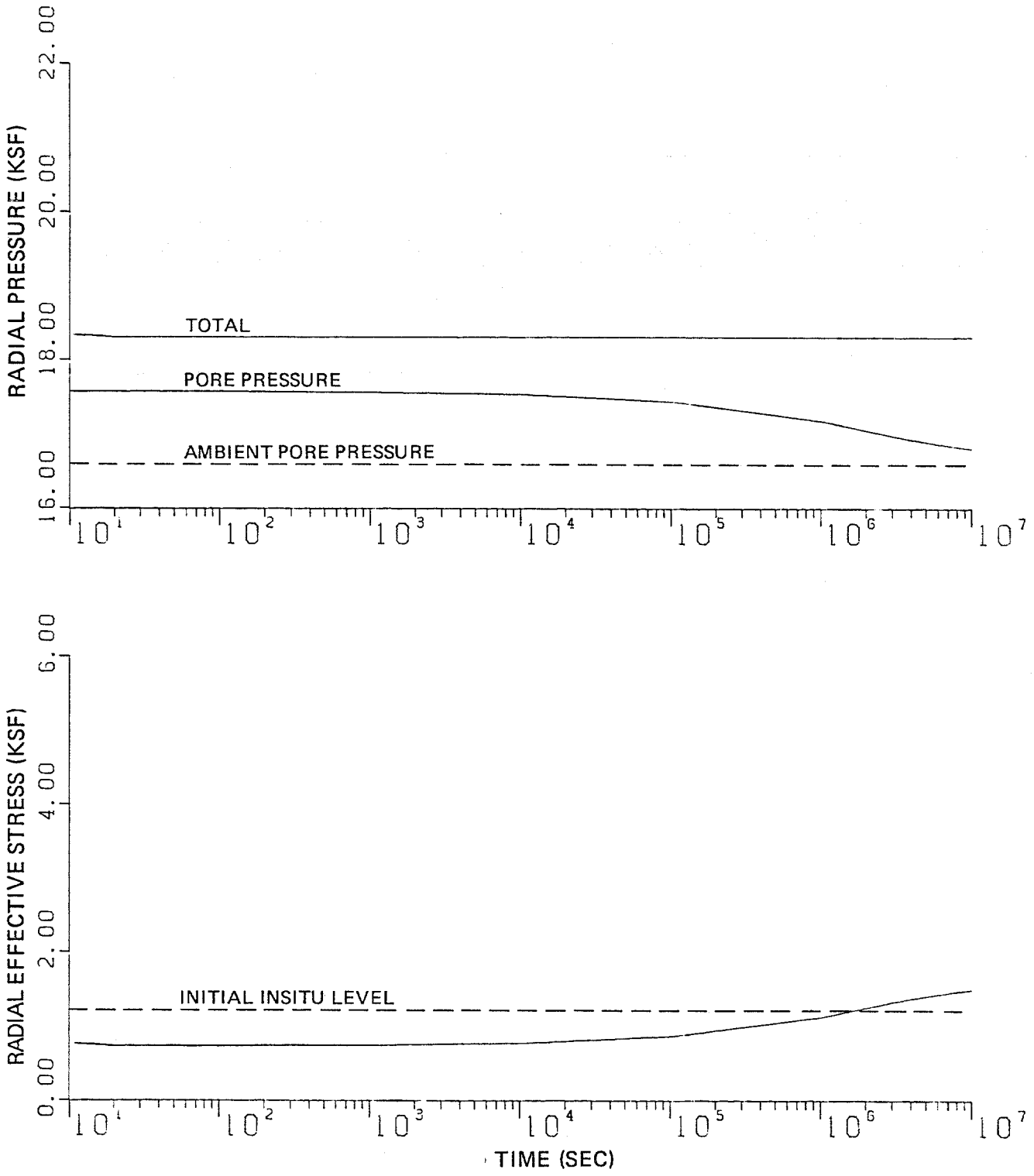

NOTE: 1 KSF = 0.0479 MPa

SOLUTION OF CONSOLIDATION HISTORY AT 148 FT. FOR 30–INCH PILE

PLATE 5.2

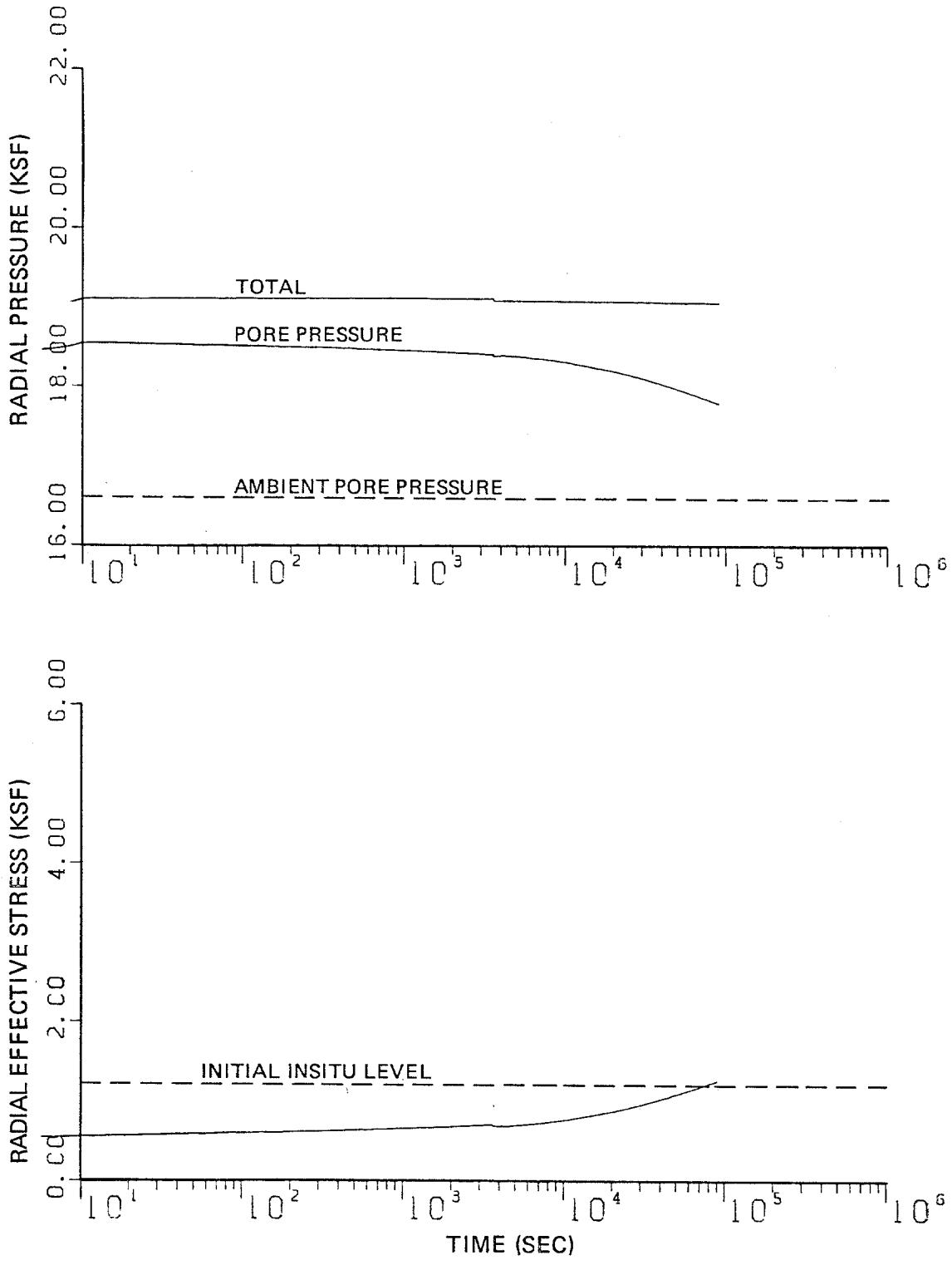

NOTE: 1 KSF = 0.0479 MPa

SOLUTION OF CONSOLIDATION HISTORY AT 148 FT. FOR X–PROBE

PLATE 5.3

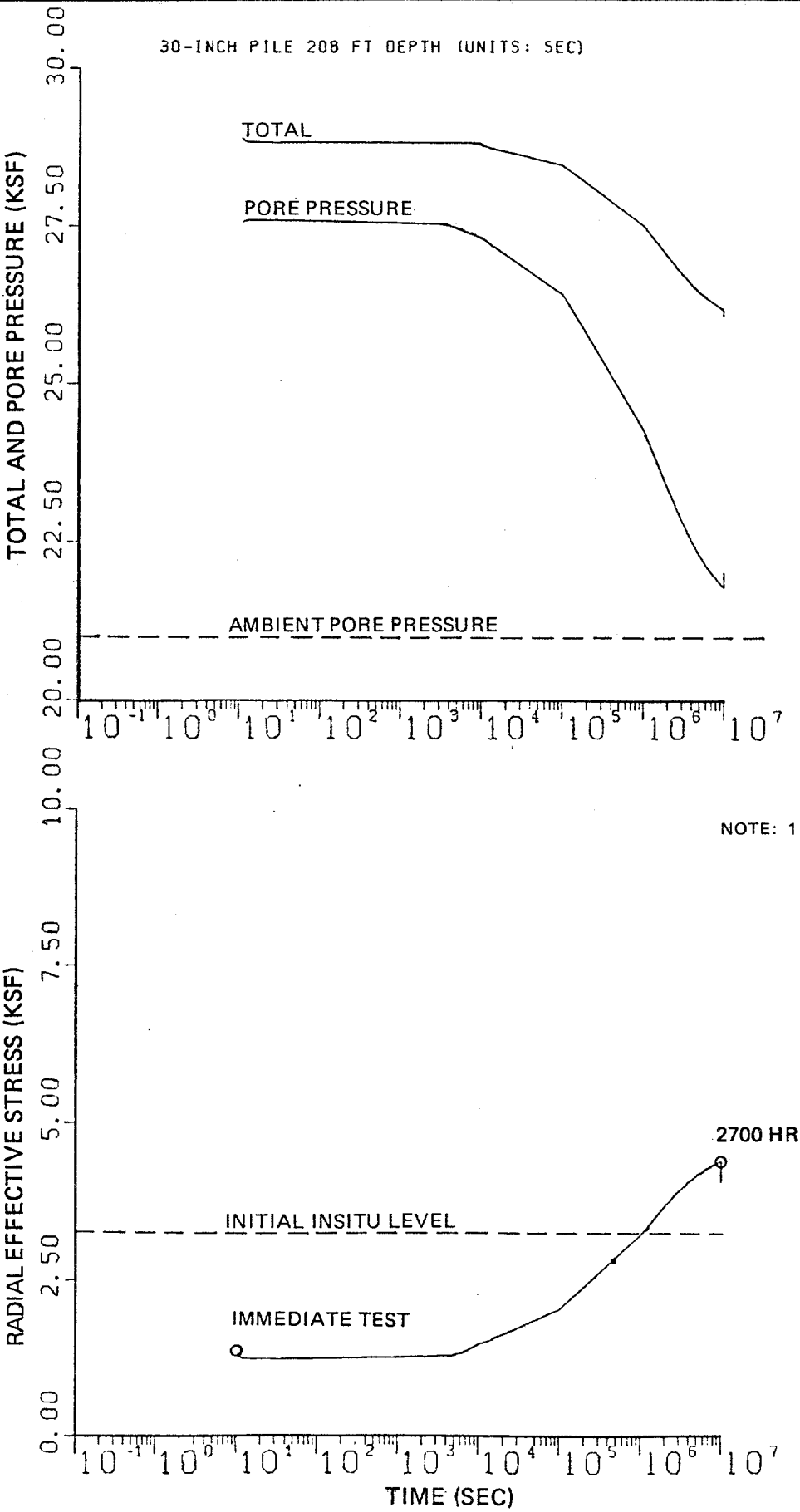

SOLUTION OF CONSOLIDATION HISTORY AT 208 FT. FOR 3–INCH SEGMENT

PLATE 5.4

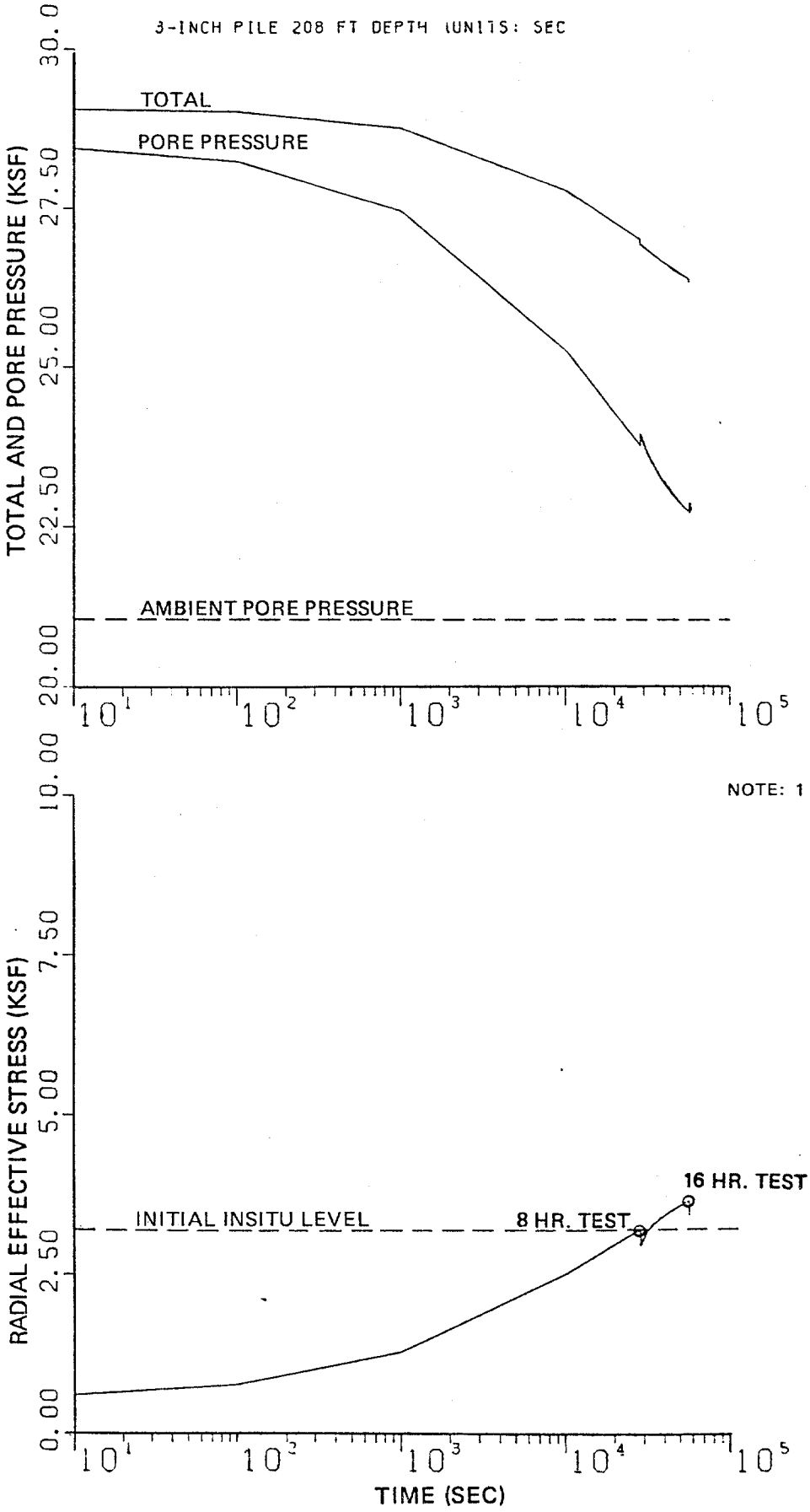

SOLUTION OF CONSOLIDATION HISTORY AT 208 FT. FOR 30–INCH PILE

PLATE 5.5

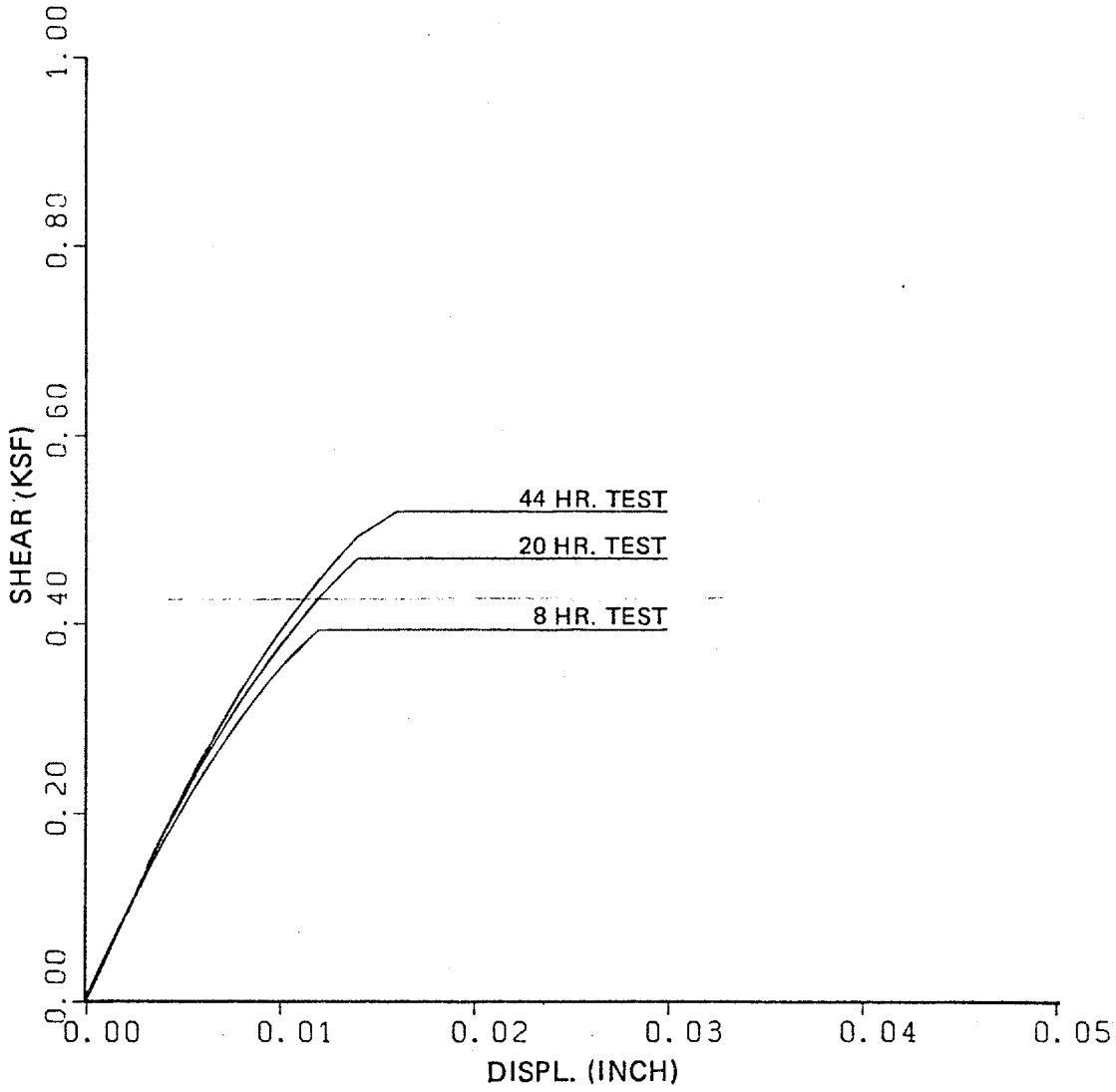

NOTES: (1) 1 INCH = 2.54 CM
(2) 1 KSF = 0.0479 MPa

T–Z CURVE FOR 3–INCH SEGMENT AT 148 FT.

PLATE 5.6

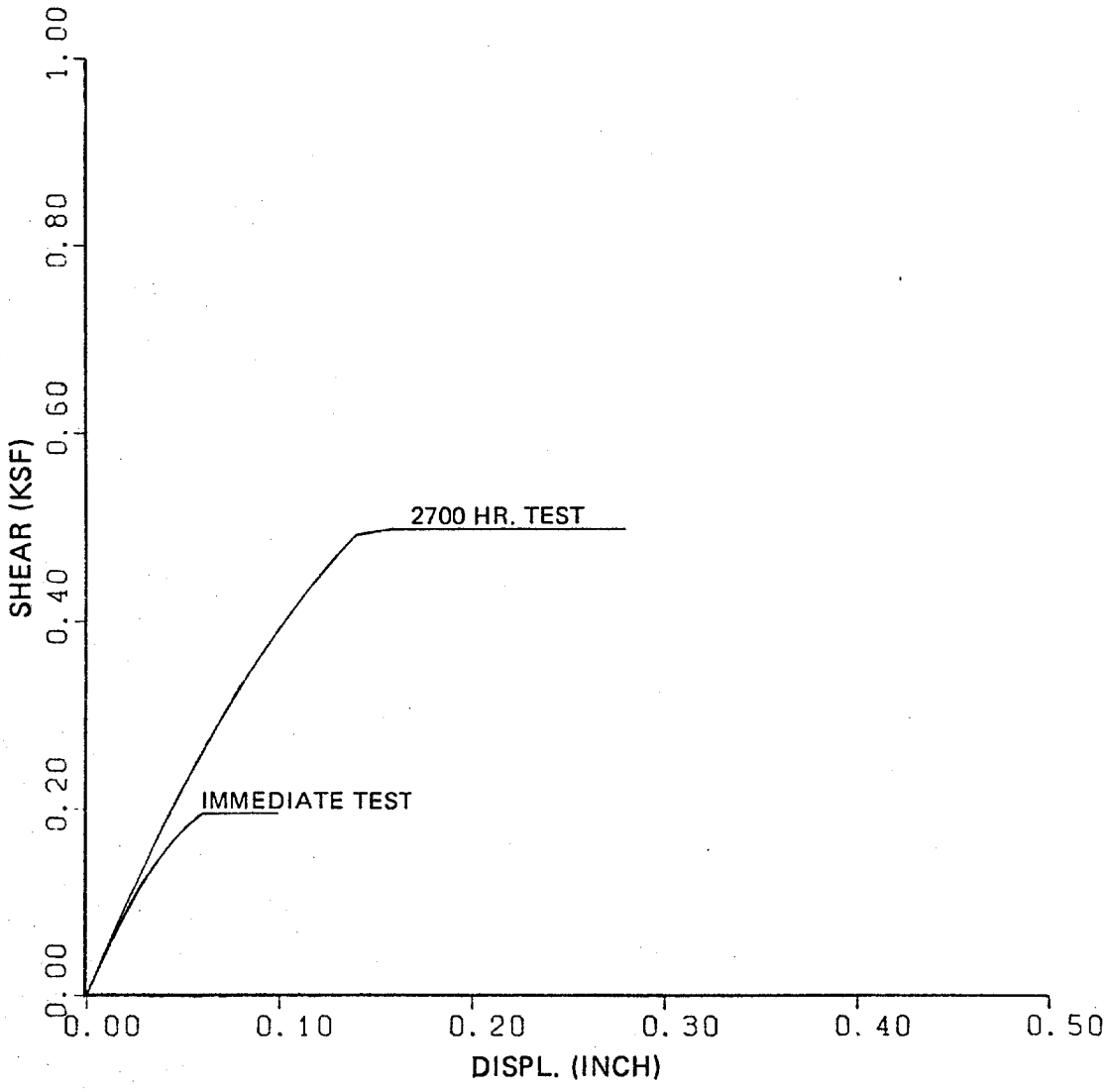

NOTES: (1) 1 INCH = 2.54 CM
(2) 1 KSF = 0.0479 MPa

T–Z CURVE FOR 30–INCH PILE AT 148 FT.

PLATE 5.7

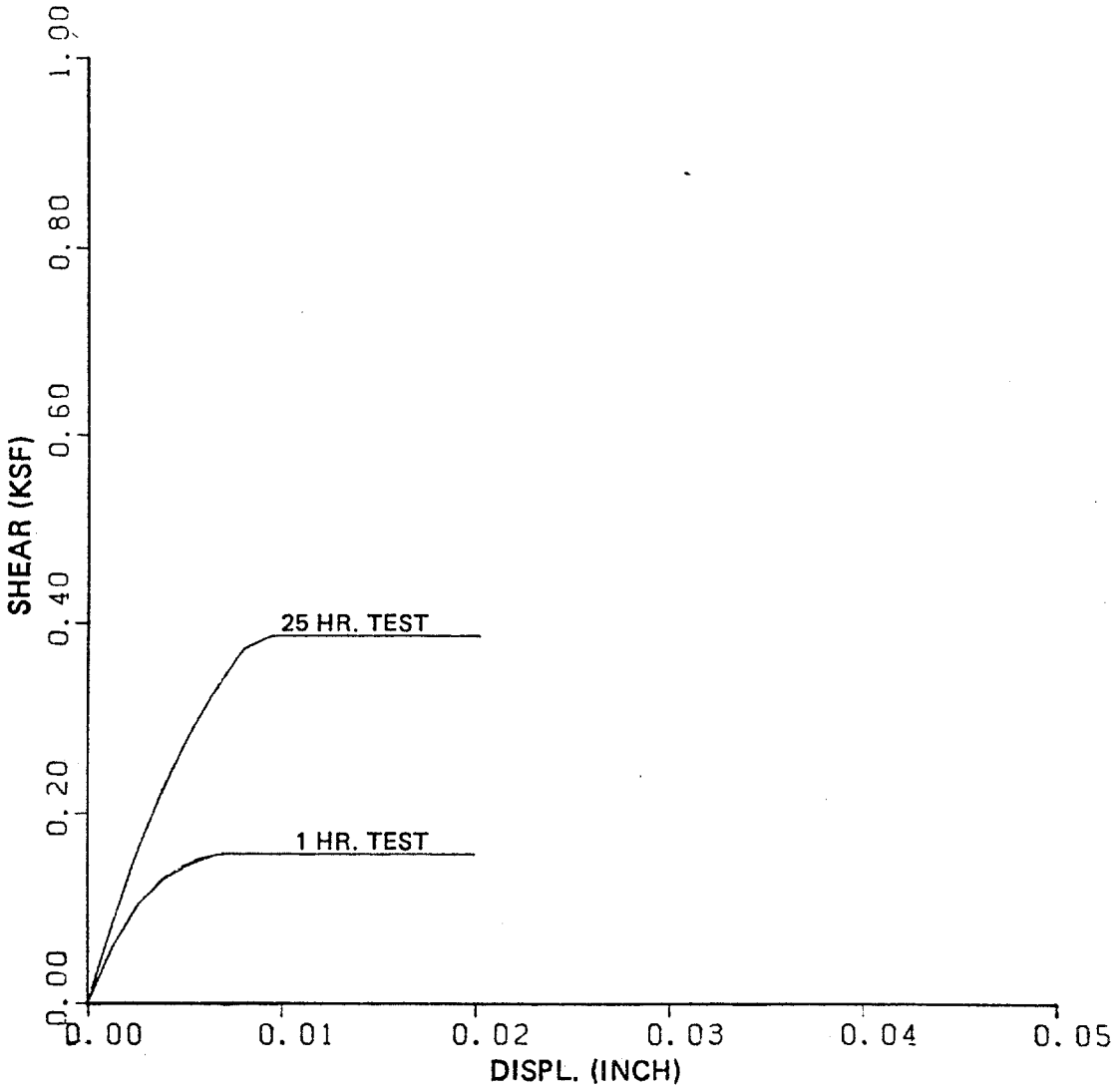

NOTES: (1) 1 INCH = 2.54 CM

(2) 1 KSF = 0.0479 MPa

T–Z CURVE FOR X–PROBE AT 148 FT.

PLATE 5.8

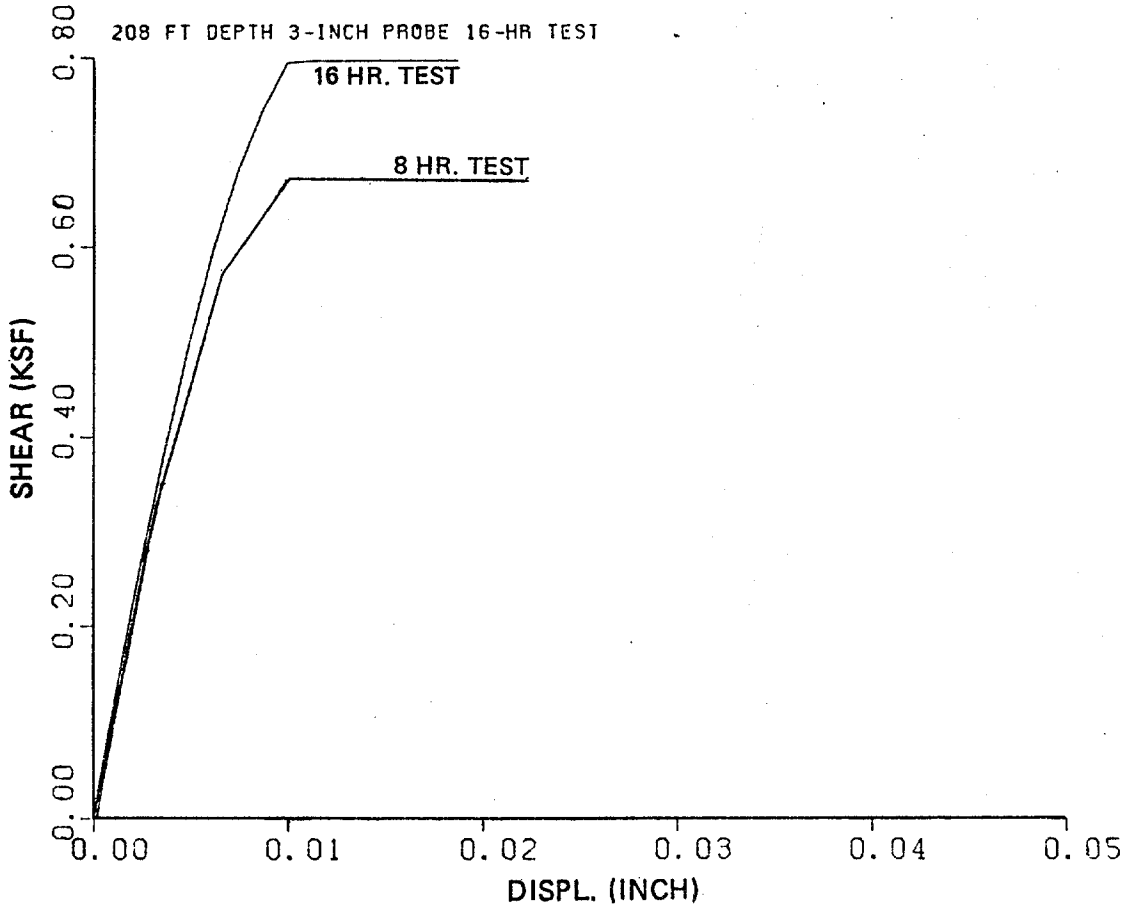

NOTES: (1) 1 INCH = 2.54CM

(2) 1 KSF = 0.0479 MPa

T–Z CURVE FOR 3–INCH SEGMENT AT 208 FT.

PLATE 5.9

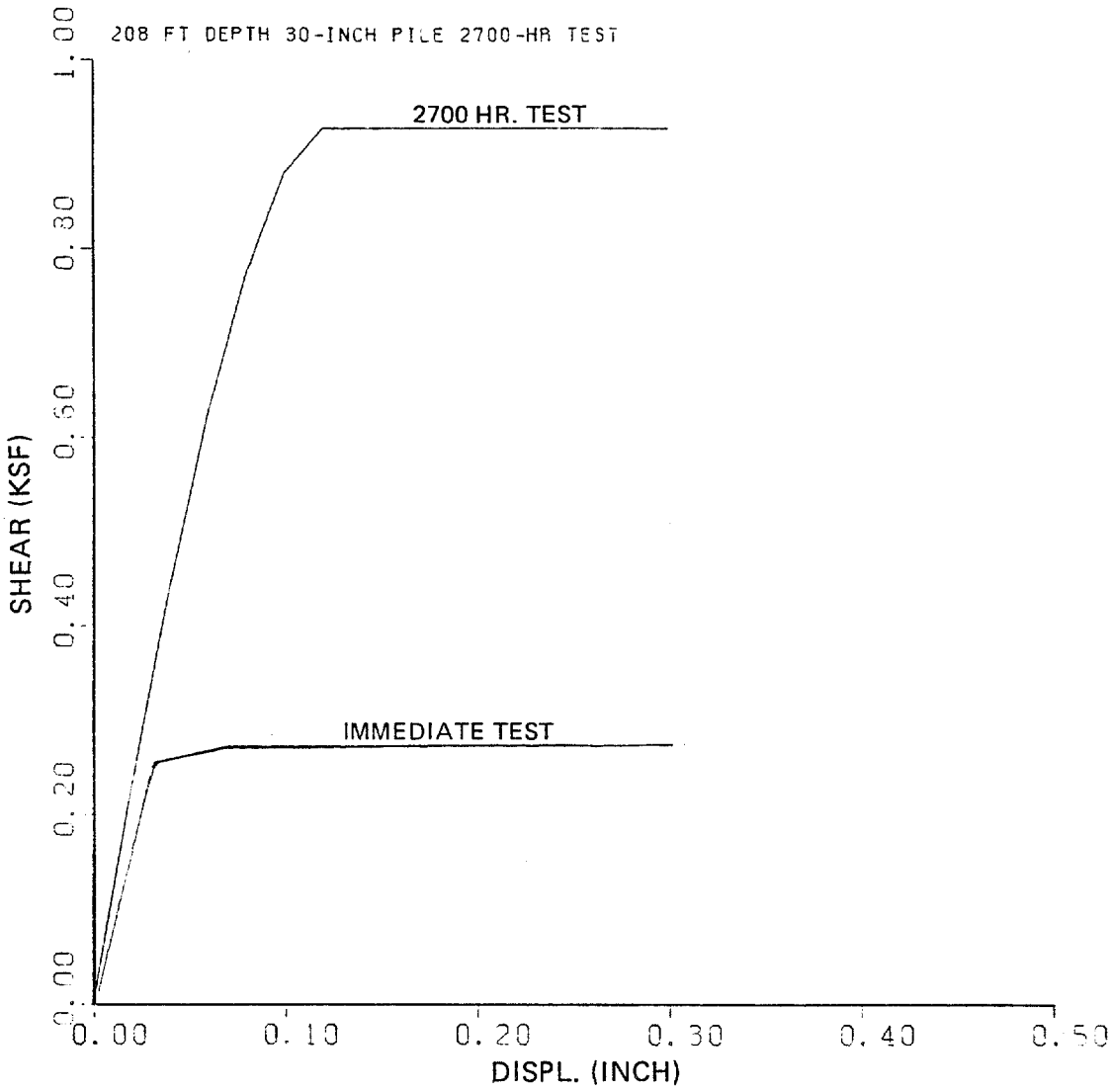

NOTES: (1) 1 INCH = 2.54 CM
(2) 1 KSF = 0.0479 MPa

T–Z CURVE FOR 30–INCH PILE AT 208 FT.

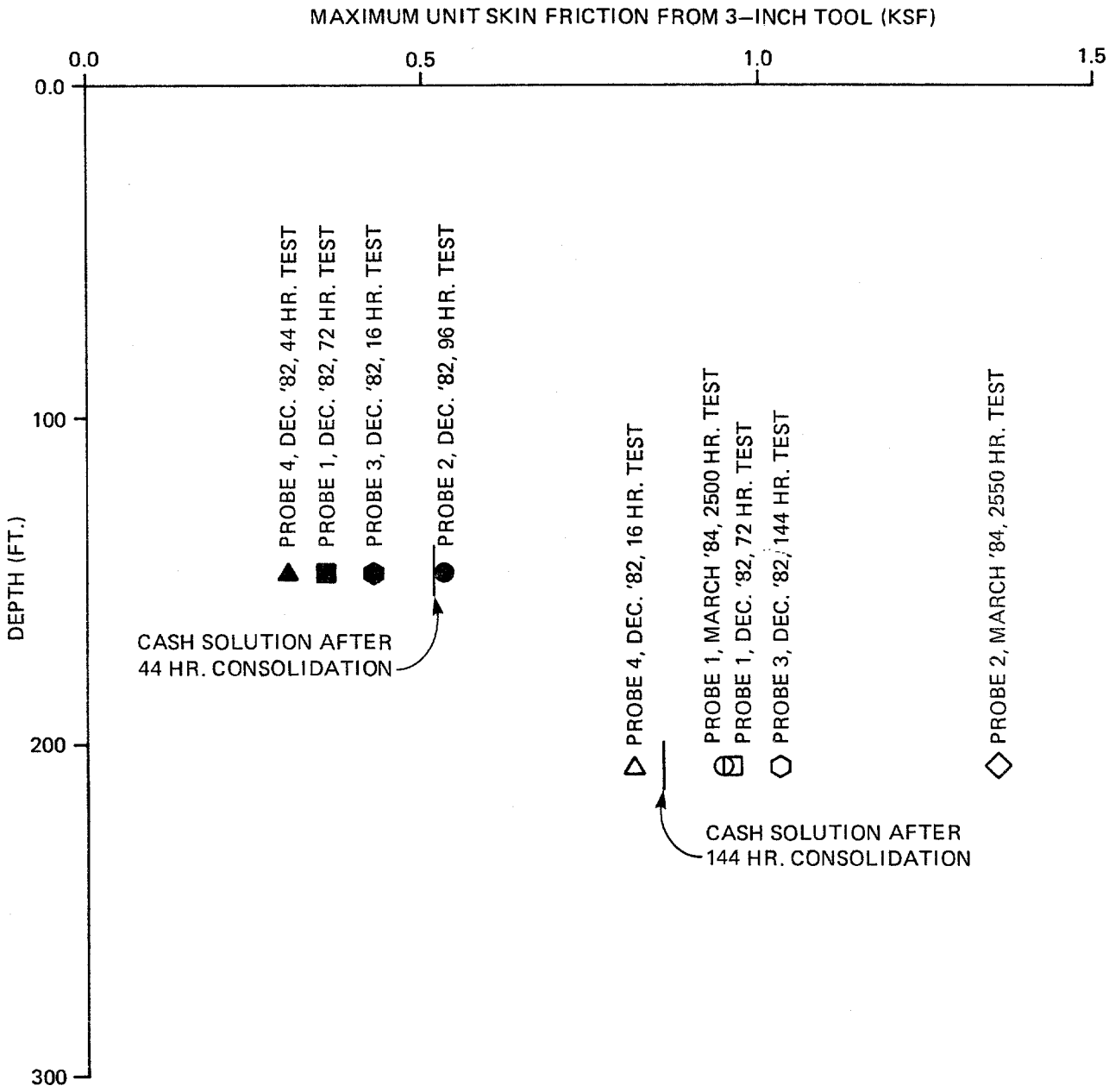

NOTES: (1) 1 FT. = 0.305M

(2) 1 KSF = 0.0479 MPa

COMPARISON OF CASH SOLUTION TO ALL AVAILABLE
3–INCH SEGMENT TEST DATA ON ULTIMATE SKIN FRICTION

PLATE 6.1

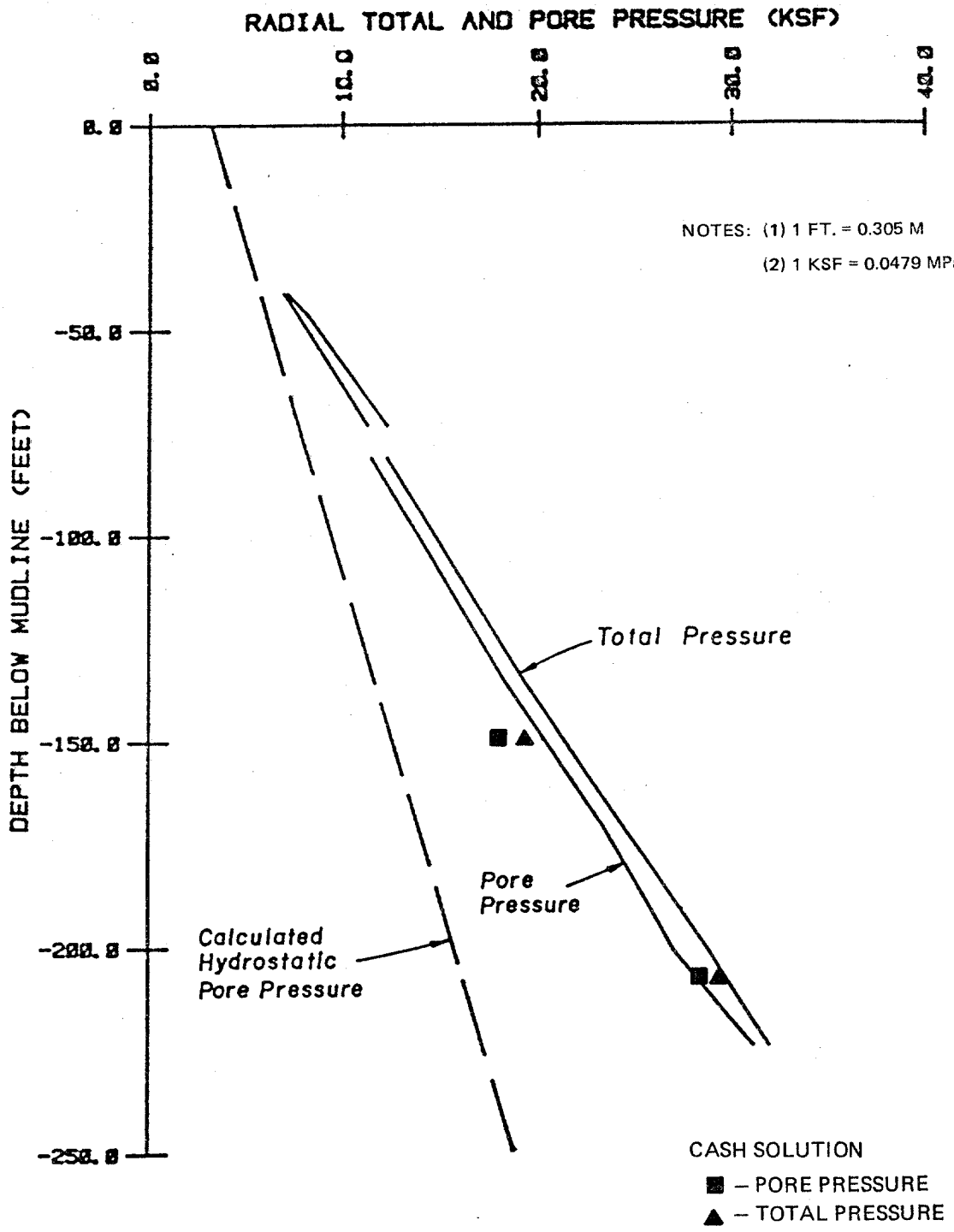

EVALUATION OF CASH SOLUTION FOR NORMAL STRESSES
IMMEDIATELY AFTER INSTALLATION OF THE 30–INCH PILE

PLATE 6.2

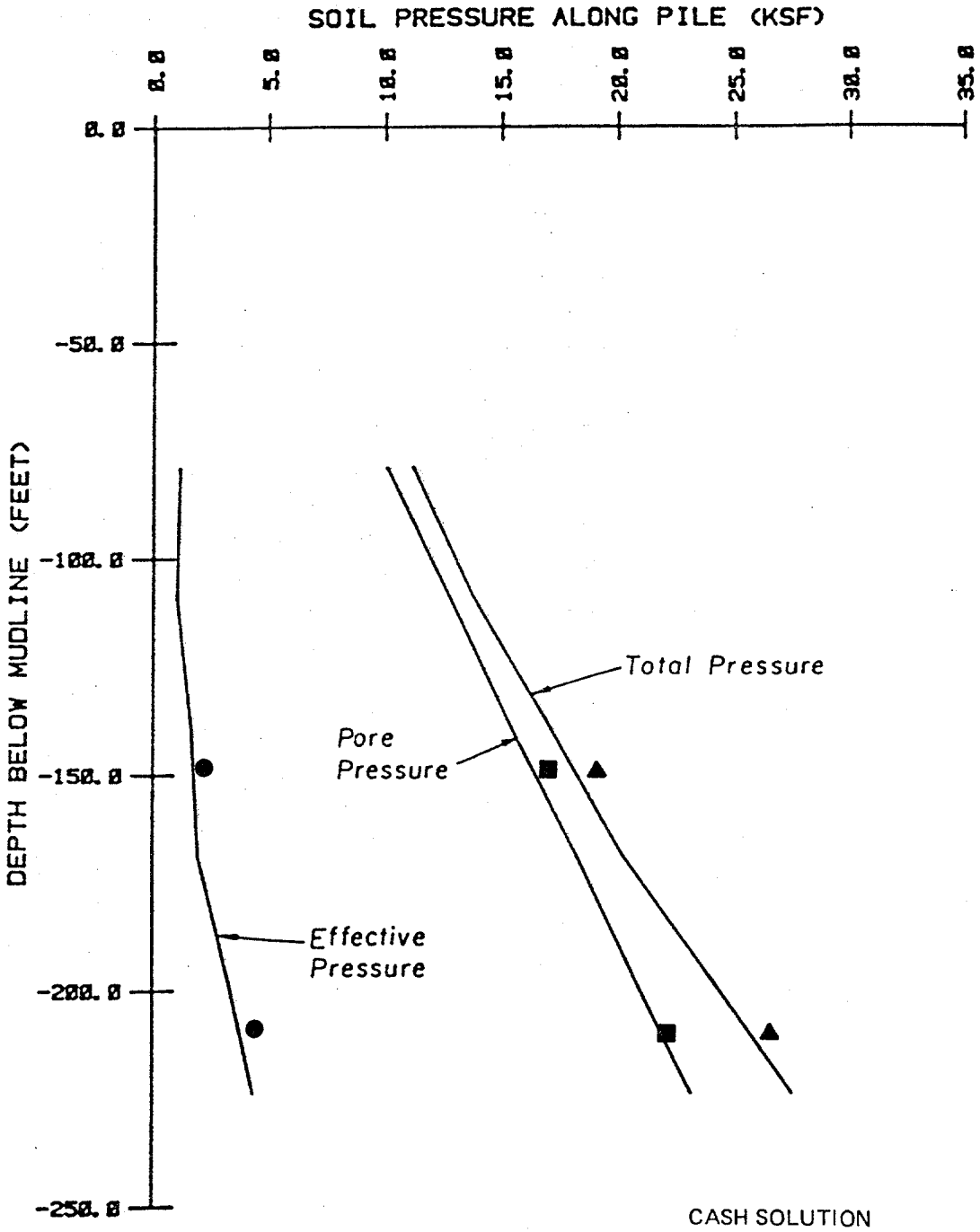

NOTES: (1) 1 FT. = 0.305 M
(2) 1 KSF = 0.0479 MPa

EVALUATION OF CASH SOLUTION FOR NORMAL STRESSES
AFTER 111 DAYS OF CONSOLIDATION OF THE 30–INCH PILE

PLATE 6.3

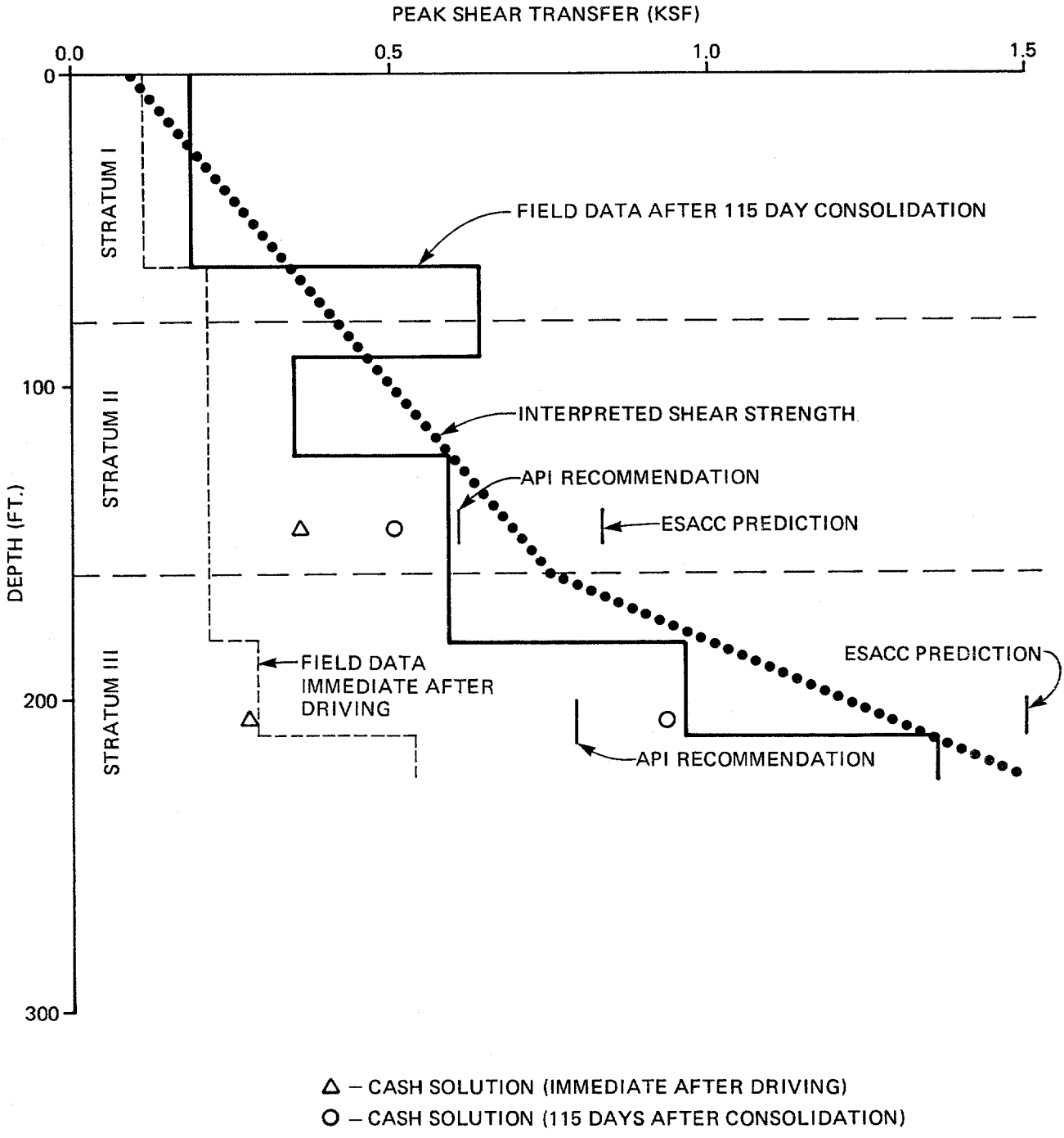

NOTES: (1) 1 FT. = 0.305 M

(2) 1 KSF = 0.0479 MPa

ASSESSMENTS OF SKIN FRICTION CAPACITY BY VARIOUS DESIGN MODELS

PLATE 6.4